MICROFLUIDIC PLATFORMS FOR MULTI-PROTEIN CROSSTALK AND ITS APPLICATION ON CELL SORTING

A Dissertation
Presented to
The Academic Faculty

by

Fangyuan Zhou

In Partial Fulfillment
of the Requirements for the Degree
Doctor of Philosophy in the
School of Mechanical Engineering

Georgia Institute of Technology
August 2019

MICROFLUIDIC PLATFORMS FOR MULTI-PROTEIN CROSSTALK AND ITS APPLICATION ON CELL SORTING

Approved by:

Dr. Cheng Zhu, co-Advisor
School of Mechanical Engineering
Department of Biomedical Engineering
Georgia Institute of Technology

Dr. Todd Sulchek
School of Mechanical Engineering
Georgia Institute of Technology

Dr. Hang Lu, co-Advisor
School of Chemical Engineering
Georgia Institute of Technology

Dr. Wilbur Lam
Department of Biomedical Engineering
Georgia Institute of Technology
Department of Pediatrics, Division of Hematology/Oncology
Emory University School of Medicine

Dr. Susan N. Thomas
School of Mechanical Engineering
Georgia Institute of Technology

Date Approved: [June 5th , 2019]

ACKNOWLEDGEMENTS

I would like to express my gratitude to my advisors, Dr. Cheng Zhu and Dr. Hang Lu, for their outstanding knowledge, support, guidance, and patience. They provided this intellectual, collaborative, and rigorous research environment for me to learn and improve in two lab cultures. It was very beneficial to learn and work with two advisors with different styles. While being critical and strict, they are supportive and constructive, and so patient with all my struggles. Being a student barely know anything in the beginning, I understand how much time and effort they have to put in me. I will always be grateful for having the opportunity to learn from someone I respect so greatly. I would also like to thank my thesis committee members for their valuable time and suggestions. Dr. Wilbur Lam, Dr. Todd Sulchek and Dr. Susan Thomas gave me honest and concrete suggestions on both paper plan and experiment details.

I am also grateful for the support of all the members from the Zhu Lab and Lu Lab. Special acknowledgments also go to Dr. Yunfeng Chen, Dr. Loice Chingozha, Dr. Kaitao Li, Dr. Lining Ju, Dr. Guillaume Aubry, Zhou Yuan, Jiexi Liao, Tel Rouse, Shivesh Chaudhary, for fruitful discussions, and for their support and friendship. Yunfeng Chen and Loice Chingozha acted as my Ph.D mentor, guided me in beginning of my projects, and always provides good suggestions in the journey of my Ph.D. A lot of the experimental designs came from the discussion with Yunfeng, who also spent a significant amount of time helping me understand the platelet biology. Kaitao from Zhu Lab and Guillaume from Lu Lab are my best ‘consultant’ over various things, from device design, fabrication to biology and thesis structure. Larissa, our lab manager, is always loving to all of us, and she

helped me a lot with materials and protocols. It is a great experience to work with everyone from the two labs in these years. In addition to my labmates, I would like to thank Yumiko Sakurai, Dr. Yongzhi Qiu, Dr. David R. Myers and a lot of other people in the Lam Lab for blood draw over the years, which is so important for my experiments.

I want to thank all my friends in GT and Emory, who have encouraged me during difficult times. The thanks also go to my friends in China, who are caring and share great moments with me.

Special thanks to my family for their unconditional love and encouragement. Though being in China, my family's support allows me devoting to this unique experience. My dear sister, Chunyuan, always my best friend, inspired me to pursue Ph.D in science and engineering.

Finally, a lot of thanks to my husband, Yuanzheng, who is always by my side no matter what, from Zhejiang University to Georgia Tech.

TABLE OF CONTENTS

LIST OF TABLES

LIST OF FIGURES

LIST OF SYMBOLS AND ABBREVIATIONS

μCP	Microcontact printing
Ab	antibody
AFM	atomic force microscopy
APC	antigen presenting cell
BFP	biomembrane force probe
BSA	bovine serum albumin
DMSO	dimethyl sulfoxide
EC	endothelial cell
ECM	extracellular matrix
FN	fibronectin
GPIb	glycoprotein Ib
HPV	Human papillomavirus
IS	Immune synapse
Ka	affinity
Koff	dissociation rate
Kon	association rate
LFA-1	Lymphocyte function-associated antigen 1
mAb	monoclonal antibody
OT	optical tweezers
PD1	programmed cell death protein 1

PDMS	polydimethylsiloxane
pMHC	peptide-loaded major histocompatibility complex
PSGL-1	P-selectin glycoprotein ligand-1
RBC	red blood cell
RT	room temperature
SMC	smooth muscle cell
SPR	surface plasma resonance
TCR	T cell receptor
VWF	von Willebrand factor
VWF-A1	von Willebrand factor A1 domain

SUMMARY

Cells use their surface receptors to anchor to and communicate with other cells and the extracellular matrix. Such processes usually involve interactions of multiple receptor-ligand pairs occurring independently, cooperatively, or antagonistically. The study of crosstalk among different receptor species can be benefitted by techniques that are efficient, high throughput, and easy to use. Conventional approaches have difficulties to control each ligand precisely or detangle measurement of cell adhesion by each receptor-ligand pair. This thesis describes the development of two platforms to address this deficiency and their applications to several problems in cellular engineering.

The first platform of an auto-alignment protein patterning approach enables a sequential ligand presentation. This allows moving cells to interact with spatially separated ligands sequentially, thus dissecting the crosstalk between different receptors by detangling temporally their ligand interactions and reporting the effect of triggering one receptor by the altered binding of another receptor. This device with multiple zones of ligand coating allows precise and tunable control over the species, the density and the zone length of surface-immobilized molecules. A parallel version of this device permits controls over various stimulations on the same chip and further improved the throughput.

This multi-zone system is first applied to provide independent evidence for the presence of an intermediate state of the major integrins on platelets and leukocytes. An intermediate state of integrin $\alpha_{IIb}\beta_3$ was demonstrated by triggering GPIb with VWF-A1 immobilized on one zone and measuring platelet adhesion to fibronectin or conformation reporter antibodies coated on another zone. Furthermore, the increased binding of integrin

$\alpha_{IIb}\beta_3$ upregulated by VWF-A1 was found in diabetic platelets. The assay required only one-drop of blood, thus potentially applicable for diabetic state monitoring upon further development. The intermediate state of integrin $\alpha_L\beta_2$ (LFA-1) was similarly studied. On human neutrophils, this intermediate state LFA-1 was upregulated by P-selectin-ligand and reported by conformation reporter antibodies. On mouse T lymphocytes, the intermediate state LFA-1 was upregulated by TCR-pMHC and reported by rolling adhesion on ICAM-1 and by intracellular calcium fluxes. The effects of "dose" were revealed through precise control of the length and ligand density of the stimulus zone and the perfusion flowrate.

The second system is to sort antigen-specific T cells based on TCR triggering studied earlier using the multi-zone device. The effective interaction of TCR-pMHC can lead to an activation of LFA-1, whose differential ICAM-1 binding amplifies the difference in pMHC binding to T cells with different T cell receptor clones. The sorting chip first triggers T cells by specific pMHC and then allows activated T cells to move laterally on a patterned ICAM-1 surface to separate cells with activated LFA-1 supported rolling. The platform was validated by two experiments: 1) sorting T cells from OT1 TCR transgenic mice specific for OVA pMHC from non-specific T cells from B6 mice, 2) characterizing OT1 T cell rolling on ICAM-1 and calcium fluxes in response to triggering by pMHCs of various biological activities. Considering its advantages including short time scale, continuous sorting manner, and module compatibility, this platform can potentially be implemented for enumeration and isolation of functional T cells.

Overall, this thesis developed an approach for studying cell multi-receptor crosstalk generalizable to various receptor mechanobiology and applied to mechanistic studies to potential clinical applications, revealing the advantages of microfluidics in disease studies

and diagnostics. In addition, the platform for functional antigen-specific T cell sorting should be valuable in a variety of clinical settings for diagnoses and functional immunotherapies.

CHAPTER 1. INTRODUCTION

1.1 Cell adhesion and multi-protein engagement in cell function

1.1.1 Cell adhesion

Cell adhesion is formed by the direct physical binding of the receptor molecules anchored on the cell surface and the ligand molecules on another cell surface or on the extracellular matrix (ECM). This adhesive binding is an important means of cells for communication with the environment, and affects various cell functions including navigation, proliferation, differentiation, survival and more [1, 2]. Physiological processes largely involve adequate cell adhesion by receptor-ligand interactions, such as wound healing and immune cell recruitment, while abnormity of cell adhesions is often associated with pathological conditions, such as thrombosis, cancer metastasis and autoimmunity. Thus, understanding the properties of cell adhesion holds a great value in pathology, clinical practice, and bioengineering device development.

Corresponding to different cell functions, cell adhesions tend to exhibit different behaviors, which can be used to evaluate the function and dysfunction of cell adhesion. For instance, firm arrest is one of the common cell adhesive behaviors, and so is continuous slow rolling [3].

When cell adhesion is measured at the cellular level, the cell adhesion strength is determined by the magnitude of the exerted force and the avidity by the likelihood of cells

adhering or departure which can be measured via techniques such as micropillar [4] and DNA force probe [5]. Rolling velocity of translocating cells is another measurement for fast association and fast dissociation interactions. Flow chamber is one way to measure the rolling velocity [3]. In addition, more measuring assays can be employed to assess other aspects of cell adhesion. Cell adhesion can also be quantified at molecular level, which requires the measurement of kinetic parameters, such as the association (Kon) and dissociation (Koff) rate, affinity (Ka), and lifetime under force, by dynamic force spectroscopy technologies [6].

1.1.2 Cell adhesion involving multi-protein engagement

The complicated and variable cell interactive functions are not easily achievable from single type of receptor-ligand binding. Instead, interactions of multiple receptor-ligand species are usually concurrently involved to fulfil cell adhesion functions [7].

In some cases, these interactions are independent, whereas in a lot of other cases, interactions are cooperative and causally related. For instance, cooperative binding induced platelet adhesion and activation occurs at vascular injury sites. In order to attach onto the exposed sub-endothelium, platelets first use glycoprotein (GP) Ib to translocate on the endothelial cell surface-immobilized von Willebrand factor (VWF) via its A1 domain (VWF-A1). This binding activates GPIIb-IIIa (integrin $\alpha_{IIb}\beta_3$) via mechano-signaling, and in turn enables GPIIb-IIIa to mediate platlet firm adhesion [8-10]. Such a sequential process enables efficient platelet recruitment during hemostatic and thrombotic processes, and also induces P-selectin expression [11] that is potentially important to other functions of platelets, e.g., in immune responses [12, 13]. Another example of cooperative interaction

laid in neutrophil recruitment to inflamed tissue, which is initiated by the engagement of selectins and followed by integrin-mediated rolling and firm arrest [14]. In addition, the adaptive immune response mediated by T lymphocyte cells also benefit from the cooperative receptor-ligand interactions. T cell receptor (TCR) on T cell surface states the recognition of peptide-loaded major histocompatibility complex (pMHC) on an antigen presenting cell (APC), which activates $\alpha_L\beta_2$ (LFA-1, CD11a/CD18) to establish concurrent binding with the APC surface ICAM-1 so as to stabilize the T cell-APC contact [2]. In some other systems, antagonistic effects are also observed between different receptors, with the function of one receptor suppressed by the ligand-binding of another. In many biological contexts, the exact nature of these interactions is largely unknown.

While the study of a single pair of receptor-ligand can enlarge our understanding of cell adhesion, a systematic study of multi-protein engagement in cellular processes is of essence to the understanding cell functions in a more comprehensive way, potentially allowing target therapy for suppression of cell abnormity functions bur retaining other functions.

1.2 Conventional tools to study surface protein adhesion kinetics

Cell adhesion to a surface consists of an initial binding and a firm attachment followed by spreading, morphological changes, migration or aggregation. Receptor-ligand binding mediates the initial cell adhesion and its kinetics have been widely studied by assays such as surface plasma resonance (SPR) by measuring surface immobilized molecules to another molecules in solution. However, cell adhesion via receptor-ligand occurs between cell surface molecules and molecules anchored on another surface (ECM

or other cells), known as 2D kinetics [15-17] whereas kinetics by assays such as SPR is known as 3D interaction kinetics. 3D assays may be insufficient in describing physiological cell adhesion because surface molecules can be clustered or linked to other molecules under physiological conditions, which may affect their binding abilities. In these cases, 2D kinetics may be more physiologically relevant [16]. Hence studies of receptor-ligand interactions between surface anchored molecules is more provocative rather molecules in a solution. 2D interaction kinetics can be measured by assays including AFM [18], optical tweezer [19], micropipette adhesion assay [17], and flow chamber [20, 21].

Flow chamber devices have been widely used as in vitro models to assess cell behavior exposed to dynamic fluid flow in a more natural, physiological environment [22-25]. A flow chamber typically consists of three parts: a polycarbonate distributor, a silicon gasket, and a glass coverslip. The coverslip can be coated with proteins, cells, or biomaterials of interest. Flow chamber studies can mimic the physiological condition and investigate hundreds of cells, yet contacts between cell and protein is loosely controlled, making it hard to investigate stimulus in right amount of time and interpret adhesion kinetics directly [3].

Micropipette adhesion assay utilize a human red blood cell (RBC) as a force transducer to detect adhesion events where RBC's low spring constant makes it an excellent candidate for sensing small forces (10-110pN) [26]. The RBC is coated with ligand of interest via covalent linking and aspirated on a micropipette connected to a piezo-driven micromanipulator [17]. On the other side is a target cell bearing the receptor of interest. The two cells are brought into repeated contact and separation at defined contact durations for tens to hundreds of times. The dependence of adhesion frequency on contact

duration enables kinetic rates to be determined from a probabilistic model at constant ligand and receptor densities, and constant contact area between the cells [15]. This probabilistic model (Equation 1) is based on the analysis of kinetics for systems which assumes a small number of bonds are formed during the adhesion events [26] and that the adhesion events are infrequent and follow a Poisson distribution [15]. Despite of the force sensitivity (10pN) and direct interpretation of adhesion kinetics from micropipette adhesion assay, only one cell can be interrogated at a time, making this a laborious, low throughput technique.

$$P = 1 - e^{-m_r m_l A_r K_a [1 - e^{-k_{off} t}]}$$

Equation 1[17]

Cell adhesion can be measured in similar principles of single cell approach using techniques such as atomic force microscopy (AFM) [18], biomembrane force probe (BFP) [27], and optical tweezers (OT) [19]. However, these 2D kinetics assays for single cell, single molecular measurements also suffer from the low throughput and high experience requirement.

1.3 Microfluidic systems for probing cell adhesion

As an emerging cell manipulation technique, microfluidics has been developed for cell adhesion and brings the benefits of precise environmental control, convenience in cell-size feature fabrication and simple operation. Microfluidics can probe cell adhesion in both initial adhering processes and later firm adhesion (including spreading, aggregation, migration and deformations) [28].

With the precise control of the environment - and in particular fluid shear - microfluidic approaches to study cell adhesion can be categorized in three groups: attachment assays, detachment assays and rolling assays.

1. Attachment assays. Microfluidic surfaces or other structural features can be functionalized by adhesive molecules to examine cell adhesion under certain shear force. As an example, Murphy and co-workers [29, 30] employed a device with a linear shear stress specific peptide and demonstrated the dependency of the adhesion of endothelial cells (ECs) and smooth muscle cells (SMCs) on peptides and shear stress by measuring the adhered cell number. Attachment assays reflect shear dependence of the cell on rate to the adhesive surfaces.
2. Detachment assays. Compared to other micromanipulation assays to detach an adhered cell, microfluidics is noninvasive and so overcomes the risk of cell damage by applying a range of shear for detachment. Surface conditions, fluid shear, and the chemical environment can all be well-controlled in microfluidics. As an example, fibroblast adhesion strength to the fibronectin (FN)-coated substrate was demonstrated as a function of surface coating concentration and shear stress by Lu et al [31]. Human papillomavirus (HPV)-infected cells were also assessed using this detachment assay by Wankhede et al. [32]. Detachment assays reflect the cell off-rate to the adhesive surfaces.
3. Rolling assay. Cell rolling is a specific cell behavior enabled by rapid on-rate and off-rate of the cell adhesion and so reveals an important mechanism

of cells interacting specific cellular cues. This behavior is prevalent in physiological processes such as neutrophil recruitment to inflammation sites, stem cells homing to bone marrow niches, and platelets adhering to injury sites. Simone et al. [33] examined the tumor cell behavior from firm adhesion and adhesive rolling for the shear regime in a microfluidic device.

Cell spreading and force measurement have also been investigated in microfluidics by employing the existing techniques of imaging cell morphology [4] and traction force measurements [4, 5].

1.4 Biological application: Platelet activation and hyperactivity in diabetes

1.4.1 Platelet activation via mechano-signaling of GPIb

Platelet plays a primary role in haemostasis, namely to stop bleeding and preserve tissue when a vascular injury happens. Vascular injury sites recruit circulating platelets in blood stream which leads to a cascade of events including platelet adhesion, activation and aggregation. Eventually, a blood clot (thrombus) formed by platelets obstructs the flow of bleeding and allows tissue repairment. A similar process also happens in the pathological conditions, known as severe thrombosis, one of the most fatal diseases where the ultra-large thrombus blocks the entire blood vessel which can cause ischemia in the heart and brain. Understanding platelet adhesion and activation in physiological and pathological conditions builds the foundation to drug discovery for preventing severe thrombosis without having excessive bleeding as a side effect.

Early adhesion and aggregation of platelets involve the binding of multiple receptor-ligand pairs. Under high shear flow conditions (> 800 s^{-1}) which exists in most arties and pathological conditions, the adhesion and recruitment of platelets on endothelia is usually initiated by the binding of platelet transmembrane molecule glycoprotein (GP) Ib to surface-immobilized von Willebrand factor (VWF) A1 domain (VWF-A1). This binding, under flow condition, then activates GPIIb-IIIa (integrin $\alpha_{IIb}\beta_3$), which provokes further binding and self-activation. Both the initial binding of GPIb to VWF-A1 and the activation are dependent on the highly shear force [34]. Therefore, the shear forces are substantial for the study of the multiple receptor-ligand interactions and the crosstalk of these surface proteins.

1.4.2 Integrin activation and conformational changes

Integrins are a group of transmembrane proteins widely existing on cell surface, and one of the major adhesive receptor families among other three (cadherin, selectin and immunoglobulin-superfamily) [35]. Integrin plays an important role in cell interaction to extracellular matrix (ECM) [35, 36] and hetero-species cells [35, 37], and thus facilitate the navigation, communication and homing of cells to the environment. Each integrin is a heterodimer composed of two components: an α subunit (18 species known in mammalian cells) and a β subunit (8 species known), which in combination create a total of 24 kinds of integrins [38]. Among the several integrins expressed on platelet surface, $\alpha_{IIb}\beta_3$ is the most abundant one whose activation and binding is essential to hemostasis and thrombosis [9, 39].

Integrin $\alpha_{IIb}\beta_3$ is a receptor to a set of ligands: fibrinogen (Fg), von Willebrand factor (VWF), fibronectin (FN) and vitronectin. As a signature attribute, the binding capacity of $\alpha_{IIb}\beta_3$ highly depends on its activation state. While residing on the platelet surface with an equilibrium between inactive and active states, integrin $\alpha_{IIb}\beta_3$ on the quiescent and discoid-shape platelet are mainly inactive, with a low affinity to its ligands. Upon activation, the change of its conformation (separation of α_{IIb} and β_3 tail by inside-out signaling, and hybrid-domain swing-out by further activation signaling) permits a high affinity to ligands, which leads to platelet arrest and aggregation [9, 39]. Although the existence of different integrin conformations was largely revealed in literature, how they correspond to the different affinity states upon various activation signals remained unclear.

1.4.3 Diabetic platelets are hyperactive

Diabetic patients have an increased risk of atherothrombosis; in these patients, platelets are hyper-reactive, meaning that they are more responsive to stimulation, form aggregates more readily, and adhere more efficiently on thrombogenic surfaces [40, 41]. As a result, up to 80% of deaths from diabetes are related to atherothrombosis [42]. Diabetic platelets are also less responsive to the standard antiplatelet therapy, such as aspirin and clopidogrel, whereas more potent antithrombotic therapy would increase the risk of serious bleeding, potentially nullifying the clinical benefits of this approach [43]. The diagnostic of thrombotic risks in diabetic patients, especially at an early stage, is thus critical. Interestingly, despite the hyperactive status, diabetic platelets remain discoid which normally corresponds to a quiescent state of healthy platelets. There lacks a sensitive assay to determine the thrombosis risk of early stage of patients clinically in an easy-accessible monitoring manner.

1.5 Biological application: T cell antigen-specific activation

1.5.1 T cell immune function with antigen-specificity

T cells play a critical role in adaptive immunity to recognize foreign pathogens and exert an immune response. The recognition of antigens and activation of T cells start with the binding of the T cell receptor (TCR) to an antigenic peptide fragment bound to a major histocompatibility complex (pMHC) on an antigen presenting cell (APC) [44, 45]. T cell receptors by alternation of receptor gene segments have a broad repertoire covering more than a million of unique biological structures. T cells can recognize foreign antigens with high sensitivity, specificity and speed, while maintaining tolerance to self-antigens that are more abundant in the environment. Albeit the difference between foreign antigen and self-antigen could be only a few amino acids, recent studies have shown that cell activation can triggered by the binding to a few antigenic pMHCs or even a single pMHC while discriminating from outnumbered endogenous pMHCs. Any abnormity in recognizing foreign antigens or tolerating self-antigens leads to immune deficiency [46] or autoimmune diseases [47]. The binding to specific antigen and subsequent triggering of activation can cause responses including chemokine release, cytotoxicity and proliferation. Therefore, it holds a great interest to study the underlying mechanism of T cell activation via TCR-pMHC interaction.

1.5.2 Conditions required for T cell activation via antigen-specific TCR

Despite the profound study in T cell activation, the mechanism of the very initial triggering through antigen specific TCR is yet elusive. Various triggering models have been proposed to describe the required T cell activation conditions [44, 45, 48].

1. Receptor occupancy model is a very early model that emphases the TCR binding affinity to antigenic pMHC [49]. This model suggests that during interaction, more T cell receptor occupied owing to the high binding affinity of the antigenic pMHC. Only pMHCs that have high affinity could give rise to a high TCR occupancy that triggers the T cell activation.
2. The kinetic proofreading model gained popularity in explaining the T cell sensitivity and specificity in discriminating antigenic and endogenous pMHCs. First adapted from DNA replication models [50], this model was then developed and modified by many groups [51-54]. The main theory is that T cell events start to happen upon a binding; only when sufficient events happen before dissociation, a T cell activates. Therefore, sufficient long TCR-pMHC binding lifetime is required for T cell activation.
3. Serial triggering model extends the kinetic proofreading model, explaining how pMHC with relatively short dwell time can also cause T cell activation [55]. This model proposed by Valitutti et al. [56] posits that a single antigenic pMHC can serially trigger many TCRs.
4. Mechano-sensor model consider TCR as a mechanosensor that mediates conformational changes. The force associated with the TCR-pMHC binding was suggested to cause conformational changes in TCR chains [57]. Recent studies by Liu et al. [58] suggested that a moderate amount of force sustains

TCR binding to antigenic pMHC but reduces the lifetime to non-stimulatory ligands.

5. Kinetic segregation model focuses more on the signal propagation process [59]. It posits that TCR-pMHC interaction (complex < 15 nm) creates a small membrane gap between T cell and APC, which excludes relatively big molecules like CD45. CD45 exclusion then triggers Lck activity and TCR phosphorylation.

Though various models are hypothesized, they are not necessarily mutual exclusive. More technological approach development allows more observant evidence to help understand this complex process.

1.5.3 Integrin activation and immune synapse

T cell activation gives rise to a serial response, including an immediate intracellular protein phosphorylation, a rapid calcium flux, surface marker activation, cytokine production, and differentiation or proliferation. Among these, surface integrin activation is critical in T cell subsequent functions, and failure leads to fatal consequences such as leukocyte adhesion deficiency (LAD) disorders [60]. Lymphocyte function-associated antigen 1 (LFA-1, also named $\alpha_L\beta_2$ for its two subunits) is the predominant integrin on T cell surface, whose functions include but are not limited to T cell trafficking on endothelial cells, homing to lymph nodes, and stabilizing T cell-APC contact [61].

One of the major functions of LFA-1 is to stabilize the contact of T cell and APC at the immune synapse [62]. The immunological synapse (IS), formed during TCR antigen recognition, is a stable region of contact initiated by TCR and pMHC but held together by

LFA-1 on T cell and ICAM-1 on APC [63]. The mature IS consists two parts: a cluster of T cell receptors in the center and a surrounding ring that incorporates LFA-1 [63, 64].

LFA-1 activation on T cells can be triggered by chemokine signaling, TCR specific interaction, and selectin binding, which consists of conformation changes of the integrin from bent, resting form all the way to an extended, open form [38, 65]. The same molecule expressed on neutrophil surface has been extensively studied to have a low affinity state, an intermediate state and a fully activated state [14, 66, 67]. However, whether the LFA-1 on lymphocyte surface shares the same sets of affinity states remains unclear.

1.6 Microfluidic surface functionalization techniques

Protein micropatterning (surface functionalization), the process to place target proteins/chemicals at well-defined locations, has a tremendous value in biological studies such as cellular adhesion [68, 69], and for certain biological assays such as combinatorial screening [70], drug discovery [71] and cell sorting [72, 73]. A variety of biomolecule micropatterning techniques have been developed over the past few decades and some typical approaches are introduced in this section.

1.6.1 Microcontact printing

Microcontact printing (μCP), namely stamping, is the most common patterning technique. It was first introduced by Whitesides and his coworkers for fast replication of patterns generated by photolithography [74, 75], and it has advanced significantly since its invention. μCP uses a polydimethylsiloxane (PDMS) stamp to transfer biomolecules of

interest to a target surface. Advanced lithography techniques can be used to make PDMS stamps with complex features and therefore allow μCP to generate patterns with complex geometries. In addition, the proper choice of materials and surface treatment methods allow sub-micron size features. However, the limitations reside when dealing with the patterns involving multiple protein species. Each stamp only carries one type of protein ink so alignment of several stamps to achieve a multi-protein pattern is required. Alignment is usually undesirable for two or more stamps, much bigger than feature size which is comparable with cell sizes.

1.6.2 Microchannel patterning

Besides surface transfer, protein in solution could deposit or be absorb to a desired surface during incubation and that solution can be guided on certain location of a surface by fluid channels. Microchannel patterning (coating in capillaries) was developed for the patterning of multiple biological cues [76]. PDMS featured with multiple microchannels is used to make contact with a substrate surface. Separated channels guide biomolecular solution to the desired regions on a substrate, thereby achieving auto-alignment in terms of the relative location of these molecule patterns. However, the location of the proteins has its constraints due to the channel walls that separate the microchannels, which is relatively large compared to the size of a cell. Direct adjacency of proteins of the interest is then not achievable and big gaps exist between protein patterns, unwanted in some applications.

1.6.3 Laminar flow patterning

The distinctive property of laminar flow in microfluidics enables another micropatterning approach: laminar flow patterning [77]. A Stokes flow, namely creeping

flow, is a type of laminar flow when the inertial term is negligible compared to the viscous term. With a very low Reynolds number (inertial force/ viscous force < 1), mixing of two solutions can hardly happen in Stokes flow. Using this distinctive property, two or multiple streams of fluid can flow next to each other without lateral mixing except for diffusion or potential chemical reaction. This phenomenon was then used in micropatterning to create no-gap protein patterns. Position of the patterns is therefore more flexible, not restricted by any channel wall between two type of proteins. This is a feasible approach for the patterning proteins that require a short-term incubation on a surface. However, many biomolecules require long-term incubation periods in order to pattern, and in these cases, using laminar flow patterning can result in a middle area contaminated by two neighboring proteins that is much larger than a cell size.

1.7 Thesis outline

This thesis presents new sets of platforms for multi-receptor crosstalk study on cell surface and for specific cell sorting based on the adhesion signature resulting from crosstalk. Microfluidics in this study enables the manipulation of small volume of liquids and small particles like blood cells, the creation of the microstructures for the desirable feature shapes and locations, the module-compatibility for different cell functions to take place. We attained the phenomena of multi-receptor crosstalk in several acclaimed species of blood cells, assessed the activation behavior and requirement in a fine-tuned well-defined manner, achieved cell of interest distinguishing.

CHAPTER 2 (Microfluidic auto-alignment of protein patterns for sequential ligand presentation) presents a new approach that permits cell surface receptor crosstalk by an auto-alignment of multi-protein patterning for sequential ligand presentation to cells. With well controlled spatial registration and protein density, this system can provide tunable mechano-stimulation dose to study cell multi-receptor adhesion and signaling cascades. Validation of the device by assessing platelet adhesion and activation revealed the threshold, saturation and reversibility of the platelet activation by immobilized ligands in drop of blood, which is not achievable by gold standard approaches. Further development of a parallel device based on the initial version enables better variation control and throughput.

CHAPTER 3 (Cell activation and receptor crosstalk on multi-zone device) presents the wide application of the multi-zone device (in CHAPTER 2) in the discovery of the activation states and the differentiation of subtle pathological conditions. In this chapter, we characterized the activation parameters, behaviors and molecular changes of platelets and neutrophils upon stimulation to reveal an intermediate state of the integrins on both cells upon activation. We successfully assessed one-drop of whole blood sample and detected the subtle differences in diabetic platelets with an amplification upon activation, which is hard to notice in other ways with such limited sample.

CHAPTER 4 (TCR-pMHC interaction under flow induces intermediate-affinity of LFA-1 to support rolling adhesion) presents the discovery of the T cell activation condition under shear flow condition and an intermediate state of integrin using the platform developed in CHAPTER 2. In this chapter, we demonstrated that T cells can be activation by rapid rebinding of TCR-pMHC interaction under flow, and that leads to

an integrin activation state supporting T cell rolling on ICAM surface. Mechanical stimulation dose of immobilized pMHC was fine controlled for the study of dose-dependent, pMHC-dependent rolling behavior. Calcium flux of T cells upon activation was also investigated.

CHAPTER 5 (Engineer microfluidic platform to sort antigen-specific T cells based on rolling behavior resulting from TCR-integrin crosstalk) employed the discovery of integrin LFA-1 lateral movement from CHAPTER 3 and the rolling property of T cells in various activation conditions from CHAPTER 4 to sort antigen-specific T cells. In this chapter, we developed a cell sorting platform that enables target T cells upon activation to move laterally by cell adhesion so to distinguish from non-interactive cells. This platform was validated by mouse primary OT1 T cell sorting from non-target cells and also implied the capability of spectrum sorting of multiple interactive cell types with various activation states.

CHAPTER 2. MICROFLUIDIC AUTO-ALIGNMENT OF PROTEIN PATTERNS FOR SEQUENTIAL LIGAND PRESENTATION

Part of the work presented in this chapter has been published in Lab on a Chip[1].

Cell adhesion plays a critical role in many cellular functions such as the hemostatic/thrombotic process, inflammatory reaction, and adaptive immune response. Many cell adhesion processes involve cross-talks between multiple ligand–receptor systems through intracellular signaling. To elucidate such crosstalk requires analysis of the synergistic or antagonistic effects of binding and signaling of multi-receptor species. Current techniques for such analysis are either labor-intensive, low-throughput, or limited in the types of ligands they can interrogate. To circumvent these limitations requires a technique for manipulating the ligand interaction with and measuring the functional response of a population of cells. We have developed a microfluidic platform for studying binding and signaling of multi-receptor species by separating their actions in space and time. The platform directs cells through a single channel and uses sequentially presented ligands for pre-processing and stimulating cells, followed by reporting of cell activation states and functional consequences. Our method sequentially patterns proteins on different spatial regions without gaps. We demonstrated the ultility of our method by using this platform to analyze the crosstalk between platelet receptors, glycoprotein Ib and IIb-IIIa, in the context of platelet adhesion and signaling under flow

[1] Zhou, F., et al. (2018). "Microfluidic auto-alignment of protein patterns for dissecting multi-receptor crosstalk in platelets." Lab Chip, 2018,18, 2966-2974

2.1 Introduction

Specific interactions of a cell with another cell or with the extracellular matrix via direct physical contact usually involves multiple receptor–ligand interactions [7]. In some cases, these interactions are concurrent and independent, whereas in other cases, the interactions are sequential and cooperative. An example of the former case is binding of two neutrophil receptors (FcγRIIA and FcγRIIIB) to a common ligand mix (total IgG), which can be treated as concurrent and independent when the bond numbers are low enough for competition to be neglected [78]. Concurrent and independent interactions result in a total bond number that is equal to the sum of two bond species [78]. As an example of sequential and cooperative binding, moving platelets use glycoprotein (GP) Ib to transiently bind surface-immobilized von Willebrand factor (VWF) A1 domain (VWF-A1), which activates GPIIb-IIIa (integrin αIIbβ3) via mechano-signaling. The sequential process enables efficient platelet adhesion during hemostatic and thrombotic processes [9], and also induces P-selectin expression [11] (Figure 2-1 a). In some other systems, the binding of a receptor can also trigger suppression of the function of another receptor [79]. In many biological contexts, the exact nature of these interactions is largely unknown.

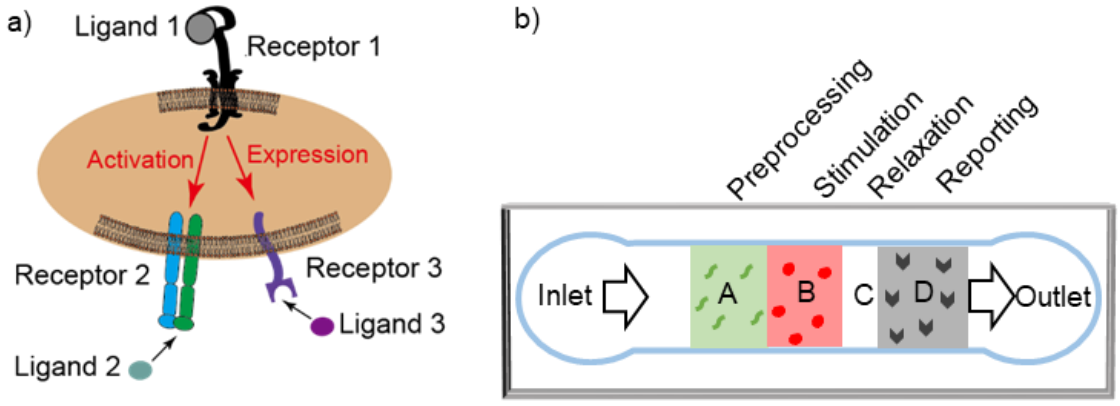

Figure 2-1 Microfluidic multi-zone channel for analysis of receptor crosstalk. a) The cell interacts with its environment via multiple receptor species that may generate synergistic or antagonist effects. Ligand binding of receptor 1 may

induce activation of receptor 2 and expression of receptor 3 to bind their respective ligands. b) Schematic of the multi-zone channel. Cell suspension will flow in from the inlet, across four zones, and out from the outlet. The cells are interrogated as they are allowed or prevented to sequentially interact via different receptors with different proteins patterned on different zones labelled as A: pre-processing, B: stimulation, C: relaxation, and D: reporting.

To analyze these synergistic or antagonistic effects among multi-species receptor–ligand interactions requires temporal and spatial control of when and where each receptor species can interact with their respective ligand or reporting antibody, in what sequence, and for how long. A recent study employed a newly developed dual biomembrane force probe to achieve this goal [80]. The study analyzed the crosstalk of GPIb with αIIbβ3 (and P-selectin) by allowing the two receptors to sequentially encounter their respective ligand (or antibody) in space and time, so as to monitor the activity change of αIIbβ3 (and surface expression of P-selectin) as a consequence of GPIb signaling. While extremely well-controlled and sensitive, this method is limited in that it requires manually moving a single cell to contact two ligand-bearing surfaces [80] and do so alternatingly; these actions are technically challenging, and of low temporal resolution and low throughput. In addition, this technique cannot recapitulate the flow condition physiological for certain cell types. We hypothesize that these limitations can be overcome with the use of well-engineered microfluidic devices that use flow to deliver cells into contact with a series of protein patterns with spatiotemporal control.

In the literature, a variety of protein micropatterning techniques have been developed, which include microcontact printing [74, 75], microchannel [76], and laminar flow coating [77]. Microcontact printing is the most common patterning technique. It uses the relief patterns on a stamp surface to print protein patterns on the substrate. While this technique can generate patterns of complex geometry, alignment of two or more stamps is technically difficult and thus lacks accuracy and uniformity [81]. Microchannels have also been used to generate protein patterns. Separate channels guide different protein solutions

to their desired regions on a substrate, thereby achieving automatic alignment. However, walls separating the microchannels are relatively large compared to the cell size, resulting in undesirable large gaps between patterns. Another patterning technique, laminar flow patterning [77], utilizes the non-mixing property of Stokes flow to create patterns. It allows two or more layers of fluid to flow next to each other without lateral mixing except for diffusion or potential reaction. Yet, diffusion could occur and is hard to control, potentially resulting in protein contamination regions much larger than the cells [82].

To study crosstalk between two cell-surface receptor species, an ideal microfluidic device system should automatically present the stimuli followed by an immediate readout of the cell status (Figure 2-1 b). Specifically, upon entering the device, the cells would first be stimulated by a protein patch with a precise dosage (concentration and time) to trigger the desired level of activation, and then be interrogated by a protein patch to report any changes in the expression, conformation, or activity of the other receptor species. Other important features include pre-screening of the cells to ensure they are not already activated upon entering the device, and a non-reactive surface between the stimulating and analyzing patches to allow transient relaxation of stimulated cells to test signal reversal in the cells. To meet these specifications requires a patterning technique for making protein patches with high-precision registration, desired pattern positions, and minimum protein contamination, which are beyond the capabilities of existing technologies.

In this chapter, we report a patterning method that combines microcontact printing and microchannel coating to achieve gapless auto-aligned patterning of multiple protein patches (Figure 2-1 b). This new approach of micro-patterning allows the placement of target ligands at well-defined locations, which can be useful for studies of cell adhesion mediated by a range of receptor–ligand species [83, 84] and for certain biological assays such as combinatorial screening [83] and cell sorting [84]. As a demonstration, we applied this method to interrogate the activation of platelets by GPIb—ligand binding, using αIIbβ3

activation and expression of P-selectin as readouts. Our results demonstrate the validity of this technical platform and show that the platform parameters can be designed to control the level of activation and its reversal. Finally, we show a potential utility of this platform in preclinical diagnostics by using it to assess platelet hyperreactivity in diabetic patients with a drop of whole blood.

2.2 Materials and methods

2.2.1 Proteins and chemicals

Monoclonal antibodies (mAbs) LIBS2 (ab62, Millipore, Billerica, MA), HIP8 (Thermo Fisher Scientific, Waltham, MA) and AK4 (Thermo Fisher Scientific) were used to coat protein patches. LIBS2 binds the β tail domain of integrin $\alpha_{IIb}\beta_3$, the epitope of which is exposed only when the integrin takes an extended conformation [85]. By comparison, HIP8 binds $\alpha_{IIb}\beta_3$ in a conformation-independent manner [86]. AK4 specifically recognizes P-selectin [87]. PE-labelled anti-A1 mAb 6G1 and FITC-labelled anti-fibronectin mAb ab2413 were from Abcam (Cambridge, UK) and used to visualize ligand coating.

GPIb ligand VWF-A1 was a gift from Zaverio Ruggeri from the Scripps Research Institute (La Jolla, CA). Integrin $\alpha_{IIb}\beta_3$ ligand fibronectin fragment (the 9-10 domains of fibronectin III) was a gift from Andres J. Garcia from the Georgia Institute of Technology (Atlanta, GA). Biotin-PEG3500-NHS were from JenKem (Plano, TX). ADP, thrombin, dimethyl sulfoxide (DMSO), apyrase, clexane, bovine serum albumin (BSA) and other chemicals were from Sigma-Aldrich (St. Louis, MO) unless stated otherwise.

2.2.2 Blood samples and platelet purification

Blood samples were drawn from volunteers who signed informed consent according to protocols approved by the Institute Review Boards of the Georgia Institute of Technology and Emory University. Blood was drawn by venepuncture from healthy subjects (20–30 years of age) or patients with type 1 diabetes (8–18 years of age) by trained nurses according to procedures approved by the Institutional Review Boards of the Georgia Institute of Technology and Emory University, respectively. Blood was drawn using a 19G butterfly needle into acid citrate dextrose containing theophylline (ACD: 85 mM sodium citrate ($2H_2O$), 72.9 mM citric acid (anhydrous), 110 mM G-glucose, 70 mM theophylline, diluted 7× with dH_2O), mixed well, and transferred to a 10 ml tube with 0.005 U ml^{-1} apyrase. Whole blood was used directly. To prepare washed platelets, blood was placed at 37 °C for 15 min and then centrifuged for 10 min at 200g. Platelet rich plasma was transferred from the supernatant to fresh tubes and centrifuged again at 1700g for 5 min. The supernatant was discarded, and the platelet pellet was re-suspended in a platelet washing buffer (PWB: 43 mM K_2HPO_4, 43 mM Na_2HPO_4, 243 mM NaH_2PO_4, 1.13 M NaCl, 55 mM D-glucose, 100 mM theophylline, diluted 10× with dH_2O, pH 6.5, conductivity 13–15) plus clexane (20 U ml^{-1}) and apyrase (0.01 U ml^{-1}). The platelet suspension was then centrifuged at 1500g for another 5 min. After discarding the supernatant, the platelet pellet was re-suspended at $<1 \times 109$ ml^{-1} in Tyrode's buffer (120 mM $NaHCO_3$, 100 mM HEPES, 1.37 M NaCl, 27 mM KCl, 55 mM D-glucose, diluted 10× with dH_2O, pH 7.3, conductivity 13–15) containing BSA (5 mg ml^{-1}) and apyrase (0.02 U ml^{-1}). The platelet suspension was placed in a 37 °C water bath for 30 min. The suspension was diluted to 1×108 platelets per ml for use in experiments.

2.2.3 Device design requirements and fabrication

Standard soft lithography was used to fabricate devices in polydimethylsiloxane (PDMS, Corning Sylgard 184, Midland, MI). Two matched silicon wafers were fabricated (SU8-2025, MicroChem). The first is a one-layer mold with a 25 μm-thick single layer for microchannel PDMS. The second is a two-layer mold, 25-μm thick each for stamping PDMS. The features on the transparency mask were transferred with UV photolithography. The surface of wafers was treated with tridecafluoro 1,1,2,2-tetrahydrooctyle-1-trichlorosilane vapor from United Chemical Technologies (Lewistown, PA) to facilitate release of PDMS from the mold. A mixture of PDMS (PDMS base and crosslinker in a 10:1 ratio) was poured on the mold and the whole preparation was left for curing for 2 h at 95 °C. After peeling off the PDMS, the devices were cut into shape and access holes were punched using 19 gauge needles (McMaster-Carr).

Plastic clamp holders were laser-cut with holes matching the inlets and outlets. Plastic holders and screws were applied to hold the PDMS device and glass substrate together. After assembly, the device was primed in vacuum to remove bubbles. The chip was connected to syringe pumps to deliver flow for protein coating.

2.2.4 Protein pattern design and preparation

Resting platelets in dynamic flow are able to bind immobilized VWF-A1 but not FN, which only binds activated platelets. In our basic design (Figure 2-1 b), therefore, after passing BSA blocked area, flowing platelets would first encounter a FN patch (preprocessing, zone A) to confirm the resting state of the platelets prior to stimulation (negative control). The resting platelets would travel downstream to encounter a VWF-A1 patch (stimulation, zone B) for controlled stimulation. Stimulated platelets would then travel further downstream to a relaxation zone C before encountering another FN patch (reporting, zone D) for reporting of platelet activation as assessed by ligand binding by

integrin αIIbβ3. To achieve this design, BSA was stamped onto zone C by microcontact printing. FN was delivered via a microchannel to zones A and D with a concentration of 0.016 or 0.16 μg/ml, and incubated for 1 h. VWF-A1 was then delivered via another microchannel to zone B with a concentration of 100 μg/ml and incubated for 1 h.

We also used two variations of the above basic design after it was fully validated. In the first variation, a conformation reporter mAb for integrin αIIbβ3 (LIBS2) or a conformation-independent mAb (HIP8) was coated in zones A and D instead of FN. In the second variation, a mAb against P-selectin (AK4) was coated in zones A and D to detect the upregulated expression of P-selectin.

We fixed the length of zones A and D to be 800 μm, long enough for analysis of platelet binding. We varied the length of zone B to program different stimulation time doses of stimulation in the device. We also varied the length of zone C to assess the sustainability and reversal of activation (Figure 2-1 b).

2.2.5 Quantification of cell binding and protein coating

The experiment was monitored using an inverted microscope (Leica EMIRBE) with a CMOS camera (Hamamatsu Orca) at 40X magnification. Phase-contrast mode was chosen for both video recording and image acquisition. Mean velocities of 15-20 rolling cells were measured for each condition with 9 fps video recording with frame by frame analysis via ImageJ software (ImageJ V1.48 National Institutes of Health) off-line. The experiment was repeated 3 times. The end-point assay was applied by counting the adherent cell number per mm^2 over an area of 36200 μm^2 after 2 min of continuous flow for 2 random fields of view. Each condition was repeated in 3 devices for each sample. Statistical comparisons were performed using the unpaired Student t-test.

Epifluorescence mode of an EMCCD camera (Hamamatsu Orca) was used to visualize the coating of FN and VWF-A1 using FITC-labelled ab2413 and PE-labelled 6G1 at saturating concentration (100 μg/ml each), respectively.

2.3 Multi-zone microfluidic device

2.3.1 Design

Our device design requirements are based on the initial application, which is to characterize receptor–ligand mediated platelet activation. The multiple surface zones should test the activation state of the platelets prior to controlled stimulation, stimulate the platelets and report the activation state afterwards. Several proteins are to be displayed with controllable density and good spatial registration to each other. The spatial resolution of the patterning should be on the order of the size of a platelet (which is 3-μm in diameter). This accuracy is required considering the fast signalling kinetics (seconds) and translocation velocity (a few μm/s) of platelets interacting with immobilized ligands. Furthermore, since platelet stimulation by GPIb–VWF-A1 mechanoreception alone is transient [8], testing platelet activation immediate after stimulation is preferable. Hence, gaps between zones should be kept as small as possible.

To achieve auto-alignment for surface patterning in the microchannels, we take advantage of the two existing techniques - microcontact printing and laminar flow patterning (Figure 2-2). The key of the process is to protect regions using physical masking or stamping of a non-ligand protein (e.g. BSA), and sequentially pattern different proteins using a combination of stamping and flow.

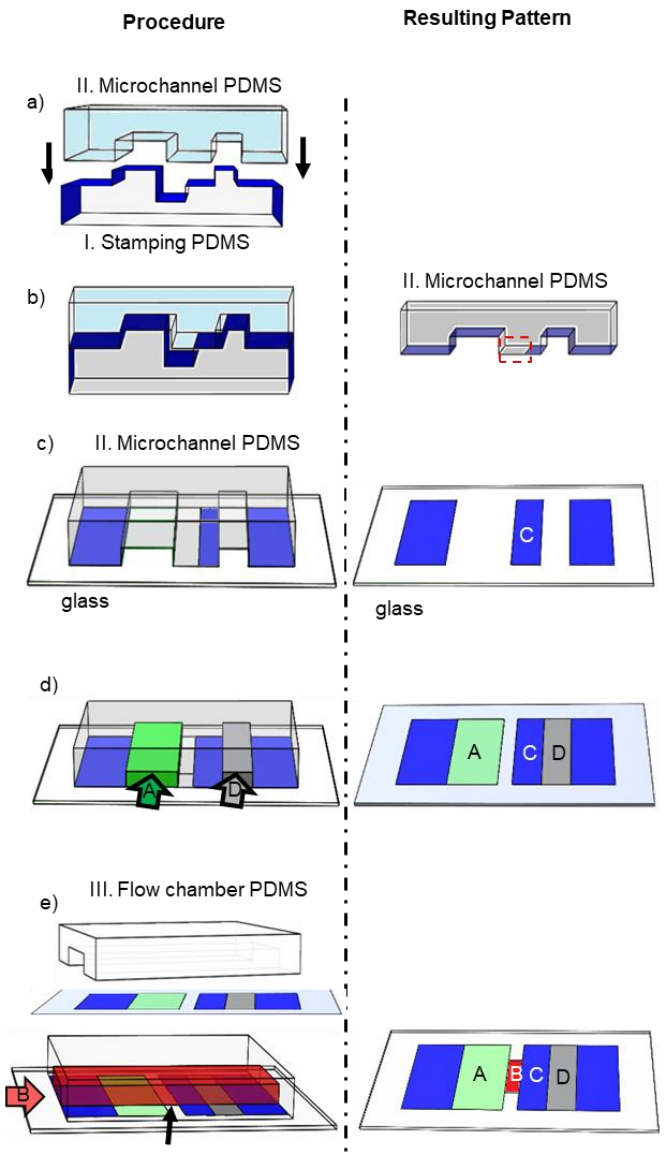

Figure 2-2 Process of patterning four proteins on four zones without gaps. The procedures are shown on the left. The resulting patterns are shown on the right. a) Two pieces of PDMS with nearly matched shapes to allow the stamping PDMS (I, bottom, light grey) pre-coated with BSA (blue) to print BSA on the microchannel PDMS (II, top, light blue). b) Upon contact, BSA was transferred from the upper surface of the stamping PDMS to the bottom surface of the microchannel PDMS except for the area boxed by the dashed red box. c) The microchannel PDMS stamps on and transfers the BSA onto a substrate glass, forming a protein patch on the relaxation zone C and also blocking the areas from the inlet to zone A and from zone D to the outlet. d) Two protein solutions flow through two microchannels (arrows) to coat zones A and D. e) A flow chamber is assembled by placing another piece of PDMS (III, white) on top of the substrate glass with flow direction perpendicular to the protein stripes. Another protein solution flows in to coat zone B.

The process is as follows. First, a stamping PDMS piece is pre-coated with BSA (I); it is put into contact with a piece of PDMS bearing microchannels with matched geometries (II) (Figure 2-2 a). This allows BSA to be transferred from the stamping PDMS to the microchannel PDMS piece wherever they are in contact. There is a region, however, where the height of the stamping PDMS is smaller than the depth of the channel PDMS piece. This area in the channel between the ridges is left blank (Figure 2-2 b, dashed red rectangle). The microchannel PDMS is then brought into contact with a glass substrate for two simultaneous actions: (1) to transfer BSA to the non-targeted areas and relaxation zone C, and (2) to create two microchannels for protein coating of glass via physical absorption of proteins from solutions that are pumped through (Figure 2-2 c). This step creates protein patterns in zones A and D on the glass surface, while leaving the middle area blank because of the protective ridges (Figure 2-2 d). BSA is then delivered through the channels to further block any uncoated areas on zones A and D so that later procedures do not contaminate them. A third piece of PDMS (III) containing the channel for cell delivery is then sealed to the surface (Figure 2-2 e). Flowing another protein solution through this channel allows zone B to be coated with no impact to the other zones because they are protected by the previously coated target proteins or BSA. As a result of this process, four protein patches can be patterned on the glass surface with all other areas blocked by BSA. Because the patterns are registered by the PDMS geometries, this approach is advantageous in that the protein patches are guaranteed to align automatically.

2.3.2 Characterization of the protein pattern

we assessed the registration of this approach by patterning the glass surface with two proteins, fibronectin (FN) and VWF-A1, and visualizing the protein patterns using their respective antibodies conjugated with two different fluorophores (FITC for FN, and PE for VWF-A1). Epifluorescent images of the patterned surface show uniform antibody staining with sharp edges in individual channels, and no overlaps when images from the two channels were registered to each other (Figure 2-3 a). To assess the accuracy of the registration, we quantified these images by taking fluorescence intensity line-plots perpendicular to the patterned stripes (Figure 2-3 b). The protein patterns have sharp and well-defined edges and relatively uniform distribution throughout the stripe. These data collectively validate the method for its ability to pattern multiple proteins with precise spatial registration and negligible cross contaminations.

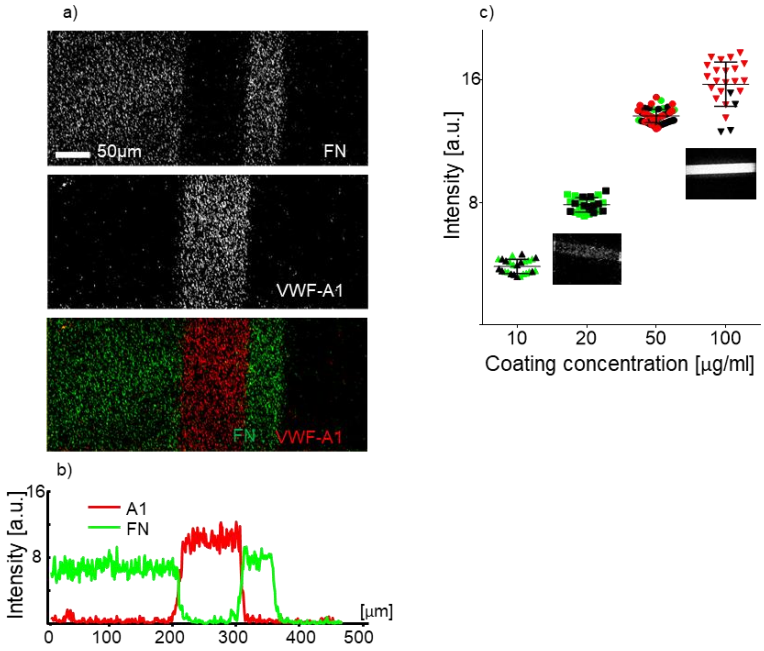

Figure 2-3 Assessment of protein coating quality. a) A three-zone device without zone C was coated with fibronectin (FN) in zones A and D and VWF-A1 in zone B. The two proteins were detected by their respective mAbs tagged by two different fluorophores and viewed by epi-fluorescence microscopy via the FITC

(green) channel for FN (top), PE (red) channel for A1 (middle) or both channels (bottom). Scale bar is applicable to all images. b) Intensity distributions of the two fluorescent antibodies along a line in the flow direction. c) Density and uniformity assessment of VWF-A1 coating. Three independent replicate tests were performed (indicated by different colors) using different devices coated with indicated concentration of VWF-A1. Each dot indicates intensity over one 20X20 μm^2 square. Two representative images were shown for VWF-A1 coating with concentration of 20 and 100 μg/ml, respectively.

To determine the consistency and robustness of the method, we measured the fluorescence intensity of the anti-VWF-A1 mAb in three independent trials using three sets of devices (Figure 2-3 c). Coating concentration of A1 was varied from 10 to 100 μg/ml for each set on different days. Fluorescence intensity increases with increased concentration. Under the same coating concentration and microscope setting, intensities for different devices were comparable on different days, suggesting that these procedures are quantitatively replicable. Together, these data suggest that our coating strategy can yield controlled and consistent surface density of the coated proteins.

2.3.3 Validation by platelet activation on multizone device

2.3.3.1 Examine platelet rolling velocity on multiprotein patches

We next tested the ability of our device to separate the two pairs of receptor-ligand cooperative binding (GPIb and integrin αIIbβ3) in space and time by measuring the velocity of platelet rolling on the respective ligands. In a device coated with FN only in zone D, washed platelets flowed passed the surface showing no sign of interaction regardless of shear rate, a condition serving as negative control [88] (Figure 2-4, annotated

as ‘do not roll’). Rolling platelets were observed over the stimulation zone, confirming the transient interaction of platelet GPIb with the surface VWF-A1 The rolling velocity first decreased with increasing wall shear stress of the flowing fluid, reached a minimum at 4 dynes/cm^2, and then increased with further increase in wall shear stress (Figure 2-4, squares), which is consistent with the previously reported catch-slip bond characteristic of GPIb–VWF-A1 binding [89]. We have also summarized the fraction of rolling cells under these conditions (Table 2-1).

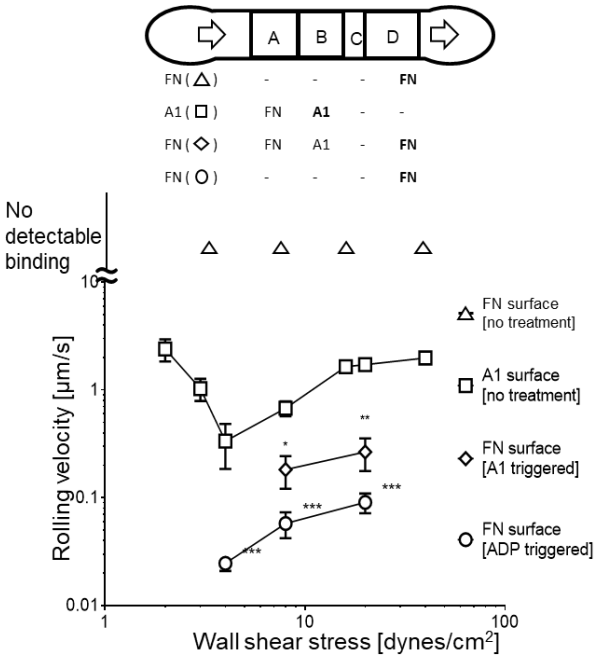

Figure 2-4 Platelet activation by VWF-A1 and ADP demonstrated by decreased rolling velocity on FN. Velocity of platelets rolling on surfaces patterned with indicated proteins is plotted vs. wall shear stress. Quiescent platelets (no treatment) did not interact with FN surface (0.016 µg/ml, coating concentration) in zone A (data not plotted), but rolled on VWF-A1 surface (100 µg/ml, coating concentration) in zone B (square) and FN surface (0.016 µg/ml, coating concentration) in zone D (diamond). (This device has no zone C.) Rolling velocity on FN surface after VWF-A1 stimulation was significantly lower than on VWF-A1 surface. As a control, platelets pre-treated with 50 µM ADP for 15 min rolled on zone A with significantly lower velocity (circle). Data are presented as mean ± sem of 15-20 cells. Experiment was repeated 3 times with consistent results and

the representative data are shown. *, ** and * denote p < 0.05, 0.01 and 0.001 by Student t-test.**

Table 2-1. Fraction of rolling cells of total interacting cells in the field of view for Figure 2-4

Shear Stress [dynes/cm^2]	2	4	8	20	40
FN	no detectable binding				
A1	75.8%	85.4%	90.2%	84.3%	89.4%
FN (A1 triggered)			77.3%	84.2%	
FN (ADP triggered)		84.1%	78.1%	83.0%	

It is known that GPIb interaction with VWF-A1 stimulates platelets, and promotes interactions with the downstream reporting zone surface coated with FN [90]. High density coating of FN (0.16 µg/ml coating concentration) firmly arrested the stimulated platelets, whereas low FN density (0.016 µg/ml coating concentration) supported their slow rolling (Figure 2-4, diamond), both of which indicated the activation of platelet surface $\alpha_{IIb}\beta_3$ with an increased ligand binding affinity after VWF-A1 stimulus. As a positive control, washed platelets were incubated with a soluble agonist ADP (50 µM, 15 min) and perfused through a device with only low density of FN coating [90]. Rolling velocity of ADP-treated platelets without VWF-A1 stimulation was significantly lower than platelets stimulated with VWF-A1 (Figure 2-4, circle). These data confirm that platelet activation can be achieved by interacting with a surface coated with A1, and this activation is weaker than the chemical agonist stimulation. This set of experiments also demonstrates that our device

allows triggering of cell activation and follow-up characterization of stimulated cells with control of the sequential timing of ligand presentation.

2.3.3.2 Platelet adhesion on ligand FN

It is reasonable to assume that the signaling amount of a cell can depend on the amount of stimulation it receives. While the stimulator dosage of a soluble agonist can easily be controlled, controlling the dosage of VWF-A1 stimulation is challenging. Indeed, how platelet activation via VWF-A1 binding is stimulation time-dependent was poorly characterized in the literature. Thus, we next characterized the stimulation time-dependency of integrin $\alpha_{IIb}\beta_3$ activation upon the stimulation on GPIb, which is realized via pre-programing the stimulation time in the device hardware. In our assay system, the stimulation time for platelets depends on both flow rate and the length of zone B. However, changing the flow rate would also change the wall shear stress, which would affect GPIb bond lifetimes with VWF-A1 and also platelet mechanosensing [89, 91]. Therefore, we made a set of devices with variable zone B lengths (50-800 μm). For a given flow rate and device dimensions, the longer the zone B, the longer the potential time for platelets to be stimulated by sequential and intermittent binding of VWF-A1. Washed platelets were perfused through devices with zone B of variable lengths, zone C of zero length, and zone D coated with high coating concentration of FN (0.16 μg/m) to arrest VWF-A1 stimulated platelets.

The effect of varying the stimulation time was assessed by measuring the number of adherent platelets per unit area in zone D (Figure 2-5). Increasing stimulation time when

zone D is relatively short (zone B length from 50 to 200 μm) resulted in a drastic initial increment in the number of adherent cells. The activation approached saturation when zone B length reached 400 μm, because further increasing the length to 800 μm did not yield more platelet adhesion. These experimental results are robust and reproducible in independent experiments on different days. This also the first demonstration of platelet activation by VWF-A1 being stimulation time dependent.

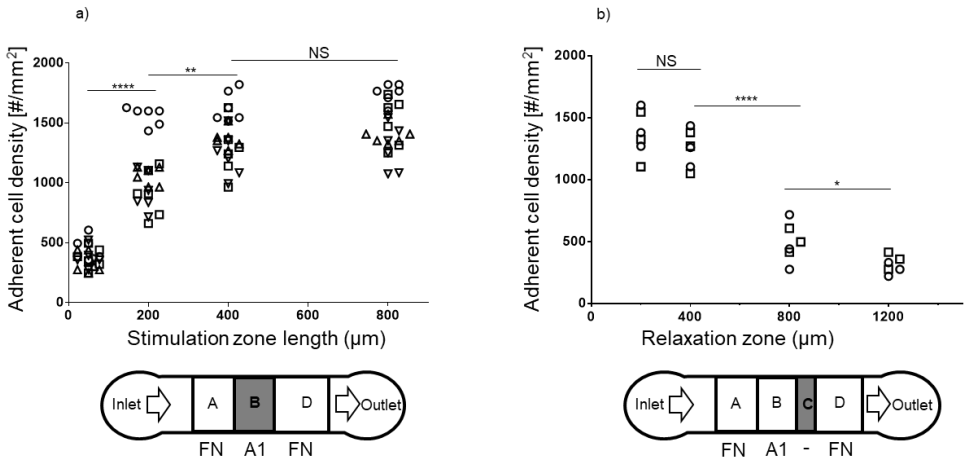

Figure 2-5 Characterization of platelet activation and relaxation. Protein patterns were made to test the effects on platelet binding to reporting zone coated with 0.16 μg/ml FN of variable length of a) stimulation zone coated with 100 μg/ml A1 and b) BSA-blocked relaxation zone. The protein patterns used in panels a have no zone C. Experiments were done by perfusing 1 × 108 platelets/ml for 2 min. Each point represents measurement from one flow chamber. Different symbols indicate data obtained from different donors. Every donor donated blood twice for repeated experiments. *, **, * and **** denote, $p < 0.05, 0.01, 0.001$ and 0.0001, respectively, by Student t-test.**

The intracellular Ca^{2+} flux triggered by GPIb is highly transient, which can fade away within seconds [9]. It is therefore reasonable to question the temporal stability of the integrin $\alpha_{IIb}\beta_3$ activation triggered by GPIb, which is downstream of Ca^{2+} flux. With the

same device, one is also able to investigate this temporal stability by pre-programming variable relaxation times with different zone C lengths in the device hardware. With blocking protein BSA on zone C, platelets are prevented from receiving any additional stimulation during the relaxation time, which varies from short (~5 s for 200 μm zone C) to long (~30 s for 1200 μm zone C), before entering the reporting zone. Again, zone D was coated with FN (0.16 μg/ml) and the effect of varying relaxation time was assessed by measuring the number of adherent platelet per unit area in zone D (Figure 2-5 b). Little decrease in adherent cell density was observed when relaxation time was short (length <400 μm). However, a steep decrease occurred when zone D length increases from 400 to 800 μm. The effect saturates beyond 800 μm. These experiments showed that platelet activation by VWF-A1 stimulation was transient (in the time scale of minute) and reversible when platelets received no further stimulation.

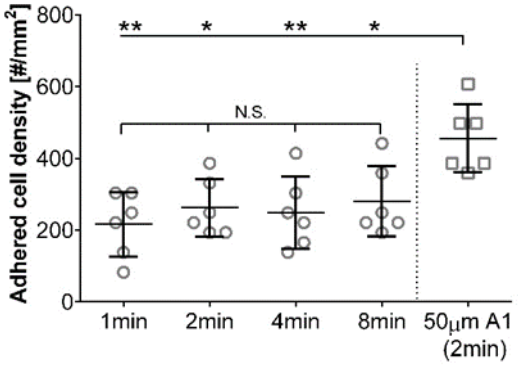

Figure 2-6 Characterization of the effect of accumulated platelets. FN was coated on device with or without VWF-A1 ahead. Platelets adhered on surface after various time span were recorded without VWF-A1, and 2min with A1 stimulation was also plotted as a reference. No significant increase in platelet adhesion was observed, but all significantly lower than the A1-stimulated condition. Each point in a and b represents measurement from one flow

chamber. *, **, * and **** denote, p < 0.05, 0.01, 0.001 and 0.0001, respectively, by Student t-test.**

We also performed another control to eliminate the alternative effect of VWF-A1 that brings platelets to the surface so accumulated more platelets adhered to the FN zone rather than stimulate the cells. In this control experiment, platelets were perfused over FN in various time spans without pre-actication by A1. No signifcant increase in platelet adhesion with longer perfusion time (more platelets) was observed, and all adhesion levels were significantly lower than that with pre-activation by VWF-A1. So even if VWF-A1 may help collect relatively more adhesive platelets, the effect is neglectable.

2.4 Parallel multi-zone device

A titration-like characterization of stimulation amount on platelets demonstrated that the cell activation by immobilized ligands was also stimulation dose-dependent in this chapter. When exploring the activation and/or relaxation conditions for cells, a range of stimulation doses is required. A thorough characterization of the cell activation also requires a variety of antibodies and ligand in the reporting region. Only one stimulation dose on a device is relatively labour intensive for researchers, especially in the exploration stage. A platform with various conditions parallel is beneficial for throughput purpose and condition control. With such a platform, researchers will be able to perform experiments for various conditions in a single run, at the same time, reducing variations resulting from device-to-device and time-to-time.

In this part, we described a more advanced version of multi-zone device – parallel multi-zone device. Not only this enables the researchers to scale up the device for various

stimulation and/or relaxation conditions, but also lessening the variation effect from the device and cell variability due to experimental time.

2.4.1 Design

To achieve this parallel multi-zone device, we modified the stamping PDMS and its matched microchannel PDMS (Figure 2-2 b, Figure 2-7 a) to be asymmetric. Instead of straight coating channel, they have changing dimensions along the protein coating channel, perpendicular to the experimental flow chamber (Figure 2-7). For instance, we designed a device with four dimensions for both the stimulation region and relaxation region.

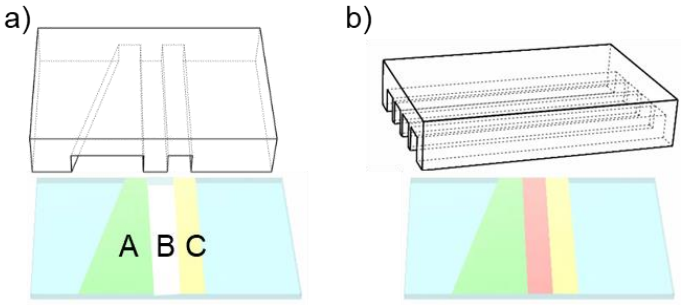

Figure 2-7 Illustration of the principle of the parallel multi-zone device. The channel PDMS are shown on the top. The resulting patterns are shown on the bottom. a) The microchannel PDMS was previous contacted by its matching PDMS carrying blocking protein BSA as in Figure 2-2 a and b. Upon contact with glass, the rest was blocked by BSA except for the middle wall. That resulted a blank area (white) in the glass surface. Area A (green) and C (yellow) were coated by two protein solutions flowing through two microchannels. b) A device with several flow chambers was then assembled by placing another piece of PDMS on top of the substrate glass with flow direction perpendicular to the protein stripes. Protein solution B then be coated (red). Asymmetricity can be applied to any of the three area. Region A was used as an example in this illustration.

The multi-zone device shares the same assembling process as the single multi-zone device described in Figure 2-2. The key change of this device is to have an asymmetric channel and/or channel wall (Figure 2-7 a). Thereupon, protein patterns have various sizes across the substrate glass. When one applies the final PDMS device with a set of channels, each channel contains different lengths of zones. Any individual zone or several zones can be modified to be the varying zone(s). Here one zone, A, was illustrated as an example.

The microchannel PDMS was pretreated as figure 2 a and b. It is then brought into contact with a glass substrate for two simultaneous actions: (1) transfer BSA to non-targeted areas, and (2) to create two microchannels for protein coating of glass via physical absorption of proteins from solution delivered through. This step created the protein patterns A and C. Note that patch A has a changing size across the substrate glass. BSA is then delivered through these channels to further block any uncoated areas on zones A and C so that later procedures do not contaminate them. Another piece of PDMS is then sealed to the surface with the channels perpendicular to the protein zones (Figure 2-7 b). Flowing through the protein solution in channels allows zone B to be coated with no impact on the other zones since they are protected previously. Thus, individual channels have a different size of zone A. These individual channels share the common inlet in practice, hence a single experiment can generate a set of various conditions.

2.4.2 Characterization of protein pattern

To realize the various zone size for individual channels but keep the size constant within a flow channel, we designed the patterning size with step increase instead of a continuous size change. However, these steps would easily cause an uneven coating on the

step edges due to bubble formation. To prevent the uneven coating affect the quality of the protein patches within individual flow channels, we designed the space of the flow channel twice of the size of a step edge fillet.

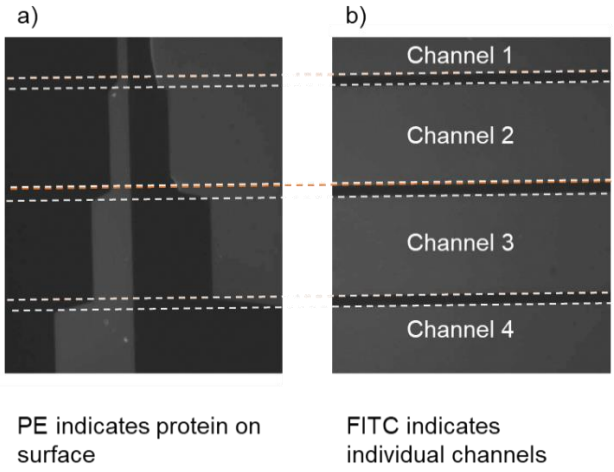

Figure 2-8 Assessment of the protein coating in individual flow channel. a) A three-zone device with only A and C coated with proteins, VWF-A1 and FN respectively. These two proteins were detected by their respective mAbs tagged by fluorophore PE and imaged by epifluorescence microscopy via N3 channel. b) The solution with fluorophore FITC was pumped in flow channels to visualize individual channels, by fluorescence microscopy via GFP channel. Dashed line indicated the edge of the flow channels. Slight uneven coating caused by the step of the protein patches was located between each channels.

We then assessed the registration of protein patches with flow channels by patterning with two proteins, VWF-A1 and FN, and visualizing the protein patches and flow channels with fluorophores (PE for protein patches and FITC for flow channels). Epifluorescent images of the patterned surfaces show the uniform and staining with sharp edges (Figure 2-8 a). There were slight uneven coating areas at the increased step edges. But they were all located between individual flow channels, indicated by the dashed lines

that derived from the fluorescent image of the individual flow channels (Figure 2-8 b). Flow channels were imaged by the same epifluorescent microscopy but in the GFP channel as a solution containing FITC fluorophore was pumped in. Hence, within the individual flow channels, protein patches are uniform and have clear edges; while across them, there are zones with various sizes to explore sizes effect to cell receptor crosstalk.

2.5 Conclusion

We developed an approach for fabricating microfluidic devices that achieves gapless protein patterning with auto-alignment for multiple protein zones. Using this approach, our microfluidic devices achieved sequentially laid-out protein patterns with well-controlled spatial registration and protein density. This system is useful for studying multi-receptor adhesion and signalling cascades such as those seen in hemostatic/thrombotic process, inflammatory reactions, and adaptive immune response. In this work, as a demonstration, we applied devices made using this approach to study platelet activation by GPIb mechanoreception through VWF-A1 binding. We characterized that such activation was dose-dependent, whereby the stimulation dose needed to achieve activation at saturation was measured. The device also allowed further investigation on the reversibility of this activation, and the quantification of its time scale.

We further developed a parallel multi-zone device based on the initial version for better variation control and throughput. With this parallel device, we are able to perform a series of stimulation doses for multi-receptor crosstalk and cell activation.

We envision that this device could be widely applied to the study of cell activation and diagnostic of cell malfunction in a diversity of biological systems, taking advantage of its precisely-controlled biochemical cues and shear environment

CHAPTER 3. CELL ACTIVATION AND RECEPTOR CROSSTALK ON MULTI-ZONE DEVICE

3.1 Introduction

One type of cells could have several distinct physiological functions; one important reason is that cells can be activated through various pathways and to distinct activation states. For instance, platelets can be activated through mechano-signaling pathways and chemo-signaling pathways, the former of which can be further categorized to the GPIb [92] and the GPVI pathways [93] and the latter of which categorized to the P_2Y_1/P_2Y_{12} [94, 95] and the PAR1/PAR4 [96] pathways. Similarly, neutrophils [14, 97] and lymphocytes [48] have their distinct activation pathways by mechano-signaling and chemo-signaling. Understanding of the various mechanistic pathways of cellular functions allows us to inhibit some pathological functions of a cell type but leave other normal functions intact by specifically suppressing one pathway.

However, the abnormality of cells in pathological conditions can be very subtle, such as platelets in diabetes, which are hyperactive but have a perfect discoid shape (indicates inactive state) [41, 98]. A general antithrombotic therapy would increase the risk of bleeding due to the indiscrimination of the inhibition on hemostasis and thrombosis. It is essential to understand the subtle differences through well characterization of different pathways so the specific pathway resulting abnormity may be targeted.

Stimulation dose control and temporal information are fundamental to activation state characterization. Relatively easy for titration of chemical stimulus, it is effortful to

control mechanical stimulation dose. Our multi-zone platform allows the fine tuning of activation dose and characterization of the resulting adhesion behavior, and so enables assessment of subtle differences of stimulation responses. Thus, it is an excellent tool for questions like this.

With the power of the platform, we were able to assess the mechanical activation pathway of platelets compared to the chemical and reveal the subtle difference of diabetic platelets. Moreover, a spatial separation of ligands resulted in a temporal ligand sensation of cells; we demonstrated separation of stimulation and function in neutrophils, assessed the time course of activation and stability of the activation states. We also investigated the effect of two stimulation components, zone length and coating density, to the resulting rolling behavior of neutrophils.

3.2 Materials and methods

3.2.1 Proteins and chemicals

3.2.1.1 Platelet study

GPIb ligand VWF-A1 was a gift from Zaverio Ruggeri from the Scripps Research Institute (La Jolla, CA). Integrin $\alpha_{IIb}\beta_3$ ligand fibronectin fragment (the 9-10 domains of fibronectin III) was a gift from Andres J. Garcia from the Georgia Institute of Technology (Atlanta, GA). Biotin-PEG3500-NHS were from JenKem (Plano, TX). ADP, thrombin, dimethyl sulfoxide (DMSO), apyrase, clexane, bovine serum albumin (BSA) and other chemicals were from Sigma-Aldrich (St. Louis, MO) unless stated otherwise.

AP5 was from P. Newman (BloodCenter of Wisconsin). PAC-1 was from BD Biosciences. ab62 (LIBS-2) was from EMD Millipore, HIP8 was from Thermo Fisher Scientific, SZ22 was from Beckman Coulter, and MBC370.2 was from Kerafast.

3.2.1.2 Neutrophil study

K2EDTA was from BD Biosciences (San Jose, CA). HI-111 was from Fisher Scientific (Hampton, NH). MEM-148 (anti-Integrin Beta 2) was from Santa Cruz Biotechnology (Dallas, TX cat. # sc-51651). mAb m25 was from BioXcell (West Lebanon, NH). rHuman ICAM-1/Fc Chimera was from R&D (Minneapolis, MN, cat. # 720-IC). P-selectin was a gift from Dr. Rodger P. McEver from University of Oklahoma Health Sciences Center (Oklahoma City, OK). EasySep human neutrophil isolation kit was from STEMCELL Technology (Cambridge, MA).

3.2.2 Blood samples and platelet purification

Blood samples were drawn from volunteers who signed informed consent according to protocols approved by the Institute Review Boards of the Georgia Institute of Technology and Emory University. Blood was drawn by venepuncture from healthy subjects (20–30 years of age) or patients with type 1 diabetes (8–18 years of age) by trained nurses according to procedures approved by the Institutional Review Boards of the Georgia Institute of Technology and Emory University, respectively. Blood was drawn using a 19G butterfly needle into acid citrate dextrose containing theophylline (ACD: 85 mM sodium citrate ($2H_2O$), 72.9 mM citric acid (anhydrous), 110 mM G-glucose, 70 mM theophylline, diluted 7× with dH_2O), mixed well, and transferred to a 10 ml tube with 0.005 U ml^{-1} apyrase. Whole blood was used directly. To prepare washed platelets, blood was placed at

37 °C for 15 min and then centrifuged for 10 min at 200g. Platelet rich plasma was transferred from the supernatant to fresh tubes and centrifuged again at 1700g for 5 min. The supernatant was discarded, and the platelet pellet was re-suspended in a platelet washing buffer (PWB: 43 mM K_2HPO_4, 43 mM Na_2HPO_4, 243 mM NaH_2PO_4, 1.13 M NaCl, 55 mM D-glucose, 100 mM theophylline, diluted 10× with dH_2O, pH 6.5, conductivity 13–15) plus clexane (20 U ml^{-1}) and apyrase (0.01 U ml^{-1}). The platelet suspension was then centrifuged at 1500g for another 5 min. After discarding the supernatant, the platelet pellet was re-suspended at <1 × 109 ml^{-1} in Tyrode's buffer (120 mM $NaHCO_3$, 100 mM HEPES, 1.37 M NaCl, 27 mM KCl, 55 mM D-glucose, diluted 10× with dH_2O, pH 7.3, conductivity 13–15) containing BSA (5 mg ml^{-1}) and apyrase (0.02 U ml^{-1}). The platelet suspension was placed in a 37 °C water bath for 30 min. The suspension was diluted to 1 × 108 platelets per ml for use in experiments. For activation by ADP or thrombin in BFP or flow chamber experiments, the platelet suspension was incubated with ADP or thrombin for 15 min before experiment.

3.2.3 Blood samples and neutrophil purification

Blood was drawn using a 19G butterfly needle into a K2EDTA tube containing 1mM EDTA. Whole blood was then added to 5mLpolystyrene round-bottom tubes, each for 2mL whole blood. Isolation cocktail (50 µL/mL) and well vortexed RapidSpheres (50 µL/mL) were then added to the whole blood and incubated at room temperature for 5 min. Separation buffer (Ca- and Mg- PBS with 1mM EDTA) was added to top up the same to 4 mL with gentle mixing before placing the tubes (without lid) into the magnet and incubate for 5 min. The enriched cell suspension was collected into new tubes and added with

additional RapidSpheres (same volume as before). The purification steps were repeated twice before the cells were ready for use.

3.2.4 Microfluidic device fabrication

Standard soft lithography was used to fabricate devices in polydimethylsiloxane (PDMS, Corning Sylgard 184, Midland, MI). Two matched silicon wafers were fabricated (SU8-2025, MicroChem). The first is a one-layer mold with a 25 μm-thick single layer for microchannel PDMS. The second is a two-layer mold, 25-μm thick each for stamping PDMS. The features on the transparency mask were transferred with UV photolithography. The surface of wafers was treated with tridecafluoro 1,1,2,2-tetrahydrooctyle-1-trichlorosilane vapor from United Chemical Technologies (Lewistown, PA) to facilitate release of PDMS from the mold. A mixture of PDMS (PDMS base and crosslinker in a 10:1 ratio) was poured on the mold and the whole preparation was left for curing for 2 h at 95 °C. After peeling off the PDMS, the devices were cut into shape and access holes were punched using 19-gauge needles (McMaster-Carr).

Plastic clamp holders were laser-cut with holes matching the inlets and outlets. Plastic holders and screws were applied to hold the PDMS device and glass substrate together. After assembly, the device was primed in vacuum to remove bubbles. The chip was connected to syringe pumps to deliver flow for protein coating.

3.3 platelet activation to intermediate state and difference of diabetic sample

3.3.1 Platelet activation reported by integrin conformation-specific antibodies

After stimulation by VWF-A1, increased binding affinity of $\alpha_{IIb}\beta_3$ for FN suggests conformational change of $\alpha_{IIb}\beta_3$ from the inactive bent conformation to an active extended conformation, which would expose the LIBS2 epitope [85]. Similarly, quiescent platelets do not express P-selectin, which could be induced upon platelet activation [12]. To further characterize VWF-A1 stimulated platelets and demonstrate the utility of the device on other proteins, additional tests were performed using the two variations of our basic design, which replaced the coating protein FN on zones A and D with a conformation-specific mAb against integrin $\alpha_{IIb}\beta_3$ (LIBS2) or an anti-P-selectin mAb (AK4), respectively reporting the extending conformational change of the integrins and the upregulated expression of P-selectin as a result of GPIb signalling. The length of zone C was set to zero in these experiments. Stimulation by 800 μm A1-coated zone B resulted in high platelet binding to zone D coated with either LIBS2 or AK4 (Figure 3-1). In comparison, platelet binding to either antibody was minimal in the absence of A1 stimulation, confirming that platelets are in the resting state (Figure 3-1). As a positive control, platelet binding to HIP8, a conformation-independent mAb [86], in both zones A and D were indistinguishable, suggesting that the increased LIBS2 binding was due to conformational change of integrin $\alpha_{IIb}\beta_3$, instead of their increased expression level (Figure 3-1). These experiments confirmed our hypothesis that VWF-A1 stimulation on platelets triggers integrin conformation change and P-selectin expression.

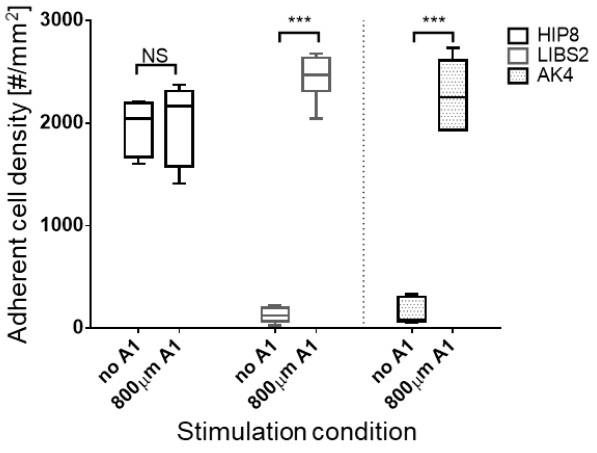

Figure 3-1 Platelet adhesion on conformation specific antibodies. Antibodies (100 µg/ml) were coated on zones A and D to report the conformational change in integrin $\alpha_{IIb}\beta_3$ (by LIBS2) and upregulation of P-selectin (by AK4) on platelets after they were stimulated by A1 in zone B of 800 µm. The conformation-independent antibody HIP8 was used as positive control, which arrested platelets in both zones A and D. By comparison, platelets were able to bind LIBS2 and AK4 in zone D but not in zone A prior to A1 stimulation. The protein patterns have no zone C. Experiments were done by perfusing 1×10^8 platelets/ml for 2 min. Data in c are presented as mean ± quarter percentile and max/min of 6 experiments. *, **, * and **** denote, $p < 0.05$, 0.01, 0.001 and 0.0001, respectively, by Student t-test.**

Platelets can be stimulated by different stimulus via distinct activation pathway such as GPIb pathway by VWF [92], GPVI pathways by collagen [93], P_2Y_1/P_2Y_{12} pathway by ADP [95] and PAR1/PAR4 pathway by thrombin [96]. We applied this device characterizing the platelet activation by immobilized ligand VWF-A1 compared with soluble agonist ADP stimulation. We measured the platelet 'dose-dependency' to immobilized VWF-A1 and ADP by either changing the length of the stimulation zone or the concentration of the pretreated ADP. A platelet suspension was perfused first through the FN zone to confirm their nonadherent resting state. The platelets then translocated on and were stimulated by the A1 zone, the length of which varied on different devices, providing adjustable doses of mechanical stimulation to platelets. Subsequently, platelets

entered the mAb zone to report the $\alpha_{IIb}\beta_3$ status. The number of captured platelets on MBC370.2 initially increased with the A1 zone length and plateaued at 400 μm, showing a mechanical dose dependency of platelet $\alpha_{IIb}\beta_3$ extension conformation. Whereas, platelet capturing on SZ22 was uniformly high and on AP5 and PAC-1 uniformly low (Figure 3-2 a), showing no sign of dose dependency. In contrast, adhesion of ADP-stimulated platelets in a single-zone flow chamber to surfaces coated with MBC370.2, AP5 or PAC-1, but not SZ22, all increased dose-dependently (Figure 3-2 b).

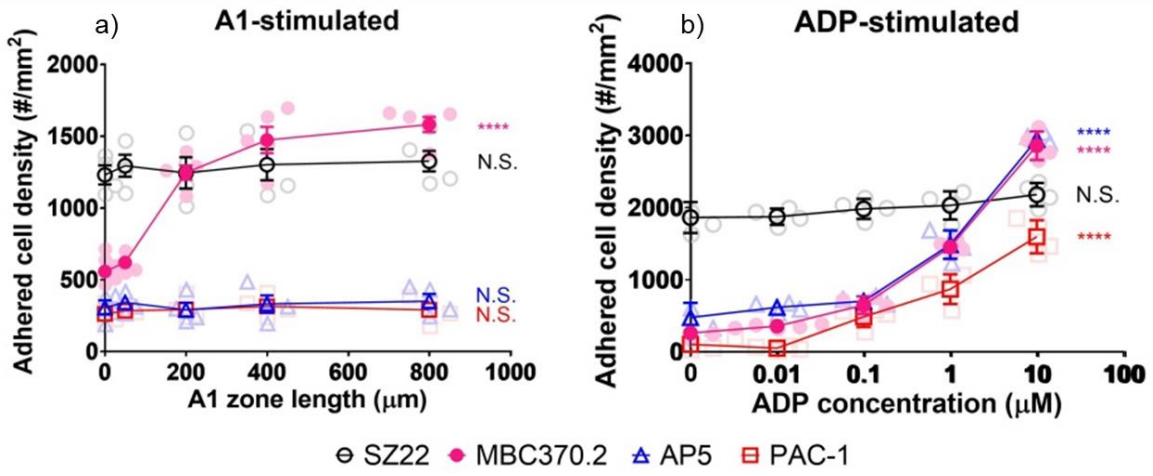

Figure 3-2 Dose-dependent mechanical and chemical activation of integrin $\alpha_{IIb}\beta_3$. Mean ± s.e.m. (n ≥ 4) platelet density on the indicated mAb zone after stimulation by the A1 zone of variable lengths (multi-zone channel; a) or ADP of different concentrations (single-zone channel; b). one-way analysis of variance (ANOVA) was used to assess whether the points in the same curve were significantly different. NS, not significant; *P < 0.05; **P < 0.01; ***P < 0.001; ****P < 0.0001.

This study suggested the distinctive dose dependencies of $\alpha_{IIb}\beta_3$ activation on mechanical and chemical stimuli: GPIbα mechano-signaling only upregulated αIIbβ3 to the intermediate state, whereas ADP evoked the emergence of active $\alpha_{IIb}\beta_3$even at low

doses. These different activation outcomes indicate distinct underlying signaling mechanisms.

3.3.2 Testing whole blood and comparing healthy with diabetic platelets

Although the use of washed platelets greatly simplifies the system for mechanistic study by removal of other blood cells and most plasma proteins, experiments using whole blood are obviously more physiological. In addition, should an assay work with whole blood, it is more likely to be usable for clinical applications. The challenge is that since whole blood is more biologically complex, experiments on whole blood are potentially prone to additional difficulties compared to assays using isolated and washed cells. We repeated the experiments as Figure 2-5a on GPIb–$\alpha_{IIb}\beta_3$ crosstalk but with whole blood and a set of devices with variable zone B length and no zone C. As with purified platelets, increased stimulation increased adhesion (Figure 3-3 a). Very low numbers of platelets adhered to FN coated zone D if the coating protein to zone B was BSA instead of VWF-A1, suggesting that platelet adhesion due to potential coating of plasma proteins onto the device was negligible under our experimental conditions. A slight increase of stimulation time (50 μm zone B coated with VWF-A1) produced a significantly higher number of adherent platelets than the BSA background ($p < 0.05$), which was further enhanced with further increasing the zone B length (Figure 3-3 a). However, even when stimulation reached saturation (zone B 800 μm), the density of VWF-A1 stimulated platelets was still significantly lower ($p < 0.01$) than platelets pretreated with agonist Mn^{2+} (10 μM, 15 min), which activates platelets to fully activated state. This suggested that the platelets under VWF-A1 stimulation were not fully activated. We then made a comparison of our approach with conventional coating approach [99] (surface coated with a mixture of VWF-A1 and

FN) for studying two pairs of receptor-ligand crosstalk. The mixture coating also yields significantly higher adherent platelets due to additional adhesion to VWF-A1. This trend is reproduced in two separate donors (Figure 3-3 a).

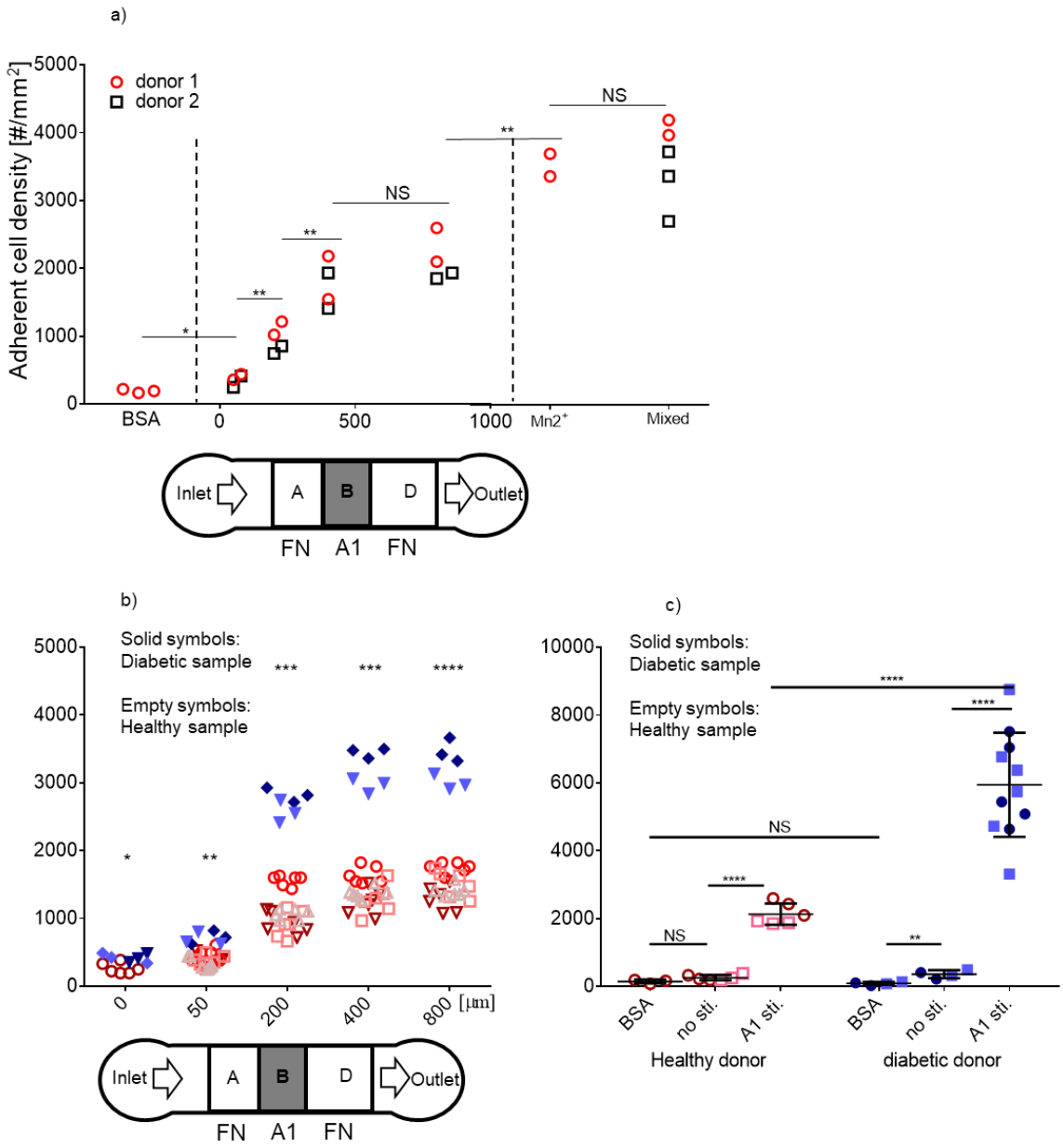

Figure 3-3 Testing whole blood and comparing diabetic and healthy platelets. a) Platelets in whole blood from healthy donors respond to different lengths of VWF-A1 (100 µg/ml coating concentration) zone from none (BSA for zone B) up to 800 µm. Conditions of platelets pre-activated by Mn^{2+} (10 µM, 15 min) or in

conventional flow chamber (a mixed of VWF-A1 and FN) were also recorded as benchmark. b) Protein patterns with varied zone B (VWF-A1 stimulus) were used to compare platelets from diabetic and healthy donors. Platelets derived from diabetic donors were statistically more responsive than those derived from healthy donors even without stimulation ($p < 0.05$). However, much more significant differences were observed when washed platelets were stimulated by varied length of zone B coated with VWF-A1. Experiments were done by perfusing 1×10^8 platelets/ml for 2 min. c) Comparison on platelets in whole blood from both healthy and diabetic donors were made for both conditions of no stimulation and VWF-A1 (800 µm) stimulation. Diabetic platelets in whole blood were statistically more responsive even without stimulation ($p < 0.01$), but much more significantly with VWF-A1 stimulation ($p < 0.0001$). Each point in a and b represents measurement from one flow chamber. Different symbols indicate data obtained from different donors. Different symbol shapes indicate different donors. Empty and filled symbols distinguish healthy and diabetic samples. n = 4 for healthy donors, n = 2 for diabetic sample. *, **, * and **** denotes $p < 0.05$, 0.01, 0.001 and 0.0001, respectively, by Student t-test**

It is known that platelets from diabetic patients are more reactive to external stimulations than healthy donors, a phenomenon referred to as platelet hyperreactivity, which includes enhanced adhesion and activation of platelets on thrombogenic surfaces [98, 100]. Adhesion and mechano-activation are important aspects of platelet function in mediating haemostasis and thrombosis. Disturbed shear can induce platelet aggregation and thrombus formation *in vivo* [101]. Therefore, platelet hyperreactivity to mechanical stimulations is closely related to thrombosis, a common disease that can be fatal [102]. To test whether platelet dysfunction can be determined by our device, we applied our device to assay the hyperactivity of platelets from patients with diabetes. We first asked whether there would be difference between diabetic and healthy samples without VWF-A1 stimulation. Washed platelets from diabetes patients and healthy donors were perfused over FN without VWF-A1 stimulation in separate devices. Significantly more ($p < 0.05$) diabetic platelets adhered to FN than the healthy group, indicating enhanced binding activity of the $\alpha_{IIb}\beta_3$ integrins on diabetic platelets before any stimulation (Figure 3-3 b).

Notably, much more significant differences between diabetic and healthy platelets were observed when the washed platelets were stimulated with additional VWF-A1 stimulation (variable length zone B) (Figure 3-3 b). The significance increased with increased A1 stimulation time (zone B 200 μm, $p < 0.005$), and even more significant for long A1 stimulation time ($p < 0.0005$ for 400 μm and 0.0001 for 800 μm, respectively). These results indicate that diabetic platelets are not only pre-activated in blood, but also are more reactive upon VWF-A1 stimulation, which is in agreement with their hyperreactivity.

Additionally, we compared activity of platelets in whole blood from diabetic and healthy donors. In a device where stimulation zone is blocked, significantly more ($p < 0.01$) diabetic platelets in whole blood bind to FN (coating concentration 0. 16 μg/ml) than a negative control where the whole device is coated with BSA (Figure 3-3 c). Further, even more diabetic platelets bind to FN after VWF-A1 stimulation at 800 μm ($p < 0.0001$). In comparison, healthy platelets only show activity after VWF-A1 stimulation, and significantly lower than diabetic platelets upon the same stimulation condition ($p < 0.0001$). These experiments demonstrated the ability of our device in distinguishing diabetic platelets in whole blood. Since one drop of blood (10 to 15 μl) is enough for one test, our assay can potentially be used for preclinical applications where frequent assessment of platelet adhesion behavior is needed.

3.4 Neutrophil activation and rolling on multi-zone device

We next demonstrated the usefulness of our platform on another biological system, neutrophils, to separate the effects of two pairs of receptor-ligand cooperative binding (PSGL-1 and integrin LFA-1) (Figure 3-4) in space and time.

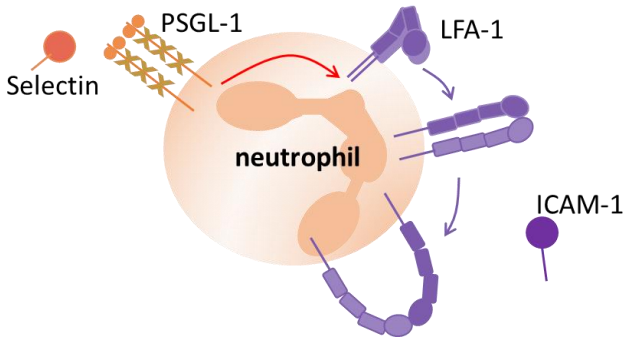

Figure 3-4 Neutrophil activation. Integrin LFA-1 can be activated through engagement of PSFL-1 to its ligand selectin and then interact with integrin ligand ICAM-1.

3.4.1 Neutrophil rolling after activation

By measuring the velocity of neutrophil rolling on integrin LFA-1's ligand under various shear conditions, we are able to assess the binding properties of the activated and non-activated integrins. Similar to the device assembling of platelet activation, a method for neutrophil activation to stimulate neutrophils and then monitor cell rolling relying on the ICAM-1 behavior, which binds to activated integrins and does not bind to quiescent integrin (Figure 3-5). The velocity of neutrophils on the reporting region was measured as a function of shear stress for different surface treatments: surface treated with ICAM-1 only, surface treated with P-selectin surface only, and two surfaces with both ligands but different patterns (Figure 3-5 a). On the surface treated only with ICAM ligand, neutrophils

were not stimulated and showed no sign of interaction regardless of the shear rate, serving as a negative control (Figure 3-5 b, annotated as 'do not roll'). Neutrophils' rolling behaviour was observed in the stimulation zone, confirming the transient interaction of neutrophil PSGL-1 with the surface immobilized P-selectin. The velocity first decreased with the increasing wall shear stress of the flowing fluid, reached a minimum at 0.2-0.3 dynes/cm^2, and then increased with a further increase of the wall shear stress (Figure 3-5 b, circle). This trend is consistent with the previously reported catch-slip bond characteristic of PSGL-1–P-selectin binding [103, 104].

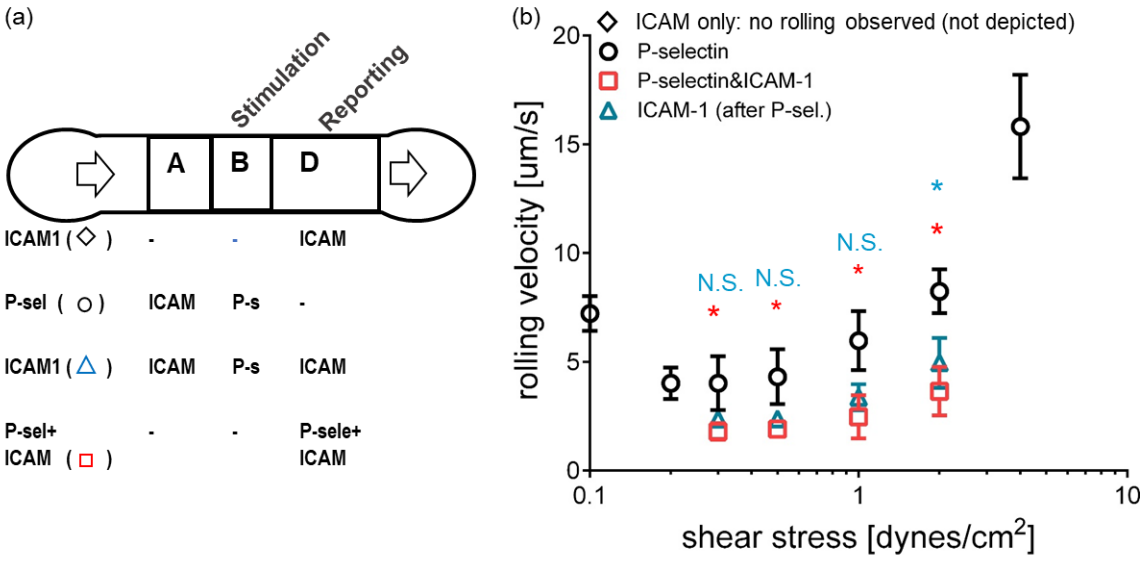

Figure 3-5 Neutrophil activation by P-selectin demonstrated by decreased rolling velocity on ICAM-1. Velocity of neutrophils rolling patterned with indicated proteins is plotted vs. wall shear stress. Quiescent neutrophils (no treatment) did not interact with ICAM-1 surface (20 µg/ml) (data not plotted), but rolled on P-selectin surface (20 µg/ml) (black circle) and ICAM-1 surface (20 µg/ml) in after stimulation by P-selectin (blue triangle). Rolling velocity on ICAM-1 surface after P-selectin stimulation was lower than on P-selectin surface. As a control,

platelets rolling on a surface with P-selectin and ICAM-1 co-presented had a lower velocity (red square). Data are presented as mean ± sem of 15-20 cells. Experiment was repeated 3 times with consistent results and the representative data are shown.

Neutrophil activation through PSGL-1–P-selectin interaction is known to promote the conformation change of integrin LFA-1 [67], and lead to the interactions with the downstream reporting zone surface coated with ICAM-1 [105]. The density of ICAM-1 (20 μg/ml coating concentration) on reporting zone supported the neutrophils' slow rolling (Figure 3-5 b, triangle), which indicated the activation of surface protein LFA-1 with an increased binding affinity after P-selectin stimulation. As a positive control, the conventional flow chamber coating approach was applied: a mixture of P-selectin (20 μg/ml coating concentration) and ICAM-1 (20 μg/ml coating concentration) was immobilized on the device. Neutrophils were able to interact with both proteins at the same time, which largely reduced rolling velocity (Figure 3-5 b, square) compared to P-selectin only. These data confirm that neutrophil activation and resulting behaviour can be separated on our platform. Together with the platelet study, this suggested that this platform can be applied to the study of cell activation and function in a diversity of biological systems.

3.4.2 Neutrophil activation threshold and intermediate state characterization

We next assessed the stimulation dose-dependency and integrin state of neutrophil activation via P-selectin binding.

How the activation level of neutrophil via P-selectin binding is stimulation dose-dependent is not well understood. We characterized the stimulation dose-dependency of integrin LFA-1 activation on neutrophils upon the stimulation on PSGL-1 by changing the length of the stimulation zone coated with P-selectin (Figure 3-6 a). Purified human neutrophils were first perfused through a stimulation zone, the length of which varied in different channels, providing adjustable doses of mechanical stimulation via immobilized ligand. Subsequently, neutrophils entered the reporting zone coated with a high density of ICAM-1 (100 μg/ml coating concentration), where activated integrin LFA-1 interacted with ICAM-1 and stopped neutrophil on site.

The effect of varying stimulation dose was assessed by measuring the number of neutrophils captured per unit area in reporting zone (Figure 3-6 a). When stimulation dose remained relatively low (zone length below 400 μm), the number of the adherent cells slowly increased with increasing stimulation doses. A significant increase of the number of adherent cells resulted for an 800 μm long stimulation pad, and further rose for the 2000 μm long stimulation zone. A mixed coating of both P-selectin and ICAM-1 served as a positive control. Another positive control by pretreatment of Mn^{2+} for 20 minutes provided the reference of neutrophil activation by chemical agonist. Further, these experimental results are robust and reproducible in independent experiments on different days.

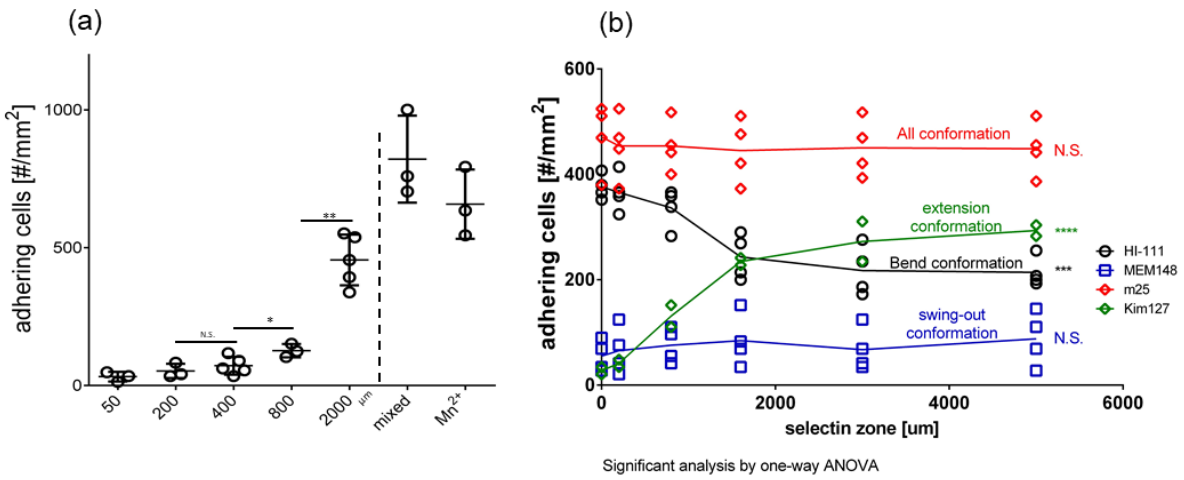

Figure 3-6 Stimulation and resulting rolling can be separated in a dose-dependent manner to show neutrophil intermediate state. The activation of neutrophils was reported by their binding to reporting zone coated with a) ligand or b) antibodies, after variable length of stimulation zone coated with 20 μg/ml p-selectin. a) ICAM-1 were coated on the reporting zone to report increased adhesion of LFA-1 after stimulation. Conventional flow chamber experiments with ICAM-1 and P-selectin co-presented were done as a positive control, as well as neutrophils incubated with Mn^{2+} for 10min. b) Antibodies (100 μg/ml) were coated to report the conformational change in integrin LFA-1 (by Kim 127 for extension conformation, HI-111 for bend conformation and MEM148 for open conformation) on neutrophils after they were stimulated by P-selectin. The conformation-independent antibody m25 was used as positive control, which arrested neutrophils in all stimulation lengths. By comparison, neutrophil binding increased to KIM127 and decreased to HI111 with increased stimulation dose of P-selectin. Whereas increased stimulation dose was not able to increase neutrophil binding to MEM148. Experiments were done by perfusing 2×10^6 neutrophils/ml for 2 min. Each point in a and b represents measurement from one flow chamber. *, **, * and **** denote, $p < 0.05$, 0.01, 0.001 and 0.0001, respectively, by Student t-test (a) and one-way ANOVA (b).**

Because integrin can be activated to different affinity states corresponding to the different conformations, which can be characterized by conformation-specific antibodies, we next applied the reporting zone with various antibodies and evaluated the integrin activation dose-dependency to the stimulation of the immobilized ligand P-selectin by measuring the number of captured neutrophils on conformation-specific antibodies. The number of captured neutrophils on HI-111 (indicates bent conformation of integrin LFA-

1) initially decreased at 800 μm and plateaued at 3000 μm, showing a mechanical dose-dependency of neutrophil LFA-1 bent conformation. Whereas, neutrophils captured on MEM148 (indicates hybrid-domain swing-out) was uniformly low, and uniformly high on m25 (for all β2) (Figure 3-6 b), showing no sign of dose dependency. This suggested that integrin LFA-1 had an extended but no further swing-out conformation upon P-selectin activation, conforming an intermediate activation state of integrin LFA-1 [65, 66].

3.4.3 Rolling supported by activated integrin is stimulation dose-dependent

It is reasonable to assume that the rolling behavior of the neutrophils stimulated by P-selectin [66, 97] would be dependent on the stimulation dose as well. We measured the rolling velocity of the neutrophils after stimulation of various zones coated with P-selectin of different lengths and coating concentrations. The coating concentration corresponds to the density of ligand on the surface, and zone length corresponds to the time of a cell travels. It is rational to suppose selectin that the length of a coated zone multiplied by the coating concentration corresponds to the total amount of ligands a traveling cell can bind to. Therefore, we hypothesized that the two effectors, the coating concentration and the length of stimulation zone, play a combinatory role as stimulation dose in activating LFA-1. We plotted the velocity of the stimulated neutrophils on ICAM-1 (coating concentration 20 μg/ml) against the stimulation 'selectin dose' (Figure 3-7). The rolling velocities of the neutrophils on ICAM-1 surface activated by various coating concentration of P-selectin exhibited exponential decrease as stimulation doses increased as expected. Among these curves, curves of 5 μg/ml to 20 μg/ml stimulation collapsed into one exponential decay

curve. This supported our hypothesis of the effect of the two factors: length and coating concentration. The more stimulation dose the neutrophils receive yielded lower rolling velocity, indicating a more activated sate of neutrophils. Whereas 50 μg/ml coating concentration yielded a different curve, which indicated an exit of the linear regime due to possible reasons such as density saturation of the ligand on substrate and occupation saturation of the receptor on the cells.

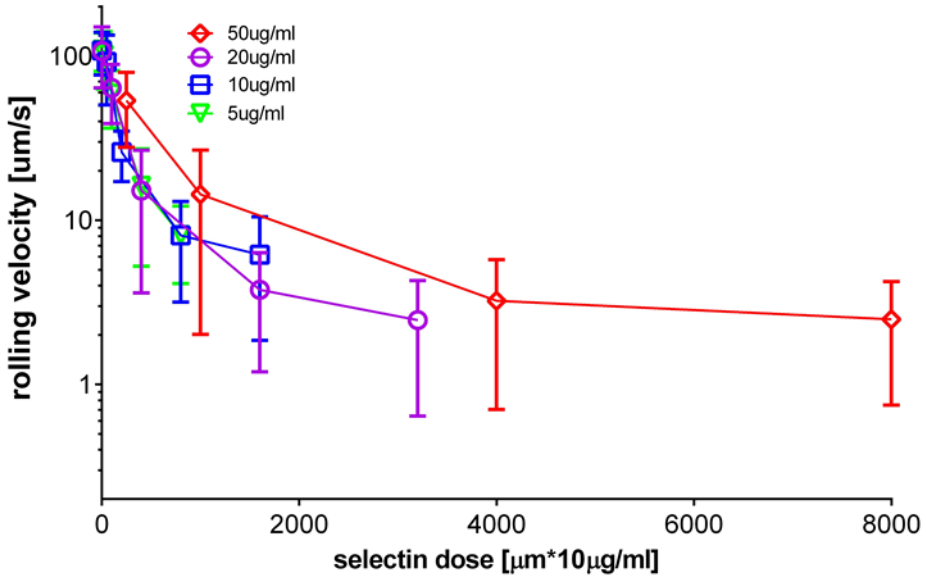

Figure 3-7 Neutrophils roll on multi-zone in a stimulation dose-dependent manner. Velocity of neutrophils rolling on ICAM-1 (20 μg/ml) surfaces after variable length of stimulation zones is plotted vs. mechano-dose (characterized by the length of stimulation zone times coating concentration). Stimulation zones were patterned with P-selectin at various concentrations for various lengths Neutrophils were perfused in the chambers with a wall shear rate of 50 s^{-1}. Data are presented as mean ± sem of 15-20 cells. Experiment was repeated 3 times with consistent results and the representative data are shown.

The rolling behavior on endothelial cells helps neutrophils locate from blood to tissue, homing to inflammation sites. We further investigated the rolling behavior of the

neutrophils on the asymmetric coating surface for potential heading guided by the patterned protein. Instead of a homogeneous reporting zone of ICAM-1, the surface was coated with asymmetric stripes of ICAM-1 by stamping, while the space between stripes was blocked with blocking protein BSA (Figure 3-8 a). With a forwarding force from flow (from the left to the right in Figure 3-8 a), cells tend to move straight forward. However, neutrophils could potentially drift laterally at the edge of stripes due to the asymmetric balance of the interaction with the ICAM-1. In our experiment, neutrophils interacted only to the ICAM-1 stripes but not space in between as anticipated (Figure 3-8 b). Extracted trajectories of individual neutrophils were plotted in Figure 3-8 c. Each color indicates one neutrophil and each dot of that color indicates the location of neutrophil in one frame. Red circles highlighted the lateral movement at the edge of the stripes. This lateral movement behavior resulted from activated integrin-supported rolling capacitates our device for a potential application in cell sorting.

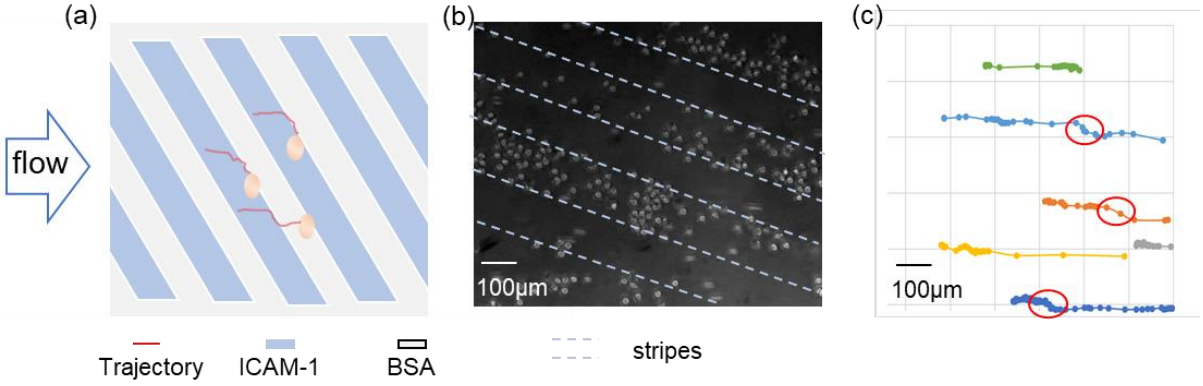

Figure 3-8 Neutrophils roll on asymmetric stripes of ICAM-1. a) illustration of the stripes of ICAM-1 surface (blue) and blocking surface (grey). Neutrophils were indicated in yellow and their anticipated trajectory in red curves. b) Neutrophils rolled and some adhered on the stripe surface of ICAM-1, but not the blocking surface. Stripes of protein pattern was indicated by dashed lines. c) Extracted individual trajectories of some representative cells. Each color

indicates one neutrophil and each dot of that color indicates the location of neutrophil in one frame. Scale bar: 100μm.

3.5 Conclusion

In this chapter, we expanded the platform on two biological systems, platelets and neutrophils, for the crosstalk study of their surface receptors.

We validated the activation state and the stimulation requirement for the platelets by GPIb-VWF-A1 interaction by characterizing integrin conformation change and P-selectin expression level in the reporting zone. This study contributed to the discovery of a new integrin αIIbβ3 activation state by demonstrating a distinct activation condition via immobilized VWF-A1 versus soluble agonist ADP in a dose-dependent manner. Moreover, the successful application of this device to assessing whole blood samples implies its potential to test a drop of blood, which is compatible with clinical application. Furthermore, using whole blood, we detected the pre-activation of diabetic platelets and their higher activation level upon VWF-A1 stimulation, which was not easily monitored by other means. Altogether, our results indicate that this microfluidic system could serve as a promising diagnostic tool for platelet hyperreactivity, which is found not only in diabetes but also in many other diseases (e.g., obesity [106], hypertension [40], etc.).

We then demonstrated that the neutrophil activation and integrin interaction can be separated in spatial and time, which is not easy to show by other means. Further assessment on the activation threshold and conformation validated the intermediate state of integrin LFA-1 after activated by the interaction of PSGL-1 and immobilized P-selectin. Moreover,

we investigated the effect of two stimulation components, zone length and coating density, to the resulting rolling behavior of neutrophils on ICAM-1 surface. The collapsed curves validated our hypothesis of these two parameters. We further demonstrated activated integrin LFA-1 - supported rolling on asymmetric stripes of ICAM-1, which leads to a lateral movement on the edge of the stripes. We envision this behavior of the activated integrin could be applied to cell sorting and the diagnostics of cell malfunction.

CHAPTER 4. TCR-PMHC INTERACTION UNDER FLOW INDUCES INTERMEDIATE-AFFINITY OF LFA-1 TO SUPPORT ROLLING ADHESION

4.1 Introduction

T cell's critical role in adaptive immunity and the extreme high sensitivity and specificity of its recognition to antigen attract intensive interests in the T cell activation study [48, 51-53, 55, 57, 107, 108] (Figure 4-1). Distinct triggering models have been proposed and modified over the past decades, including affinity-based model [49], kinetic proofreading model [50, 51], serial triggering model [55, 56], mechano-sensor model [57, 58] and so on [44, 59] (details in 1.5.2). Despite the intensive study, this triggering process is still under debate. Further observation could help to add more understanding to this process.

Integrin LFA-1 is expressed on all leukocytes and comprehensively studied in neutrophil for its conformation, affinity state and function: bent, resting state of the LFA-1 results in low affinity to its ligands; extended conformation of LFA-1 supports slow rolling; open conformation facilitates firm adhesion which usually require chemokine stimulation [67]. After T cell triggering by TCR, one of the most important regulation is the integrin LFA-1 activation [65] (Figure 4-1). However, the activation state of this predominant integrin remained elusive on T cells. The integrin in an immunological synapse (IS) facilitate firm adhesion and demonstrated fully activation state [62], yet the formation of an IS could last hours which involves activation processes like chemokine

stimulation [109, 110]. It also remained a question whether the activation of the integrin requires to be in an IS.

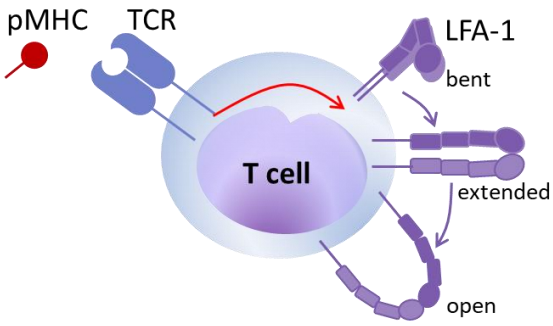

Figure 4-1 T cell stimulation by specific pMHC. Stimulated by specific pMHC, T cells can be triggered with a change in integrin LFA-1.

New technology development always allows advanced observations that facilitate more finding and add knowledge to existing models. With the power of controlling mechano-stimulation dose precisely, permitting fast rebinding interaction under flow and allowing two receptor-ligand interaction spatially separated, the multi-zone device is an excellent tool for the investigation of T cell stimulation under flow and the resulting behavior. We applied this platform to study T cell activation under flow by measuring the velocity of moving cells on both the antigen surface and integrin ligand surface in a separated, dose-dependent manner. Calcium flux monitoring was also added to validate the activation and distinguish the calcium pattern of T cells stimulated by pMHC with various potency. This study added an observation to the current knowledge of T cell activation, of the T cells interacting with surface-immobilized pMHC in a flow condition and triggering a state that supported T cell rolling on ICAM-1 surface.

4.2 Materials and methods

4.2.1 Chemicals and proteins

RPMI 1640 1X w/ L-glutamine was from Corning Inc. (Corning NY). Mouse Erythrocyte Lysing Kit was from R&D systems (Minneapolis, MN). Molecular Grade Water was from Corning Inc. (Corning NY). Trypan Blue was from Sigma-Aldrich (St. Louis, MO). Mouse CD 8+ T cell enrichment kit was from STEMCELL Technology (Cambridge, MA). Recombinant mouse ICAM-1-Fc chimera was from BioLegend (San Diego, CA). EZ-Link™ NHS-PEG4-Biotin was from ThermoFisher Scientific (Waltham, MA).

pMHCs (including OVA, Q4R7, Q4H7, G4, VSV) were from Emory NIH tetramer core facility (Atlanta, GA): OVA (SIINFEKL), Q4R7 (SIIQFERL), Q4H7 (SIIQFEHL),G4 (SIIGFEKL), VSV (RGYVYQGL).

4.2.2 Primary mouse T cell purification

4.2.2.1 Spleen grinding and RBC lysis

Mouse spleen was collected into 1mL of R10 buffer (RPMI 1640 1X w/ L-glutamine, added 100mL FBS, 10mL P/S, 10mL Hepes, and 10mL sodium pyruvate per 1L RPMI). Together with 3 mL R10 in a 70 μm cell strainer placed on the top of a 6 cm petri-dish, collected spleen was grinded using a 3 mL syringe plunger end. The cell suspension was collected with 3 mL R10 washing the plunger end, cell strainer and petri dish and then centrifuged at 1500 rpm for 7 min. The supernatant was discarded, and the cell pellet was resuspended with 2 mL of 1x lyse buffer (dilute 0.2mL of 10X M-lyse buffer

in 1.8 mL of molecular grade wafer) and incubated 2.5-3 min at room temperature. The reaction was stopped by adding 8 mL of 1x wash buffer (dilute 800 µL of 10x wash buffer in 7.2 mL of molecular grade water) to make a 10 mL in total. Cell counting was done by taking 10 µL of solution for 10 times dilution with 0.04% Trypan Blue (0.4% Trypan Blue diluted with 1x PBS). After cell counting, the solution was centrifuged at 1500 rpm for 9 min at room temperature before discarding the supernatant.

4.2.2.2 CD8 T cell purification

The splenocyte pellet was resuspended at a concentration of 1×10^8 cells/ml with EasySep Buffer (PBS + 2% FBS) in a 5mL FACS tube, plus Normal Rat Serum (50 µL/mL) to prevent non-specific binding and CD8+ T cell isolation Cocktail (50 µL/mL), followed by an incubation of 10 min at room temperature. SA Rapid Spheres (125 µL/mL) was added and incubated for 5 min at RT before Easy Sep Buffer added to the mixture for a total volume of 2.5 mL. The tube was then placed on the EasySep magnet without cap for 3min. Solution was collected by pouring to a 15 mL tube with an addition of Easy Sep Buffer to make a final volume of 5 mL for cell count. Cell solution was centrifuged for 7 min at RT at 1500 rpm before discarding the supernatant and resuspending in R10 or HBSS to make 2 million/ml concentration.

4.2.2.3 CD8 T cell depletion

The splenocyte pellet was resuspended at 100 million/mL in Easy Sep buffer (PBS + 2% FBS). After adding biotin-antiCD8 (cl 53-6.7 0.5 mg/mL) to a final antibody concentration of 25 µg/mL, the solution was incubated at 4 degree for 20 min on a rotator. The splenocyte solution was then transferred to a 15 mL tube, with additional 10 mL Easy

Sep Buffer to stop the reaction before cells resuspended to 100 million/mL in Easy Sep Buffer. Dynabeads M-280 streptavidin (125 µL beads per 1 mL of cells) was taken before thorough vortexing for a wash with 1 mL Easy Sep. Cell suspension and beads were mixed for an incubation of 15 min at 4 degree on a rotator. The cell-bead-mixture was then transferred to a 5 mL FACS tube, plus Easy Sep Buffer till a final volume of 2.5 mL before placing the tube on an EasySep magnet for 3 min. The liquid was poured gently out into a 15 mL tube while the FACS tube was kept on the magnet. The solution was then centrifuged and resuspended in R10 or HBSS to a concentration of 2 million cells/mL.

4.2.3 Microfluidic device fabrication

Silicon wafers were fabricated in clean room with negative photoresist (SU8 2025, MicroChem). Wafers were then used to mold devices in polydimethylsiloxane (PDMS, Corning Sylgard 184, Midland, MI) by standard soft lithography. The stamping wafer, the coating channel wafer and the experimental device wafer are all one-layer molds for a 25 µm-thick single layer PDMS for stamping, channel coating and experiment flow. The features on the transparency mask were transferred with UV photolithography. The surface of wafers was treated with tridecafluoro 1,1,2,2-tetrahydrooctyle-1-trichlorosilane vapor from United Chemical Technologies (Lewistown, PA) to facilitate release of PDMS from the mold. A mixture of PDMS (PDMS base and crosslinker in a 10:1 ratio) was poured on the mold and the whole preparation was left for curing for 2 h at 95 °C. After peeling off the PDMS, the devices were cut into shape and access holes were punched using 19-gauge needles (McMaster-Carr). Plastic clamp holders were laser-cut with holes matching the inlets and outlets. Plastic holders and screws were applied to hold the PDMS device and

glass substrate together for protein coating. Assembled devices were taken out of the holders gently for experiment under microscope.

4.3 T cells interact with immobilized pMHC under flow

Unlike static condition where cells have a long time interacting with the surface, the flow condition provides a chance to investigate the rapid contact scenario. We assessed the interaction between OT1 T cells and its ligands under flow condition by measuring velocity and adhering cell density. Flow channels were coated with ligands of OVA, Q4R7, Q4H7, G4, or VSV at a coating concentration of 25 μg/ml, and BSA blocking coating served as a negative control. Cell behavior was highly dependent on the shear rate: higher shear rate resulting in cell moving, while lower shear rate resulting in cell adhering. Hence, I applied wall shear rate of 25 s^{-1} and 15 s^{-1} for the measurement of velocities of the moving cells and density of the adherent cells respectively. Mean velocities of the individual moving cells near surface were measured for each coating conditions at the same wall shear rate (Figure 4-2a). Inserted figure indicated the number of moving T cells and adherent cells at this condition, which demonstrated the dominance of the moving cell numbers. Moving cells on OVA and Q4R7 surface had significant lower mean velocities than the rest conditions, suggesting interactions between the T cells and the surfaces. We also assessed the adherent cell density on surfaces under the low shear rate (Figure 4-2b) to further validate the cell-surface interactions. Three distinct groups were shown by the adherent cell density measurement: OVA and Q4R7 (high density), Q4H7 and G4 (medium density), and VSV and BSA (low density), which agreed with antigen affinity differences reported in literature [108, 111].

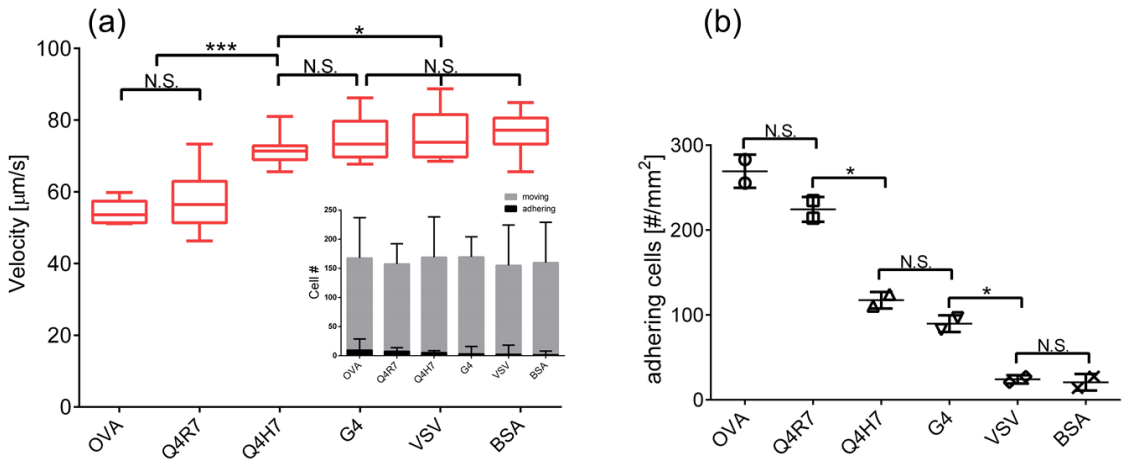

Figure 4-2 The observation of T cells interacting with immobilized OVA under flow. a) Velocity of the OT1 T cells moving on the pMHC surface (25 μg/ml) under a shear rate of 25 s^{-1}. Inserted graph represented the number of moving T cells and adherent cells. Data are presented as mean ± se of 15-20 cells. Experiment was repeated 3 times with consistent results and the representative data are shown. b) Adherent cell density of OT1 T cells on each pMHC surface under a low shear rate of 15 s^{-1}. Each dot indicated one experiment. *, **, * and **** denote, p < 0.05, 0.01, 0.001 and 0.0001, respectively, by Student t-test.**

To test whether the velocity reduction of cells on surfaces of OVA and Q4R7 was induced by the flow and channel difference, we also measured the velocities of cell above of surface (Figure 4-3). The data of the velocities of cells near surface (red) were replotted from Figure 4-2 a, while the velocities of the cells above surface were plotted as comparison (black). Among all surface conditions, the velocities of cells above surfaces showed no sign of significant difference, suggesting that any velocity difference of the cells near surface was due to the ligand-coated surfaces. Together with Figure 4-2, this suggested that OT1 T cells can interact to surface coated pMHC under flow conditions.

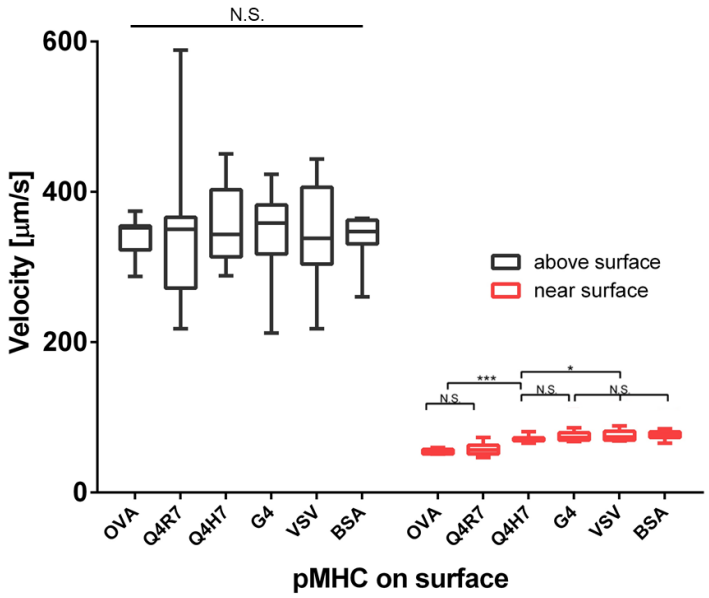

Figure 4-3 The velocity of T cells in the flow. A comparison of velocities above the surface (black) and near the surface (red). Velocities of the OT1 T cells moving above the surface, meaning no interaction to the surface, had no significant difference among the various pMHC coating. The velocity data of 'near surface' T cells were the replotted from Figure 4-3. This confirming that the difference of moving velocities of near surface T cells on various pMHC surface was not due to the flow condition. Data are presented as mean ± se of 15-20 cells. Experiment was repeated 3 times with consistent results and the representative data are shown.

To further assess the TCR-pMHC interaction by the behaviors of the cells, we analyzed the instantaneous instead of mean velocities of three groups of OT1 T cells with frame-by-frame tracking. Ten representative cells for each group were plotted in Figure 4-4, cells classified as adhered on OVA surface, moving on OVA surface, and moving on BSA surface, respectively. The cells classified as adhered cells (Figure 4-4 a) had an instantaneous velocity largely at 0 µm/ s^{-1} with occasional movement. Cells on the BSA surface, as the opposite, were flowing without stop, at an average speed of 75 µm/ s^{-1} (Figure 4-4 c). The variation of the velocity was caused by cell fluctuation and the

limitation of the spatial resolution. Velocity of OT1 cells moving on the OVA coated surface showed frequent stops and rapidly regained movement (Figure 4-4 b). This suggested the rapid rebinding and dissociation between TCR on OT1 cells and pMHC OVA coated on surface under flow.

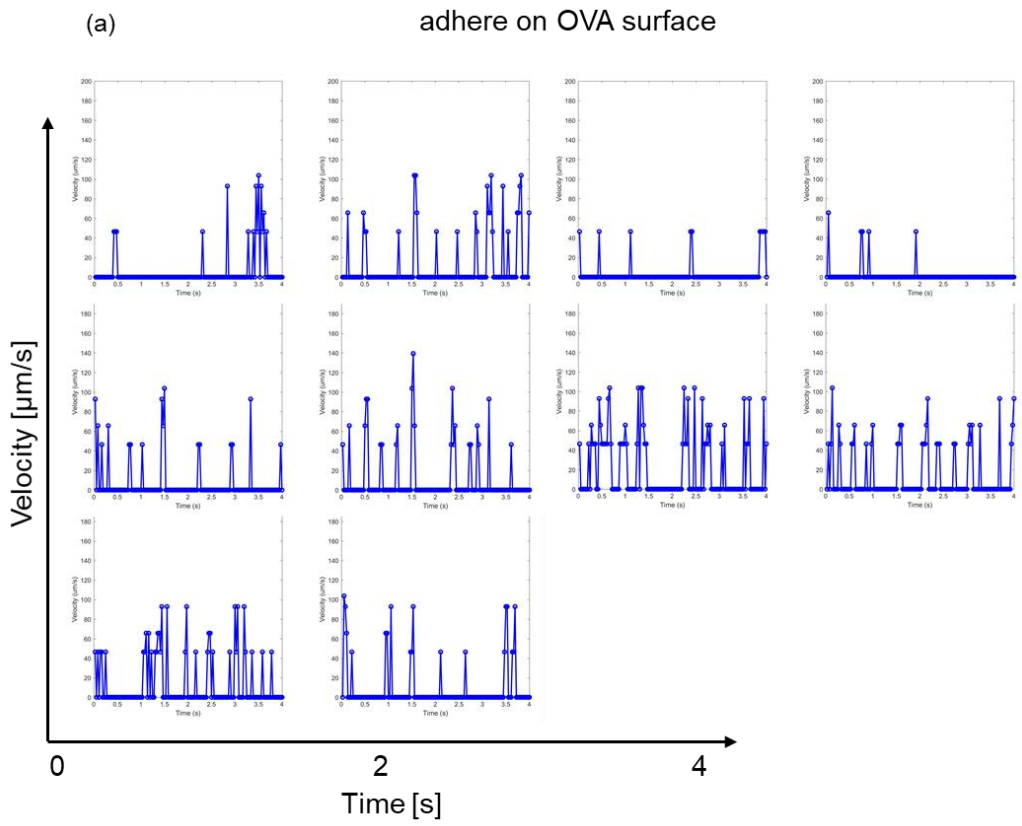
(a)
adhere on OVA surface
Velocity [μm/s]
0
2
4
Time [s]

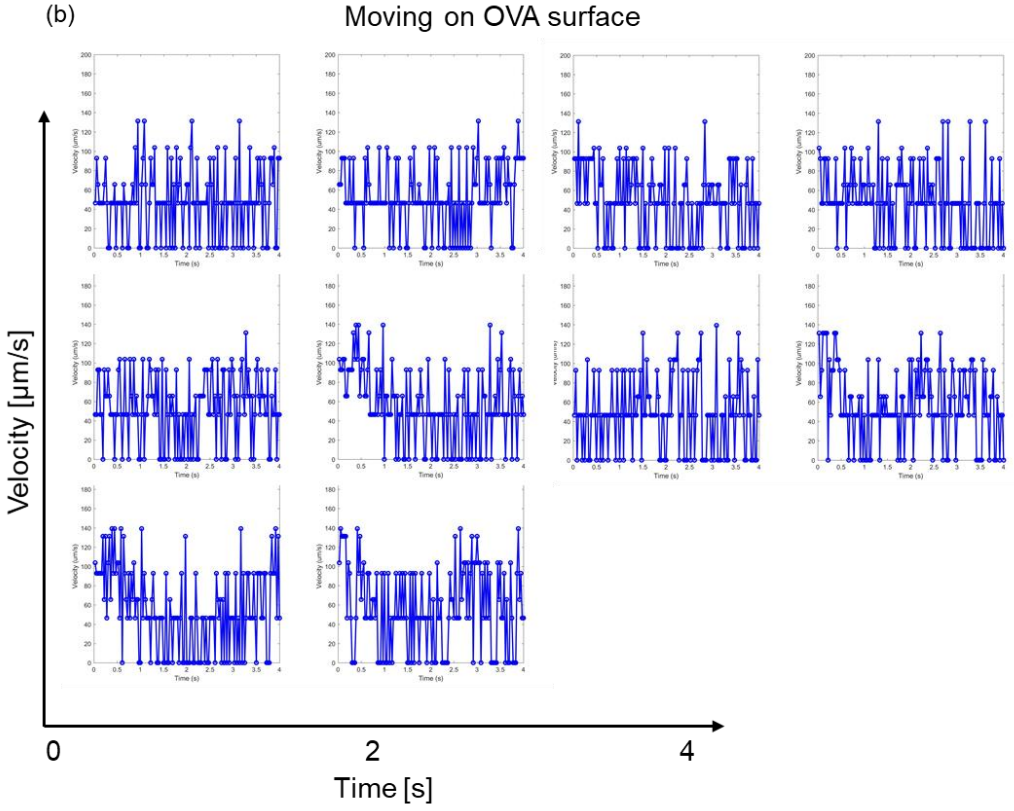
(b)
Moving on OVA surface
Velocity [μm/s]
0
2
4
Time [s]

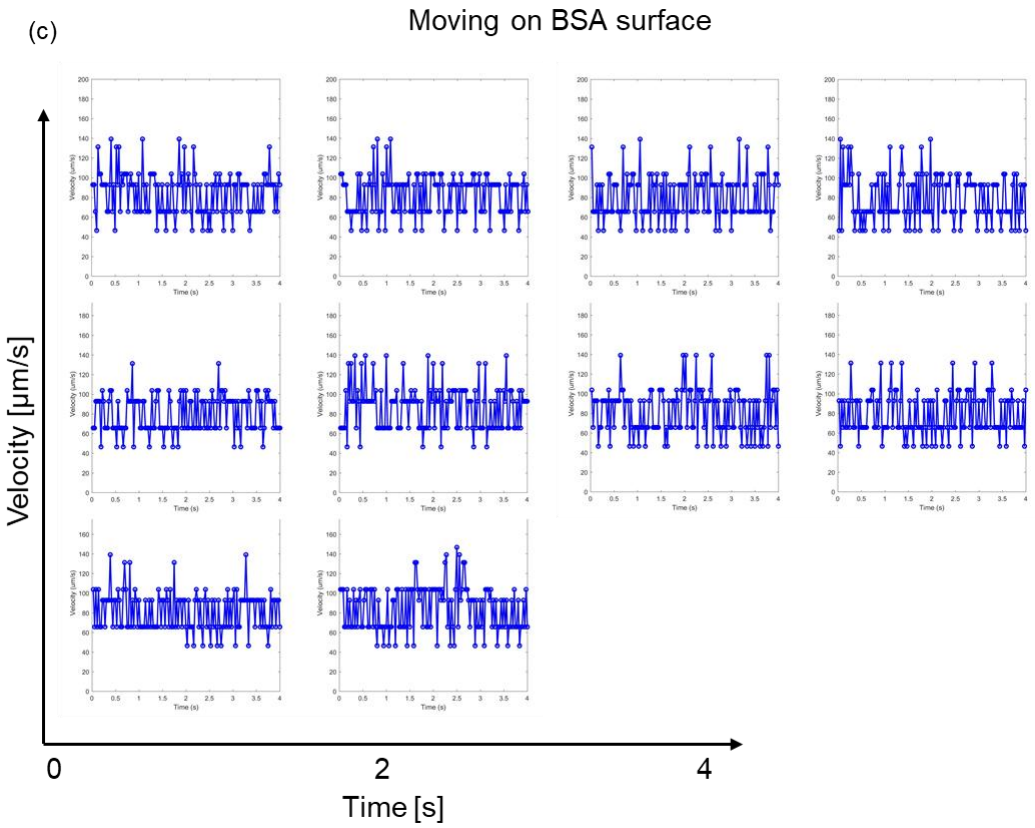

Figure 4-4 Instantaneous velocities of T cells on surface. Cell velocities analyzed for 10 representative cells for each condition: a) adherent T cells on OVA pMHC surface, b) moving T cells on OVA surface and c) moving T cells on BSA surface. Each panel represents one cell. Videos were taken under 10x magnification at 36 f/s and analyzed frame by frame for 4 seconds for each cell.

Together with reduced mean velocities and increased adherent cell on pMHC surface, this study indicated that T cells can interact with surface-immobilized pMHC and form the rapid rebinding under flow condition.

4.4 T cell LFA-1 activation stimulated by TCR-pMHC interaction

T cell receptor interaction with pMHC upregulates integrin activation and function in immune synapse [62]. Thus, it is reasonable to assume that the TCR-pMHC interaction under flow would also generates the integrin LFA-1 activation. To test this, we coated the microfluidic channels pMHC OVA ligand with or without ICAM-1, which binds to activated LFA-1. Flow carried OT1 T cells were delivered (25 s^{-1}) and cells were allowed interaction with the surfaces; the number of adherent cells was measured to assess the T cell interaction. The adherent T cells on OVA/ICAM-1 surface were significantly more than OVA alone surface (Figure 4-5), indicating an additional interaction to the ICAM-1. Channels coated with ICAM-1 alone served as a negative control, to confirm that the integrin LFA-1 was not activated in the beginning. Another non-specific pMHC, VSV [111], was also tested as a negative control, where channels were concurrently coated with VSV and ICAM-1. Very low level of adherent cells on VSV/ICAM-1 surface indicated that the interactions of T cells on OVA and OVA/ICAM-1 surface were specific. This study showed that interaction of T cell LFA-1 and ICAM-1 facilitated T cell adhesion under flow when pMHC OVA was at present, and this synergetic effect of TCR and integrin LFA-1 was highly specific.

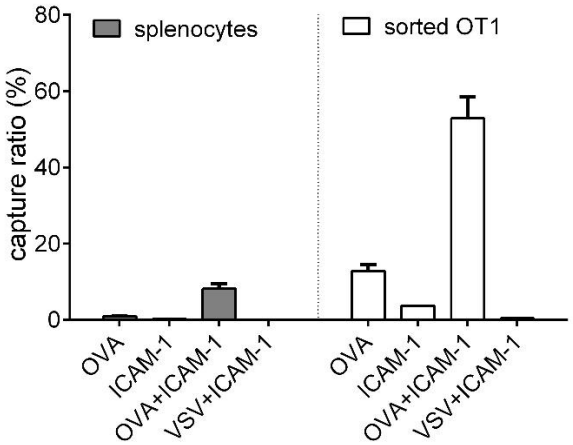

Figure 4-5 Synergetic effect of TCR and integrin LFA-1 on T cell adhesion. Adherent cell fraction of OT1 T cells was calculated as 'captured on surface / (captured on surface + collected in outlet)' on each surface under a low shear rate of 25 s-1. Splenocyte sample includes other cell populations besides OT1 T cells. OVA and VSV coating concentrations were 25 μg/ml and ICAM-1 coating concentration was 20 μg/ml. Each dot indicated one experiment. *, **, * and **** denote, p < 0.05, 0.01, 0.001 and 0.0001, respectively, by Student t-test.**

Although we showed that TCR can interact with pMHC under flow condition and the interaction can recruit integrin-ICAM-1 interaction, it is still unclear whether engagement of the integrin LFA-1 on T cell surface must occur while TCR-pMHC interacts consistently as in an immune synapse. To temporally separate these two interactions, we applied our multi-zone device to address this question by functioning the stimulation zone with immobilized pMHC OVA (coating concentration 25 μg/ml) and reporting zone with ICAM-1 (coating concentration 20 μg/ml) (Figure 4-6 a). The length of the stimulation zone can be tuned to achieve various levels of stimulation dose and measure the adherent cell density at the reporting zone. For a given flow rate (shear rate = 15 s^{-1}) and device dimension (1mm wide), a low adherent cell density was present at both no stimulation (BSA instead of OVA coated on the stimulation zone) and low stimulation dose (50 μm length) (Figure 4-6 b). Increase of adherent T cells on ICAM-1 reporting zone started when stimulation zone size increased to 200 μm and the adherent density kept rising at 400 μm and 800 μm. A hypothesized saturation of the adherent cell density was not observed for the given stimulation dose, indicating that a higher dosage may be required to achieve further stimulation. Positive controls were done by delivering cells onto a surface coated with a mixture of OVA and ICAM, or by pretreating the T cells with agonist Mn^{2+} (10 μM, 15 min), which activated T cells to fully activated state. This suggested that the TCR-

pMHC and LFA-1-ICAM-1 interactions can be spatially and so temporally separated, where the activation level of LFA-1 by TCR-pMHC interaction can be tuned by the stimulation zone size.

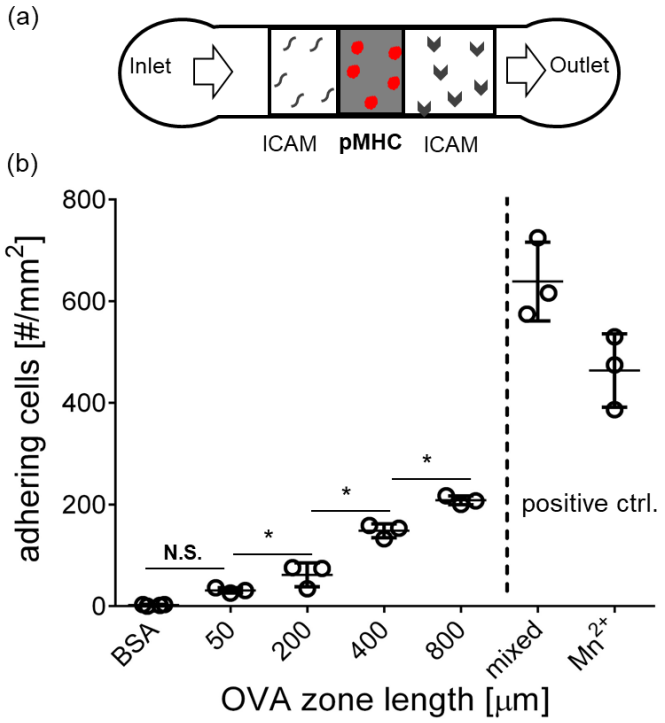

Figure 4-6 Stimulation and probing activation can be separated in a dose-dependent manner. a) Schematic of the multizone microfluidic channel for T cell stimulation and reporting. Highlighted pMHC zone is size-variable for different dose of stimulation. b) The activation of T cells was reported by their binding to reporting zone coated with ligand ICAM-1 (20 μg/ml coating concentration), after variable length of stimulation zone coated with 25 μg/ml pMHC OVA. Conventional flow chamber experiments with ICAM-1 and OVA co-presented were done as a positive control, as well as T cells incubated with Mn^{2+} for 10min. Dots indicated individual experiment. *, **, * and **** denotes p < 0.05, 0.01, 0.001 and 0.0001, respectively, by Student t-test**

It is known in literature [14, 97, 112] as well as demonstrated in chapter 3 that integrin LFA-1 activated by selectin interaction can support neutrophil rolling. Whether the integrin LFA-1 on T cell surface can support rolling and whether this can be enabled by TCR interaction all remained unclear. We next measured the velocity of pMHC stimulated T cells on ICAM-1 surface upon various stimulation doses to assess whether and how the velocity will be affected the activation dose.

Length of the stimulation zone was demonstrated to be an activation dose factor in Figure 4-6. It is intuitive to think that coating concentration could be another factor of activation dose. We varied the size of the stimulation zone with coating concentrations: 10 µg/ml, 25 µg/ml, and plotted the velocity of T cells on ICAM-1 surface as a function of zone length for these two coating concentrations. Lower velocity indicates a stronger interaction between cell and surface molecules. As expected, the longer the stimulation zone was and the higher the coating concentration was, the slower the cells moved on the ICAM-1 reporting zone (Figure 4-7), which suggested a more activated state.

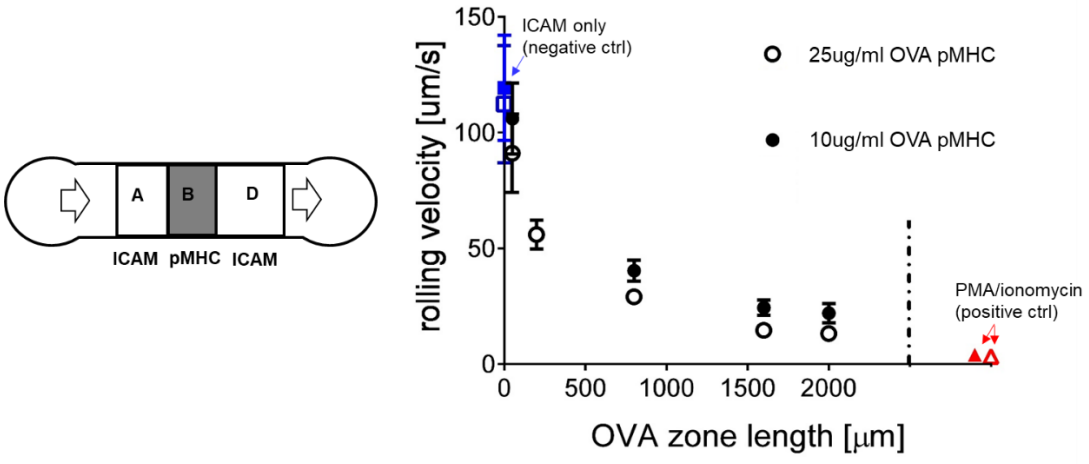

Figure 4-7 Activated OT1 T cell can roll on ICAM-1 in a mechano-dose-dependent manner. Velocity of T cells rolling on ICAM-1 (20 μg/ml) surfaces is plotted against the length of OVA zones. The stimulation zones with variable lengths were patterned with pMHC OVA concentrations of 10 μg/ml and 25 μg/ml. T cells were perfused in the chambers with a wall shear rate of 25 s^{-1}. Negative control of T cells on ICAM-1 surface without pre-stimulation was plotted at dose = 0 and positive control of T cells incubated with PMA/ionomycin for 10 min was plotted at right after dash line. Data are presented as mean ± sem of 15-20 cells. Experiment was repeated 3 times with consistent results.

It's reasonable to speculate that zone length corelates to the total time a cell is possibly allowed for stimulation and the density of the surface molecules corelates to the 'frequency' of a cell can interact to ligands. As 'time x frequency' is the total number of bonds a moving cell could possibly form, then the 'coating concentration × zone length' would also corelates to the total number of bonds that cells are allowed to bind. Thus, we plotted the rolling velocity of pMHC stimulated T cells on ICAM-1 surface against a combined stimulation dose factor 'coating concentration × zone length' (Figure 4-8 a). We observed the decrease of the velocity of T cells on ICAM-1 surface after a region of pMHC OVA, indicating a more activated state of the T cells. Interestingly, the velocity curves of all three OVA coating concentrations exhibited exponential decrease as the stimulation length increased. As they were plotted in the same combined 'stimulation dose' axis, these curves collapsed into one exponential decay curve. The negative control and the positive control were provided, by the velocities of the T cells on the ICAM-1 surface without stimulation and of the T cells pretreated with the PMA/ionomycin (which activates T cells to fully activated state), respectively. This supported our hypothesis of the effect of the two factors on T cell activation dose.

We further assessed the effect of other pMHC ligands beside OVA. Q4R7 and Q4H7 are two alterations of OVA peptide and have lower affinity and potency to OT1 T cells [108]. We compared the velocity curve of the T cells on ICAM-1 after stimulation by these two pMHC with the fitted exponential decay curve of T cell velocity stimulated by the OVA (Equation 2) (Figure 4-8 b). Notwithstanding the fact that both Q4R7 and Q4H7 stimulated T cells had lower velocities compared to the OVA stimulated cells, Q4R7 curve, had a similar fitted 'steady state' velocity as OVA fitted curve (Equation 3), but not Q4H7 curve (Equation 4). This suggests that the velocity of T cells with a sufficient stimulation of Q4R7could potentially reach as low as OVA stimulated cells, while Q4H7 curve, conversely, could not reach the same rolling velocity even with abundant stimulation (fitted 'steady state' velocity of ~ 55 $\mu m/s^{-1}$ in Equation 4). This difference could be related to the pMHC binding kinetics for the fact that T cells bind to both OVA and Q4R7 with a catch-bond, but to Q4H7 with a slip-bond [111].

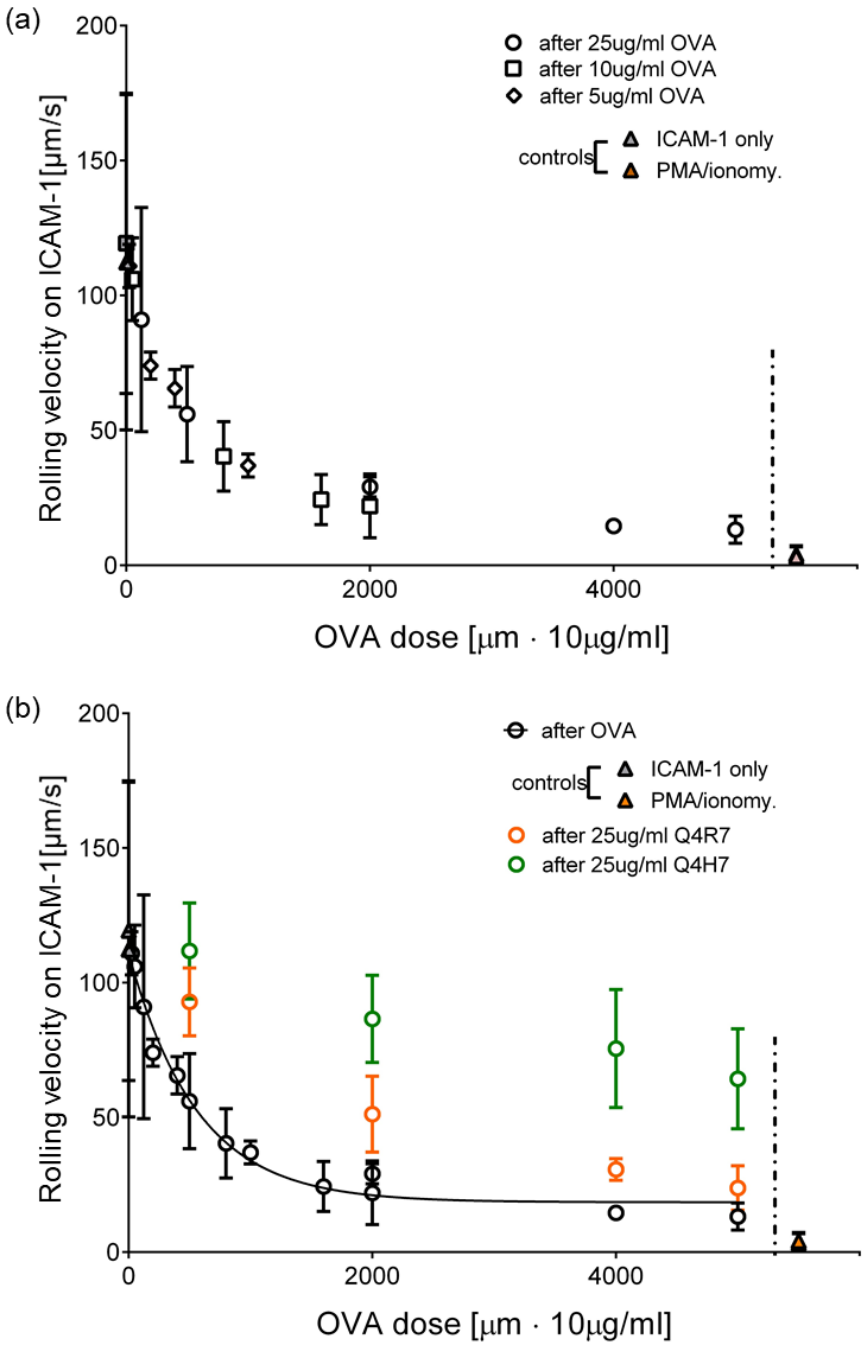

Figure 4-8 Stimulation factors for pMHC activated T cell rolling on ICAM-1. a) Velocity of T cells rolling on ICAM-1 (20 μg/ml) surfaces is plotted vs. mechano-dose (characterized by the length of stimulation zone times coating concentration). The stimulation zones with variable lengths were patterned with various pMHC OVA concentrations from 5 μg/ml to 25 μg/ml. T cells were perfused in the chambers with a wall shear rate of 25 s^{-1}. Negative control of T cells on ICAM-1 surface without pre-stimulation was plotted at dose = 0 and

positive control of T cells incubated with PMA/ionomycin for 10 min was plotted at right after dash line. b) Rolling velocities of T cells stimulated by two weaker ligands were compared to OVA. One exponential fitting was done to collapsed OVA stimulation curves (black). Data are presented as mean ± sem of 15-20 cells. Experiment was repeated 3 times with consistent results.

$$V_{rolling} = 96.1 \times e^{-0.001826x} + 18.2$$

Equation 2 Velocity fitting of T cell activated by OVA

$$V_{rolling} = 97.8 \times e^{-0.001323x} + 17.7$$

Equation 3 Velocity fitting of T cell activated by Q4R7

$$V_{rolling} = 67.1 \times e^{-0.000864x} + 58.9$$

Equation 4 Velocity fitting of T cell activated by Q4H7

We first demonstrated the interaction of the T cells to the surface immobilized pMHCs by measuring the velocity and adherent cell on pMHC surfaces. Instantaneous velocity of the T cells of each behavior was provided to further confirm the rapid re-binding behavior of the T cells to the surface pMHC OVA. An activation of the T cells by the pMHCs, especially by OVA, were observed by measuring the increased adherent cells on ICAM-1 surface with OVA concurrently at present or separated in a multi-zone device.

We then assessed the velocity of the T cells on ICAM-1 surface in a pMHC stimulation does-dependent manner, by varying the length of stimulation zone and coating concentration. Different activated integrin behaviors were observed for various pMHCs by fitting velocity curves for the ultimate rolling velocity of various pMHC stimulations. Hence, we demonstrated that T cells interacts with surface pMHCs and this interaction activates integrin LFA-1 in a dose-dependent and pMHC-dependent manner.

4.5 Calcium response of pMHC-stimulated T cells

Since calcium is an immediate downstream signal from TCR activation (within minutes) [113, 114], we further monitored the calcium flux of the T cells upon stimulation of the pMHCs to confirm the activation and investigate the different resulting behaviors by these pMHCs. Mouse OT1 T cells carrying calcium indicating dye (Fluo-4) were perfused into microfluidic channels coated with different pMHCs (25 μg/ml) for a distance of 800 μm and monitored under epi-fluorescent microscope at a frame rate of 0.5 f/s and exposure time of 200 ms (Figure 4-9). Negative control of BSA blocked surface were provide for each condition as a reference. In general, the calcium flux magnitudes were as expected, strongest for OVA stimulated cells (Figure 4-9 a) and less for other alterations. Q4R7 (Figure 4-9 b) was the closest to OVA among all alternations and G4 (weak pMHC, Figure 4-9 d) and VSV (irrelevant pMHC, Figure 4-9 e) did not show a significant difference compared to BSA blocked surface. This suggests that the strength of TCR binding translates to downstream signaling.

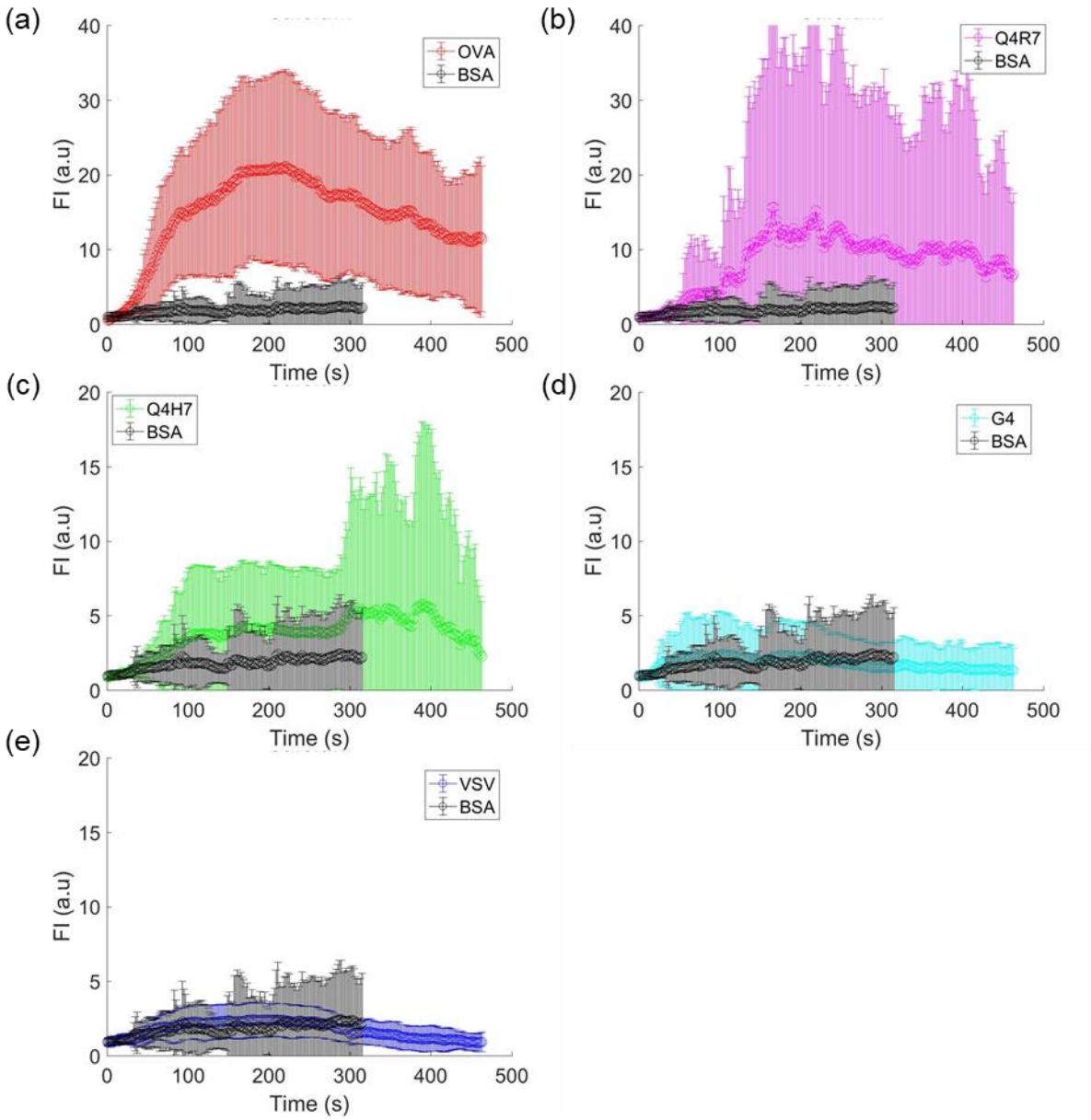

Figure 4-9 Calcium of pMHC-stimulated T cells indicates activation. Calcium flux of OT1 cells upon stimulation of pMHC a) OVA, b) Q4R7, c) Q4H7, d) G4, and e) VSV. BSA control (black) served as a reference for each condition. Data are presented as mean ± se of 15-20 cells. Experiment was repeated 3 times with consistent results.

We next quantified the calcium flux data on the single cell bases to further investigate the effect of each pMHC by assessing the peak calcium intensity (Figure 4-10 a), the area under curve (Figure 4-10 b) of each cell, and the response ratio of the calcium flux curve of the population (Figure 4-10 c). The general trend was as observed in calcium trace where OVA stimulated cell showed the strongest response and less for other alternation pMHCs. Additionally, this analysis illustrated the reason of the different activation level upon various pMHCs. The fact that cells upon OVA (or Q4R7) stimulation were more activated appeared in calcium response in two ways: 1) the stronger response, which was shown by the peak intensity value and the area under the curve, 2) the higher percentage of responder cells, which was shown by the response ratio of the cell.

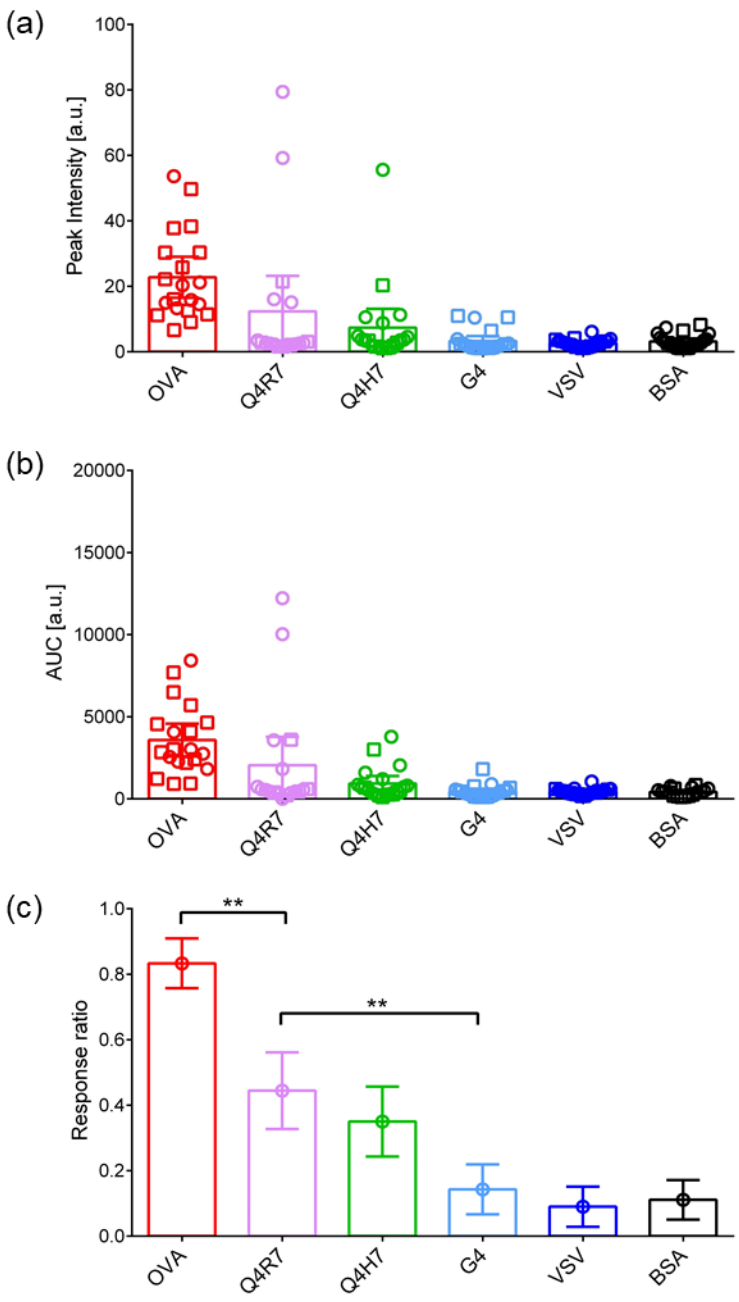

Figure 4-10 Quantitative analysis of calcium response upon various pMHC. T cell calcium flux data from Figure 4-9 were analyzed and plotted by a) calcium peak intensity and b) area under curve for single cells (each dot for one cell), and c) cell response ratio of all collection. For binomial distribution with event probabilities Pk, an estimate of the i-th event probability was set as the associated standard error s.e.m. *, **, * and **** denotes p < 0.05, 0.01, 0.001 and 0.0001, respectively, by Student t-test.**

To understand the difference of the pMHC stimulated activation and non-specific activation of T cells, we assess the calcium flux of anti-CD3 antibody stimulated T cells with or without flow condition. Microfluidic channels were coated either with OVA (25 μg/ml) or anti-CD3 antibody 2C11 (50 μg/ml). BSA blocked channels served as a negative control and reference. Surprisingly the 2C11 stimulated T cells, which usually serves as 'positive control' for stimulation, had lower calcium flux level compared to OT1 T cells with flow condition. When we investigated the effect of the flow to triggering the calcium flux, OVA stimulated cell demonstrated a significant lower calcium flux without experiencing the flow compared to cells that experienced flow; yet the 2C11 stimulated cells did not shown a sign of magnitude difference whether they experienced flow before videoing. This coincided with the fact that binding of anti-CD3 antibody to T cells do not require force to trigger stimulation, thus providing additional evidence that force between pMHC and TCR facilitates the T cell stimulation.

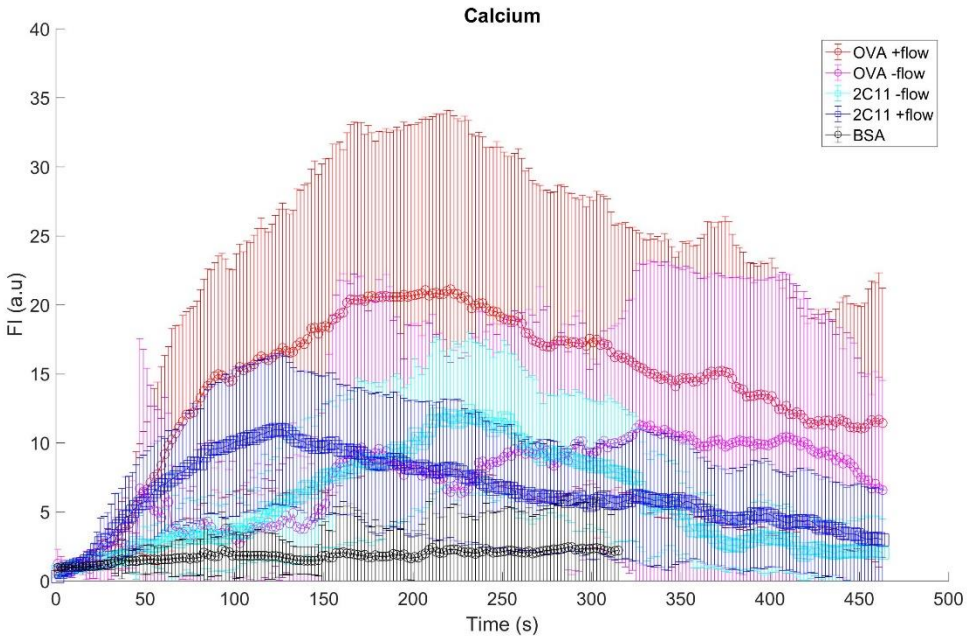

Figure 4-11 Anti-CD3 stimulation triggers calcium with or without shear. Calcium fluxes of anti-CD3 antibody 2C11 and pMHC OVA stimulation were compared with or without flow condition. Data are presented as mean ± se of 15-20 cells. Experiment was repeated 3 times with consistent results

4.6 Conclusion

In this chapter, we demonstrated the activation conditions of T cells by specific pMHC and characterized the resulting rolling behavior of pMHC activated T cells. We first demonstrated the rapid rebinding of TCR-pMHC interaction by assessing the T cell moving velocity (for mean velocity and instantaneous velocity) and adherent cell density on immobilized pMHC surface under flow condition. T cell activation was then observed when cells were exposed to OVA and ICAM concurrently or spatially separated in multi-zone device. A further investigation on the mechanical stimulation dose of the immobilized pMHCs was conducted by varying the coating concentration and length of stimulation zone.

By fitting the activation resulted rolling velocity of T cells on ICAM-1 surface, we demonstrated the ultimate velocity differences of various pMHCs. Together, we demonstrated that T cells interact with surface pMHCs and this interaction activates integrin LFA-1 in a dose-dependent, pMHC-dependent manner. Furthermore, calcium flux of T cells upon various pMHC stimulation revealed two reasons of the difference activation behavior: the response intensity level and percentage of the responder cells upon stimulation. We demonstrated the effect of the force between TCR-pMHC interaction by monitoring the calcium flux of T cells after experience a shear condition or always in a stationary condition. Compared to anti-CD3 antibody stimulation which does not require a force, T cell stimulated by OVA pMHC showed a higher calcium flux magnitude when experiencing shear. This suggests that the force is an integral part of TCR-pMHC engagement and signaling. This study adds more evidence to T cell triggering models with repeated bindings under force. Further studies on instantaneous signaling monitoring during interaction will better define the triggering mechanism.

CHAPTER 5. ENGINEER MICROFLUIDIC PLATFORM TO SORT ANTIGEN-SPECIFIC T CELLS BASED ON ROLLING BEHAVIOR RESULTING FROM TCR-INTEGRIN CROSSTALK

5.1 Introduction

T cells' critical role in adaptive immunity makes it important to assess T cell phenotypes and functionality in both fundamental study [115, 116] (such as pathogenesis [117], tumor immunology [118] and autoimmunity [119]) and clinical practice [120-122] (such as vaccine targeting [123] and immunotherapy evaluation [121, 122]). Enumeration of certain antigen-specific T cells provides information of the patient's healthy state as target T cell may proliferate as the cognate antigen grows [122]. Sorting and *in vitro* expansion of the certain target T cells have a great value in adaptive immune therapy as the effective T cells originate from the patient so cause no transplantation rejection response.

Antigen-specific T cells upon activation give rise to surface marker activation and subsequent effector functions such as cytokine production, cytotoxicity, differentiation and proliferation. Literature has shown that high adhesion affinity of TCR-pMHC binding is not for sure leading to T cell functioning [124]. Conventional approaches to identify and separate specific T cells are usually based on the adhesion strength of TCR-pMHC interaction, such as the use of multimerized pMHC with a fluorophore [125-128]. With the increase of the multimer number, sensitivity of the TCR recognition advances [127]. However, the nature of this approach results in the lack of the assessment of the T cell

functionality. Therefore, additional functional tests are required to validate the selected cells, such as activation biomarker expression and cytokine releasing. Recently researchers also applied the activation property of integrin LFA-1 to antigen-specific T cell selection in a flow cytometry-based assay by pre-incubating lymphocytes with peptide induced APCs for a time from minutes to hours [129]. This approach overcame the low affinity of TCR-pMHC by using a tetramerized ICAM-1-fluorochrome complexes to bind to activated integrin. However, optical based assays are limited in the number of antigen specificities aby the spectral overlap since physiological polyclonal T cells have a spectrum of responses. In addition, serial flow cytometry for detection is restricted by the sample size. Alternative to flow cytometry-based detection and sorting, microfluidics provides easy operation on cell manipulation and module compatibility, allows small sample size (~10μL to 10mL) and high throughput.

Microfluidic devices for cell sorting have been developed for various kinds of cell selection [130-133]. Majority of them are based on the physical properties of target cell such as size [134-136], density [137], stiffness [138] and electromagnet property [139]. Sorting approaches based on the cell adhesion have been developed in recent decades [140-143], yet focused on the interactions of adhesive molecules [73] such as selectin [73] and integrin whose affinities (K_D~0.1 μM to ~1 μM [144]) are much higher than signaling interactions like TCR-pMHC (K_D ~1 μM to ~100 μM [145]). In this chapter, we developed a microfluidic platform that exploited the rolling properties of activated integrin (learned in CHAPTER 4) to facilitate T cell sorting. With the microfluidic power of precise protein patterning, cell manipulation, and module-compatibility, this platform consists of an activation zone for antigen-specific T cell activation and a sorting zone for responsive cell

selection. In the rolling sorting manner, the sample was fed into the device and collected without stop. This continuous sorting motion not only permits a potential high throughput but also simplifies the operation and allows extra microfluidic modules for immediate follow-up test. This system has potential advantages for follow-up target cell screening and function evaluation.

5.2 Materials and methods

5.2.1 Chemicals and proteins

RPMI 1640 1X w/ L-glutamine was from Corning Inc. (Corning NY). Mouse Erythrocyte Lysing Kit was from R&D systems (Minneapolis, MN). Molecular Grade Water was from Corning Inc. (Corning NY). Trypan Blue was from Sigma-Aldrich (St. Louis, MO). Mouse CD 8+ T cell enrichment kit was from STEMCELL Technology (Cambridge, MA). Recombinant mouse ICAM-1-Fc chimera was from BioLegend (San Diego, CA). EZ-Link™ NHS-PEG4-Biotin was from ThermoFisher Scientific (Waltham, MA). pMHCs (including OVA, Q4R7, Q4H7, G4, VSV) were from Emory NIH tetramer core facility (Atlanta, GA).

5.2.2 Primary mouse T cell purification

The methods of mouse T cell purification from both OT1 transgenic mouse or wildtype B6 mouse are the same as in 4.2.2 (Primary mouse T cell purification). Briefly,

mouse spleen was collected for grinding and RBC lysis, followed by a negative purification of CD8 T cells with mouse CD8+ T cell enrichment kit (STEMCELL Technologies) with the EasySep protocol.

5.2.3 Microfluidic device fabrication

Devices were molded from silicon wafers in polydimethylsiloxane (PDMS, Corning Sylgard 184, Midland, MI) by standard soft lithography. Stamping PDMS was made from a 25 μm-thick one-layer wafer fabricated in clean room (IEN, GT) with negative photoresist (SU8 2025, MicroChem). Sorting device was from a two-layer wafer with a 12 μm-thick first layer and 13 μm-thick a second layer. The features on the transparency mask were transferred with UV photolithography. The surface of wafers was treated with tridecafluoro 1,1,2,2-tetrahydrooctyle-1-trichlorosilane vapor from United Chemical Technologies (Lewistown, PA) to facilitate release of PDMS from the mold. A mixture of PDMS (PDMS base and crosslinker in a 10:1 ratio for sorting device and 5:1 ratio for stamp) was poured on the mold and the whole preparation was left for curing for 2 h at 75 °C. The PDMS pieces were cut into shape and the device PDMS were punched using 19-gauge needles in inlets/outlets holes while stamp PDMS not. Instead stamp PDMS was treated with plasma before gently covered with protein solution, incubated in DI water sprayed petri-dishes for 1 hour at RT. Protein solution was then washed off with DI water and the stamp dried in air before transferring the protein to substrate surface.

5.3 Design criteria

We have demonstrated in the Chapter 4 that T cells can be activated by the immobilized pMHC on surface and resulted in rolling on ICAM-1 surface. We also

demonstrated that activated LFA-1 on neutrophils can support lateral movement on inclined ICAM-1 surface. It is reasonable to suppose that rolling behavior of activated T cells on ICAM-1 surface could also lead to a lateral movement if the inclined ICAM-1 stripes are patterned. Together, the study before provided a foundation to the feasibility of a platform that recruits the activated LFA-1 to amply the difference of antigen-specific T cells with non-specific cells, where TCR-pMHC interaction usually has a low affinity (K_D ~1 μM to ~100 μM) [145] compared to activated integrin (K_D ~0.1 μM to ~1 μM) [144]. With the activation of the adhesive molecule LFA-1, T cells can more reliably adhere to target surface or slowly roll, but the specificity remained due to the activation specificity. Rolling neutrophils can move laterally on an pattern of inclined stripes of selectin [146] and ICAM-1 (CHAPTER 3). We hypothesized that same integrin LFA-1 can also support T cell rolling laterally upon activation.

Our platform design requirements are based on the application of distinguishing target cells from a polyclonal population. The target T cells in a mixed population should be specifically activated by its specific pMHC to a state where LFA-1 on the surface could roll on ICAM-1 surface. The activated T cells in the polyclonal population are then delivered to the next module, sorting zone, where interacting T cells roll on the ICAM-1 surface. The requirement for the activation module is to fully activate the target cells, so a sufficient contact between cell and the pMHC needs to be guaranteed. The requirement for the sorting zone is to selectively distinguishing target cells from the rest T cells and a continuous separation of the cell populations is preferable.

5.3.1 Scheme of the activation and sorting steps

To achieve activation and selection of target T cells, we designed the two-module device as in Figure 5-1. Target T cells in a polyclonal population will be stimulated in the activation zone where an array of pillars is designed to increase the contact surface area and allow collisions between the T cells and the pillars to facilitate the TCR-pMHC interactions. After activation of the target T cells by the specific pMHC in activating zone, cells will be delivered to the sorting zone where the surface is functioned by inclined ICAM-1 stripes. Whereas the activated LFA-1 can interact with the ICAM-1 surface, at the edge of each stripe, T cells see two distinct areas: ICAM-1 surface and BSA-blocked surface. With an uneven interaction between cells and the surface, cells will be guided to move along the stripe edge, thanks to the flow shearing force along the channel. Hence, a lateral movement is achieved only in the interacting cells besides the longitudinal movement, while nontarget cells stay on the original side as the buffer is kept perfusing. At the end of the sorting zone, the target cells will be collected at the ‘collection outlet’ and rest cells at the ‘discard outlet’.

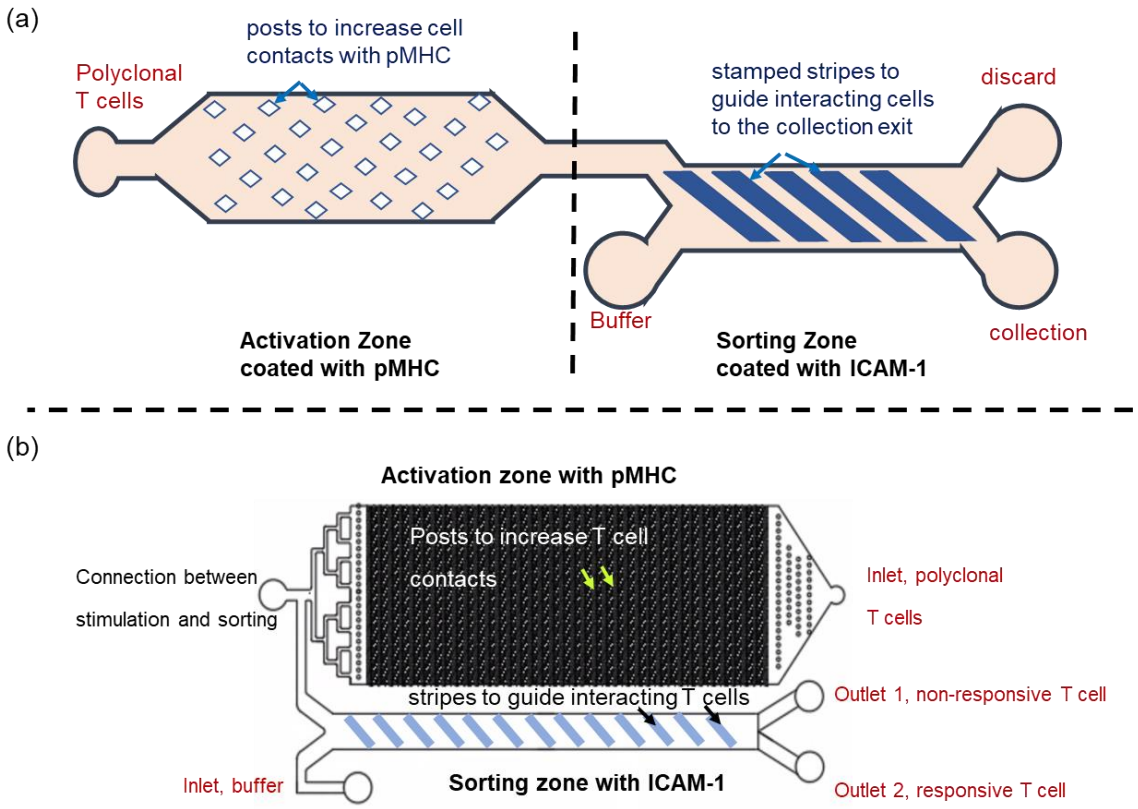

Figure 5-1 T cell sorting platform. a) Scheme of the platform. It consists of two parts: activation zone (left) coated with target pMHC and sorting zone (right) coated withICAM-1. Pillar array is designed to increase the contact surface area in activation zone inclined stripes is stamped to guide the target cells to move laterally in the sorting zone. Two inlets: cell inlet and buffer inlet. Two outlets: collection outlet and discard outlet. Two zones can be separated. b) real device design. The two zones wrapped up to fit the substrate size. The connection outlet/inlet was for the coating feasibility of the two part with two different protein patterns.

5.3.2 Fabrication and experimental set-up

Device was molded from a two-layer master (silicon wafer, features fabricated with negative photoresist SU8), where pillars (h = 25 μm) in activation zone (Figure 5-1 a) were through the ceiling to the bottom while ridges (h = 13 μm) in sorting zone (Figure 5-1

b)were only on the ceiling. Matched stamp PDMS was used to pattern the inclined stripes of protein on the surface of the sorting zone. After protein ICAM-1 stamped on the surface of sorting region, markers were made to indicate the locations of the stamp pattern for the assembling of the device. Device PDMS was also treated with plasma before make contact with the glass substrate. Once contacted, activation zone was then coated with pMHC by perfusing the solution from the inlet to the 'coating outlet' without contamination to the sorting zone, and incubated for 1 hour. The blocking protein BSA was at last introduced to the whole device with the 'coating outlet' blocked. The 'coating outlet' was then blocked for the whole experiment.

Cell solution and buffer were delivered to the device by syringe pump, which was controlled by a MATLAB program (code in Appendix C).

5.4 Activation region

5.4.1 Pillar array design and simulation

Although a pillar array significantly increases contact area, a good design of the pillar array is required to have sufficient collision rates. The shape of the pillars was designed as diamond instead of traditional round to eliminate the cell sticking at the stagnation point. 5 designs based on the design criteria in literature [147] were fed into the COMSOL simulation. An example of the simulation result of the design #1 was shown with the red lines indicating streamlines (Figure 5-2 b). Streamlines were plotted 10 μm apart (on the order of a cell size) to illustrate all possible the location of the original cell. With every streamline illustrated has efficient collisions to the pillars ('collision' defined as a distance < 3 μm to a pillar), it means a cell could form sufficient collisions to the pillars

regardless of the starting position in the chamber. The criteria for sufficient collisions is defined as one collision of a cell to pillars in every 4 rows. By this criteria, three designs were selected for experimental test (Figure 5-2 a).

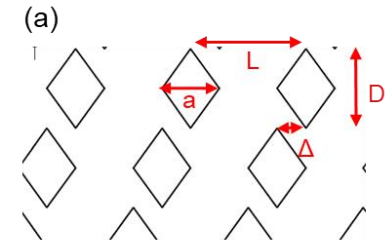

	L	D	a	Δ
#1	100	100	50	25
#2	100	150	50	40
#3	150	200	50	40

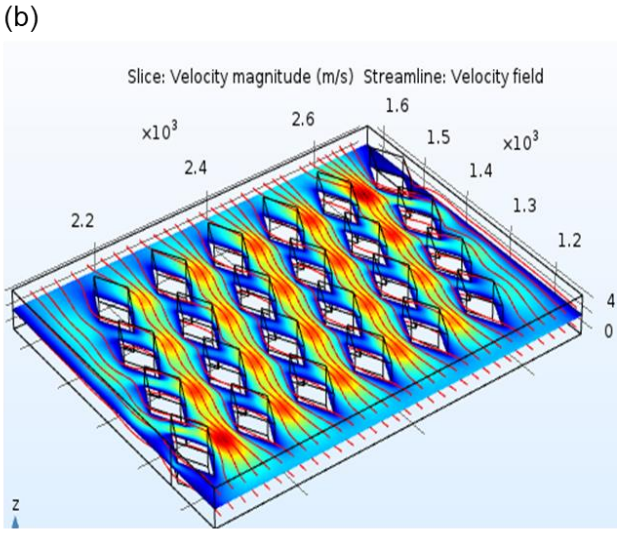

Simulation: collision in every 4 rows

Figure 5-2 Simulation identified the feasibility of the pillar array designs. a) illustration and parameters of the three designs; b) example of the simulation result on design #1. Red lines were streamline 10 µm apart.

We then tested the collision rate of the 3 designs (Table 5-1) whose collision rate was confirmed by the COMSOL simulation. Efficient collisions (at least 1 collision in every 4 rows) were achieved experimentally for all three, indicated by the distance of a cell centroid to pillar surface ≤ 3.5 µm (typical radius of mouse T cells is 3 µm). However, a design with bigger sizes yields bigger chamber size for activation, which limits the throughput of the sorting assay. Considering both the collision number over the entire device and the cell clogging issues, Design #2 were selected for the rest of the experiments.

collisions	2min chamber	5min chamber	Clogging issue
#1	~56	~140	cell clogging
#2	~36	~90	rare
#3	~25	~63	very rare

Table 5-1 Experimental quantification of the collision rate revealed sufficient cell-surface contact. Collision rate of each design were presented of 15-20 cells from different starting locations.

5.4.2 T cell activation characterization after activation region

To design the right size of the activation zone so to enable both activation and throughput, we assessed the time for T cells activation in microfluidics. A cell trap device [148] was applied study T cell activation by measuring the calcium flux trace of individual cells (Figure 5-3 a). Device was coated with specific pMHC and T cells were trapped in stationary condition to have contact with the surfaces. Calcium trace of individual single cells revealed a rise of calcium activation from 120 s to 240 s. Note that calcium is an upstream signal for LFA-1 activation and that this experiment only indicates the activation of T cells under stationary condition, while an activation under flow condition may be faster with shear force involved. However, this experiment provided an order of magnitude estimation of the activation of the T cells.

We then designed two activation zone chambers with the pillar array #1 and lengths that allows 2 min and 5 min travel of the T cells under a shear condition of 25 s^{-1}. Activation

was defined as calcium intensity reach 2x of the mean of the original population. Only target cells were perfused into the chamber and the ratio of the activated cells of the outlet were plotted (Figure 5-3 b). While 2min-chamber already allowed an activation ratio of ~70%, a 5min-chamber enabled majority (~85%) of the population activated.

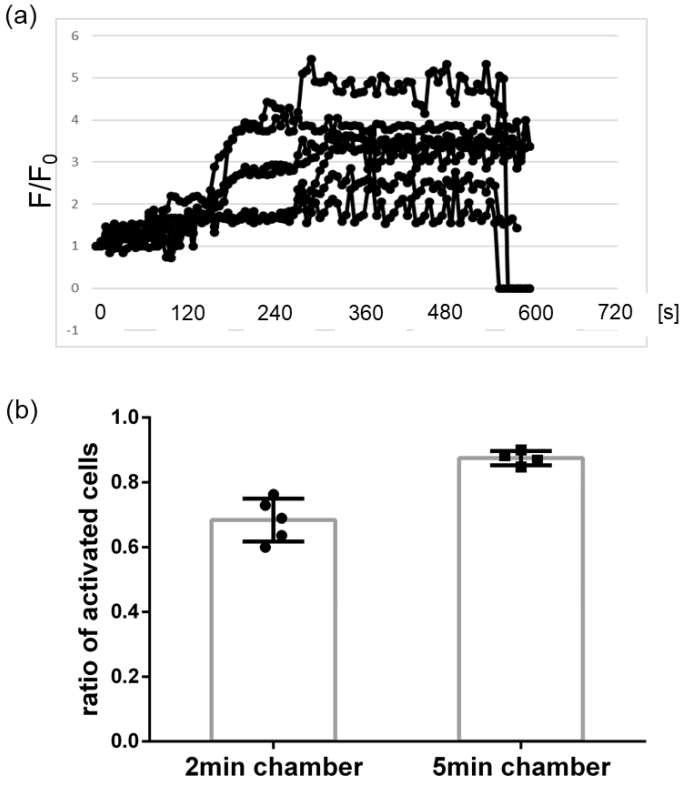

Figure 5-3 Cell activation by calcium flux was realized in activation chamber. a) calcium flux of the T cells in cell traps. Data are presented as the traces of 8 cells. Experiment was repeated 3 times with consistent results. b) ratio of activated cells for two activation zone designs indicated by a calcium intensity 2x of the original mean intensity. Data are presented as mean ± se of 4-5 experiments. Each dot indicates one experiment.

With assessment by both simulation and experimental test, we selected three designs for pillar array that enables sufficient collision rates. One of them was finally

chosen due to the collision per length efficiency. Cell trap calcium monitoring allowed a good estimation of the time course of T cell activation. A further validation was achieved by two length designs of the activation chamber. With these, an activation ratio of ~85% was achieved in the activation zone.

5.5 Sorting region

The purpose of the sorting region to laterally move the activated T cells to the collection side and keep the non-interacting T cells in the original side (namely the discard side).

5.5.1 Analysis of T cell rolling in inclined stripe area

To facilitate cell rolling laterally, several parameters are critical to link cell rolling ability to rolling trajectories and lateral displacement: coating concentration, angle of the inclined stripes and flow pattern. We first assessed the lateral movement of the pre-activated T cells by measuring their trajectories on four different patterns of ICAM-1 stripes: 5˚, 20˚, 45˚, 60˚ (Figure 5-4, a). Note that the ICAM-1 stripe patterns were stamped on the surface by manual alignment and a misalignment of ~3˚±1.5˚ was observed in 10 times alignment measurements by imaging the off-alignment of target mask pattern and stamp position. Videos of the cells moving under a flow of 25 s^{-1} were taken for analysis of the individual cell trajectory by ImageJ. The angle of the individual trajectories in reference to the horizontal direction were also measured in ImageJ and quantified in Figure 5-4 b. The green mark for 45˚ and 60˚ highlighted the feasibility of the use of these two

designs. With an angle degree of 2˚ over a sorting region with 3 cm, target cells are able to travel 1 mm laterally according to calculation. Considering the fact that cells are not always in contact with the surface and by some conditions move to the stream above surface, we designed a 5 cm long sorting region to enable lateral movement.

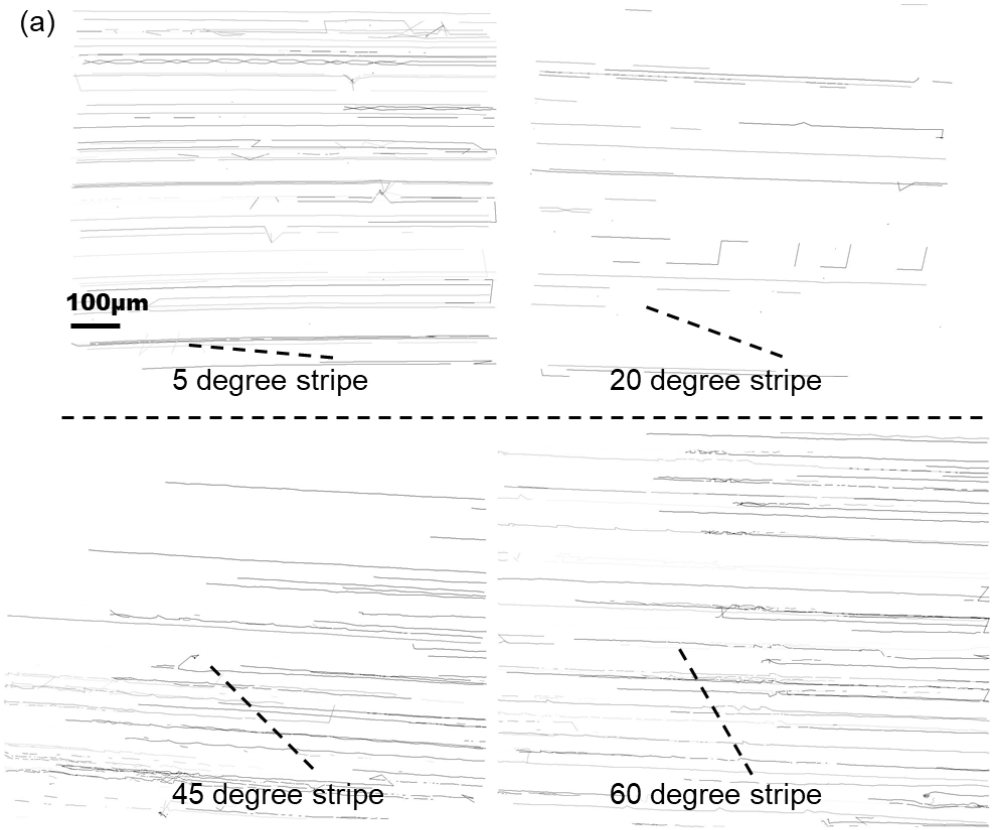

(b)

Stripe angle	5	20	45	60
Trajectory angle	0-0.05	0-0.5	0-3.5	0-2.5

Figure 5-4 Stripe inclination angles affected activated cell lateral movement. a) Four examples of cell trajectories for indicated stripes of patterned ICAM-1. Each line illustrated a single cell. scale bar: 10 μm. b) quantification of the trajectory angles for each design.

5.5.2 Sorting platform design and experimental setting

In general, although a surface interaction could allow cell lateral movement, only a small fraction of cells interact with the surface, whereas the majority of the population remains in the flow stream. A shallower channel could force the cells to make contact with the surface; however largely increases additional clogging issues. We designed an array of ceiling ridges that are perpendicular to the flow direction to force cells making a contact with the surface and allowed enough space in between eliminating clogging issue (Figure 5-5, a). Design parameters were listed in Figure 5-5 b.

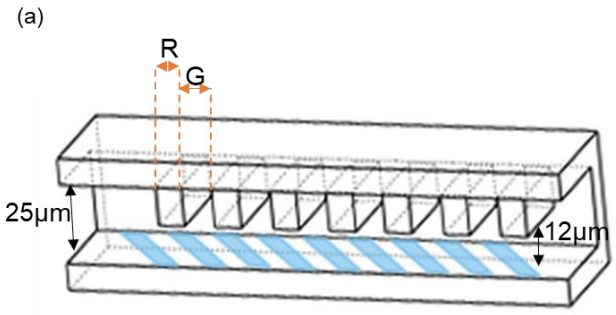

(b)

Designs	#1	#2	#3	#4
ridge (R) (μm)	50	100	200	250
gap (G) (μm)	200	300	200	500

Figure 5-5 Ceiling ridge design in the sorting zone. a) cross-view illustration of the sorting zone. Blue stripes on the bottom indicated stamped ICAM-1 patterns and ridges on the ceiling were perpendicular to the flow direction. b) designed ridge parameters for difference cell sizes.

To determine the suitable coating concentration for cell lateral movement, we assessed a set of coating concentrations for stamping ICAM-1 surface. Pre-activated T cells were delivered into a 5cm-long channel where surface coated 45˚ ICAM-1 stripes. The lateral movement was quantified by the ratio of the cells ending up at the collect outlet out

of all (Figure 5-6). The lateral movement was observed to have a significant increase when the coating concentration was increased at 5 µg/ml and saturated from 10 µg/ml to 30 µg/ml. A decrease of the lateral movement occurred at 50 µg/ml, largely due to the depletion of the firm adhesion of the interactive cells on the surface, showed by a decrease of cell number at collection outlet but no sign of change at discard outlet. Thus, a range of 10 µg/ml to 30 µg/ml coating concentration was selected for our sorting zone patterning.

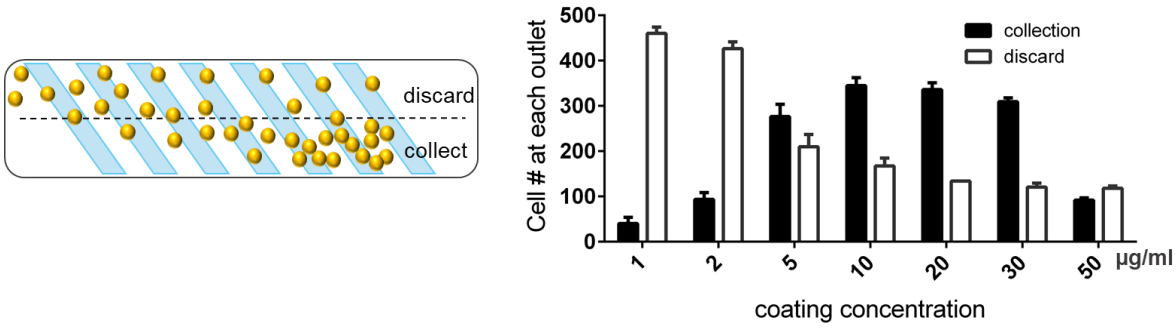

Figure 5-6 The concentration of ICAM-1 affected the lateral movement of target T cells. Ratio of lateral movement was depicted as collect/total (left). Flow left to right. Data are presented as mean ± se of 3 experiments. *, ** and * denote p < 0.05, 0.01 and 0.001 by Student t-test.**

5.5.3 Stop-flow pattern facilitate cell-surface interaction

The portion of cells missed the opportunity to interact with surface at the trade-off between increase cell contact and eliminating clogging (when channel is too shallow). Cells are uplifted away from the surface in a Poiseuille flow condition by the Segré–Silberberg effect [149, 150]. Without inducing the clogging issue, another way to increase contact is to diminish the Segré–Silberberg effect by settling cells on the surface without flow. However, cell settlement on the surface without flow may cause firm adhesion instead of

rolling, and a flow force is still necessary to cell lateral movement. Thus, we introduced the Stop-flow pattern to facilitate cell contact and resume flow once in contact (Figure 5-7).

We first assessed settlement of a cell when the flow stopped (Figure 5-7 a). The instantaneous velocity was measure frame by frame in 36 f/s video. The mean velocity of 5 cells decreased when the flow stopped at t = 10 s and finally reach complete stop at t = 20 s. A flow stops at least 10 s is preferable for the effect contact of a cell to the surface. We tested different Stop-flow patterns by measuring the lateral movement of the pre-activated T cells. The ratio of the two side of the channel was plotted at the beginning of the channel (~ 1 for a even distribution from a common inlet) and at the end of the channel for different patterns (Figure 5-7, b, c). The patterns of a 15s stop with a 30s flow or 1min flow yielded best performance among all. We picked the 1min flow + 15s stop for the purpose of a higher throughput.

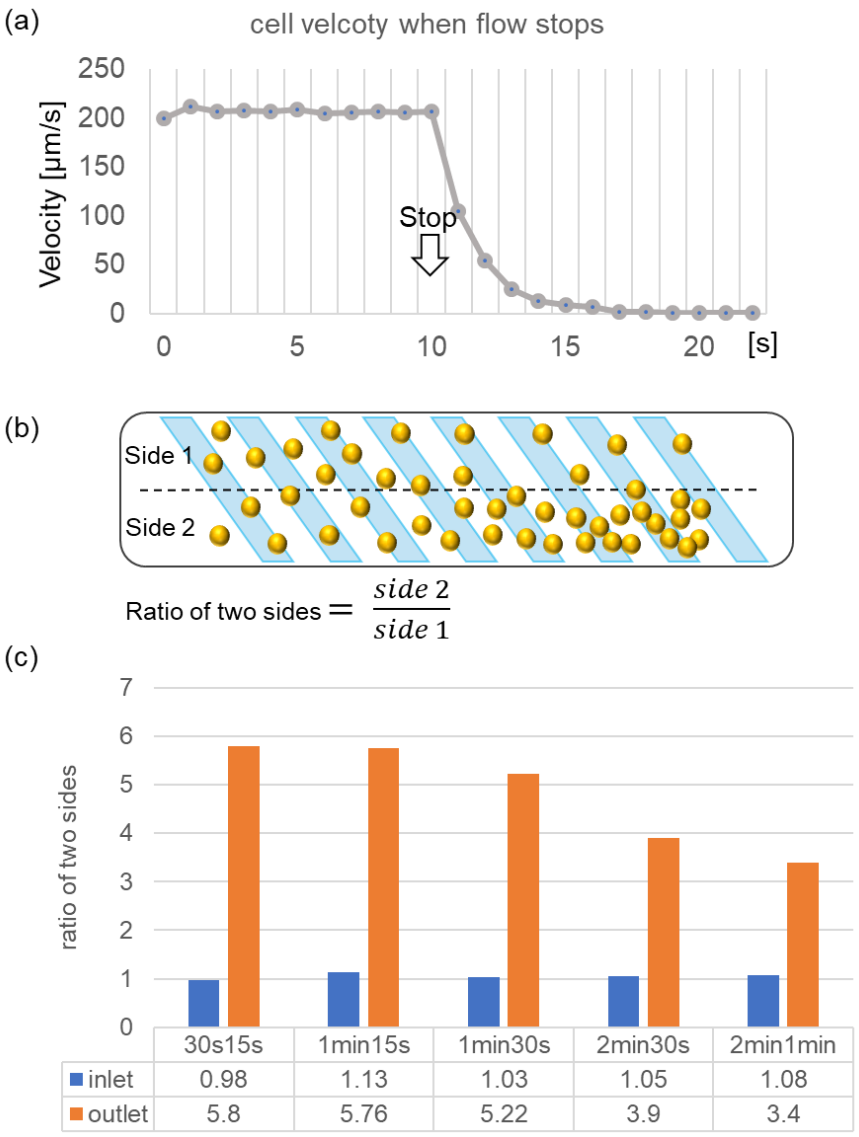

Figure 5-7 Stop-flow pattern allow better lateral movement. a) mean velocity of 5 cells in a flow-stop condition. Flow stopped at t = 10s. b) illustration of ratio of the two side, for an even distribution of cells, ratio = 1 at the beginning. c) ratio of two side plotted for five stop-flow patterns listed on the bottom. Exact numbers of ratios were listed in the table below the graph.

In this section, we assessed the angle and coating concentration of the ICAM-1 stripes on surface for cell lateral movement and employed ceiling ridges and Stop-flow

patterns to facilitate it. With these, we finalized the sorting region design and experimental setting.

5.6 Sorting performance

5.6.1 Mock sorting of target OT1 T cells from a mixture with B6 T cells

To demonstrate the sorting ability, we first assessed the lateral movement of the stimulated cells and non-stimulated cells in separate channels. The ratio of lateral movement was calculated as before, cells in collect outlet / total cells in both outlets (Figure 5-8, a). Stimulated OT1 T cells were activated prior in the activation zone coated with pMHC, whereas non-stimulated T cells experienced the activation zone with BSA blocking coating. The sorting platform yielded a lateral movement of ~65% for stimulated cell population and very specific to the non-stimulated cell population (< 3%). This justified the ability of this platform to distinguish cells able to interact and roll on ICAM-1 surface from the non-interacting cell.

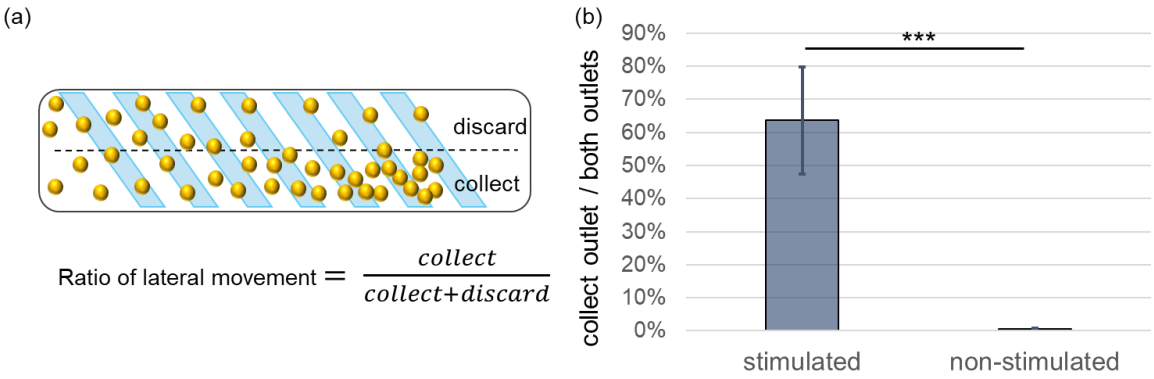

Figure 5-8 Lateral movement of the stimulated cells and non-stimulated cells. a) illustration of the ratio of lateral movement as collect/total. Flow left to right. b)

lateral movement of the stimulated and non-stimulated OT1 T cells. Data are presented as mean ± se of 3 experiments. *, ** and * denote p < 0.05, 0.01 and 0.001 by Student t-test.**

We assessed the sorting performance from a polyclonal population, by creating a mixture population of cells by target: non-target = 1:1. Buffer was delivered to main a flow on the collect side (Figure 5-9 a), so the cells only stay on the discard side if no lateral movement occurred. T cells from wildtype spleen of B6 mouse (Figure 5-9, a, blue) were incubated with a cell membrane dye CellTracker^{TM} for image, while T cells from transgenic OT1 mouse (Figure 5-9, a, yellow) were incubated with same volume of PBS buffer. Ratio of potential sorted cells for each population was calculated as number of cells on the collect side out of two sides. We imaged the cell locations every 1 cm along the region to assess the distinguishing ability (Figure 5-9, b), so to estimate the most economic location for collection. Although the absolute value of the ratio of sorted cell differed from day to day, the two cell populations can be distinguished in repeated experiments.

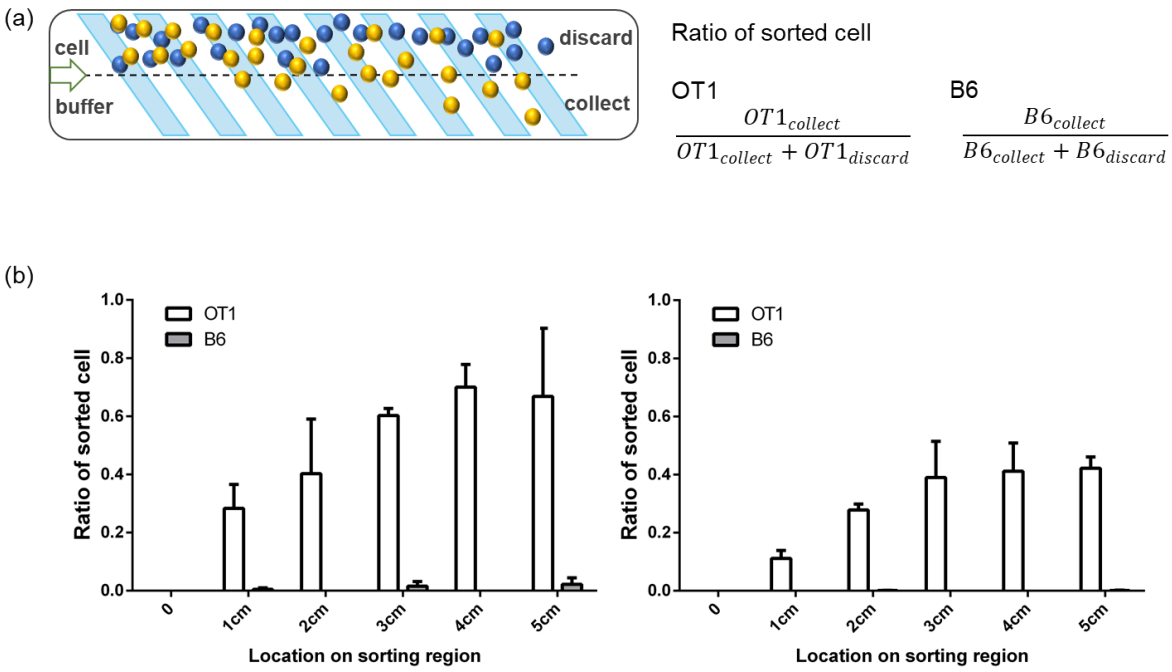

Figure 5-9 Primary OT1 T cells sorted from a mixture with non-target B6 T cells. a) illustration of the lateral movement and ratio of sorted cells for each population. b) Sorting performance of OT1 and B6 in a mixture on two separate days. Data are presented as mean ± se of 2-3 experiments. Experiment was repeated 3 times with consistent results.

We validated the antigen-specific T cell sorting in the platform by demonstrating the lateral movement of two populations in separate or mixed condition. OT1 T cells, which are specific to OVA pMHC [151], achieved 40%-60% sorting while non-specific B6 T cells remained in the original discard side (> 97%). Further purification is possible, for instance, by repeatedly application of the mixed population to the same sorting system, as many multi-stage separation processes do [152, 153].

5.6.2 Sort strong agonist activated T cells from weak agonist activated

Lateral movement of interacting cells is a continuous spectrum outcome before collected as ‘collect’ or ‘discard’. Therefore, this lateral movement-based device allows more than distinguishing target and non-target cells. A potential assay of enumerating and sorting several groups of T cells with various interacting ability to the surface can be illustrated. We assessed this ability by distinguishing two population of ‘targeted’ cells but stimulated by two distinct pMHCs that activates the T cells differently as shown in Chapter 4.

A mixture of OT1 T cells was created after inactive OT1 T cells experiencing strong pMHC OVA and weak pMHC G4 respectively in two activation zone (Figure 5-10, a). As before, a 1:1 ratio of mixture was delivered into sorting zone on the discard side when the buffer was perfused at the collect side (Figure 5-10, b). The ratio of the potential sorted cells for each population was calculated as number of cells on the collect side out of both sides. We imaged the cell locations every 1 cm along the region to assess the separation ability (Figure 5-10,c). To eliminate the potential effect of the cell tracker dye to the surface molecule interaction, dye application was flipped for the two populations in the experiment (dyed G4 stimulated cells on the left graph, OVA stimulated cells on the right). Significant differences started at the first monitoring spot (L = 1cm) and the differences persisted along the sorting region, which means a clear distinguishing between OVA stimulated T cells and G4 stimulated ones.

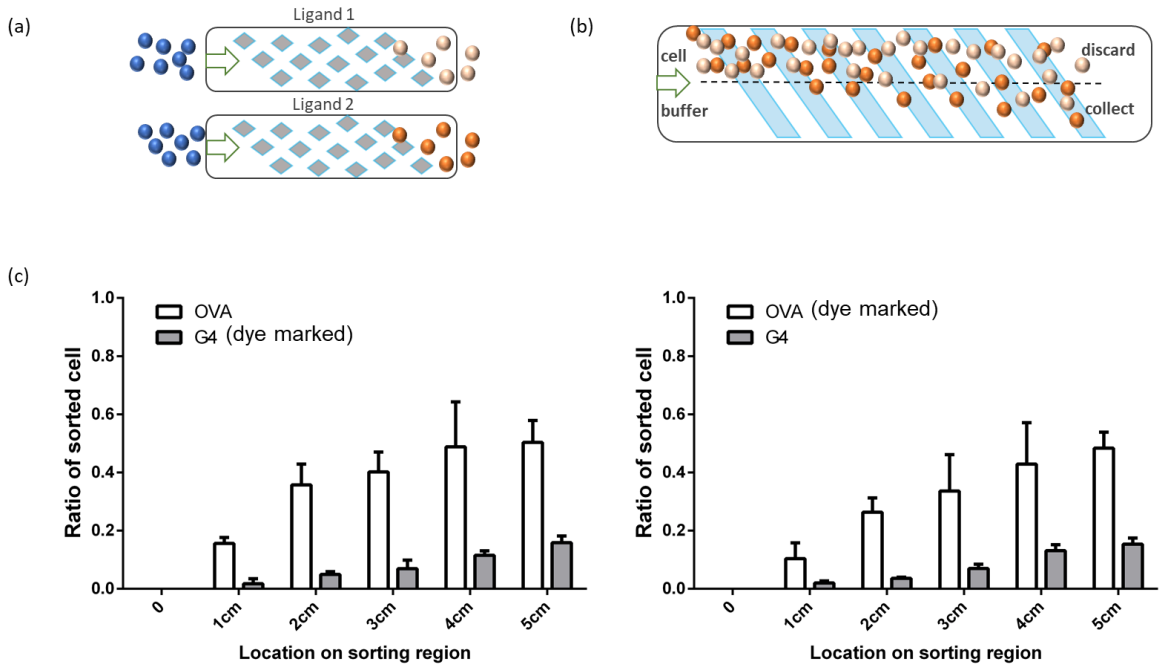

Figure 5-10 Distinguish OVA (strong ligand) stimulated and G4 (weak ligand) stimulated T cells. a) Two populations of the inactive OT1 T cells from same batch was activated in two activation chambers. b) The mixture of the two populations in sorting region. c) The ratio of potentially sorted cells for two populations along the channel. Data are presented as mean ± se of 2-3 experiments.

We further assessed the capability of the platform separating T cells with activation levels more similar to each other (Figure 5-11). In fetal thymic organ culture, pMHC Q4R7 was identified as the weakest negative selectors and Q4H7 as the strongest positive selectors [154], making Q4R7 and Q4H7 the closest selection ligands in affinity spectrum [111]. These two ligands were used in two separate activation chambers. Dye application was flipped for these two population in two separate experiment (dyed Q4H7 stimulated cells on the left graph, Q4R7 stimulated cells on the right). Started with a mixture of 1:1 ratio, the final collected population yielded an enrichment of target cell fraction from 50%

to ~55% of the stronger pMHC stimulated cells. These two ligands of similar activation potency defined the separation resolution of the system. However, additional iterations of enrichment may increase the enrichment further.

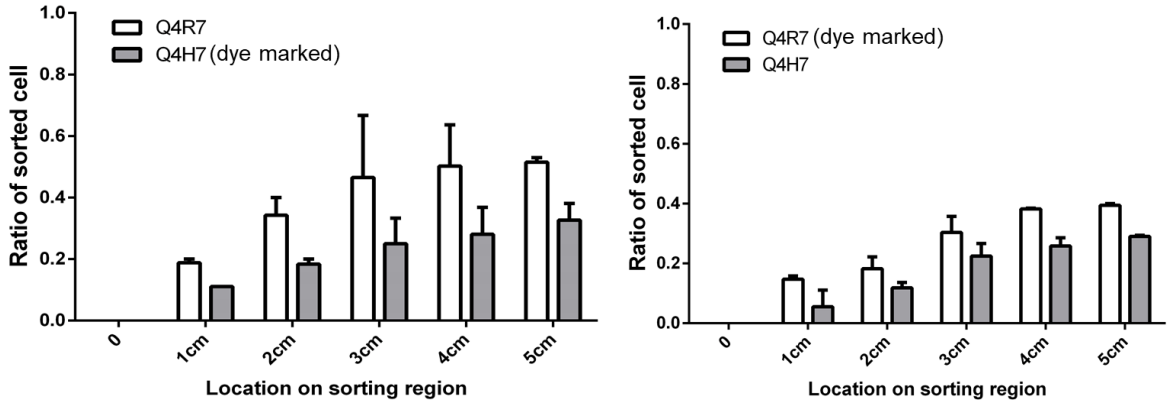

Figure 5-11 Assessment of the distinguishing capability by two populations stimulated by two pMHCs with close potency. The ratio of potentially sorted cells for two populations along the channel. Data are presented as mean ± se of 2-3 experiments.

We validated our hypothesis of distinguishing cells with different levels of activation, namely interactive ability to the stripes. A clear difference between OVA stimulated and G4 stimulated OT1 T cells were demonstrated in the sorting platform, where OVA stimulated T cells were significantly enriched from the original population. A test of the close-potency ligands (Q4R7 and Q4H7) were also applied for device capability assessment. Though enrichment of the cells stimulated by the stronger ligand was not as obvious, a difference between the two populations persisted throughout repeats with or without dye marker flipped.

5.7 Conclusion

In this chapter, I developed a platform for antigen-specific T cell sorting by activating target T cells in an antigen-coated chamber array through TCR-pMHC binding and drafting the activated interactive T cells moving laterally by integrin-ICAM-1 interaction. The efficiency of the sorting was improved by the pillar array design of the activation zone and designs in sorting zone including stripe angels, ceiling ridges, and stop-flow pattern. We validated this platform by mouse primary OT1 T cell sorting from non-target cells and demonstrated the ability to distinguish strong ligand activated cells from weak ligand activated.

Further improvements are needed for better sensitivity and higher cell collection ratio. Iterative cycles of enrichment can be one of the options. Physiological cell types and whole blood performance need to be tested before broad applications. Nevertheless, with the high specificity of the sorting, this platform would allow selection of cells in interest for sequencing or follow-up studies on these cells. The ability for distinguishing cells with different activation levels may allow a potential application of ‘interactive cell chromatography’ where a polyclonal population can be disassembled in a spectrum regarding the cells’ potency.

CHAPTER 6. CONCLUSIONS AND FUTURE DIRECTIONS

6.1 Summary

Cell adhesion through receptor-ligand interactions is an essential way for cells to sense and respond to the environment. Although extremely common in cellular processes, multi-receptor crosstalk lacks an efficient technique for profound study with precisely controlled ligand stimulation, detangling measurement of the effect by several receptor-ligand interactions. In this thesis, two high-throughput platforms regarding cell multi-receptor crosstalk were established: 1) multi-zone platform, which allowed the study of receptor crosstalk in a spatially and temporally separated way with precise control of stimulation; 2) cell sorting platform, which take advantage of the knowledge of T cell intermediate adhesion signatures learned on multi-zone device and applied it in a sorting device.

An auto-alignment protein patterning technique was first developed for sequential ligand presentation in a multi-zone device in CHAPTER 2. Contacting the ligands separated spatially detangled the adhesion measurement of the several pairs of receptor-ligand interactions, but retained the triggering effect of one protein to another on cells. The species, the concentration and the zone length of surface-immobilized molecules can be well-controlled, so as to provide precise, tunable doses of mechano-stimulation to study cell multi-receptor adhesion and signaling cascades. Advanced parallel version of this device could allow controls over various stimulations on the same chip and further improve the throughput.

In CHAPTER 3, I exploited the multi-zone device on two biological systems, platelets and neutrophils. The characterization of the platelet integrin adhesion behavior and conformation upon various dose of mechano-stimulation contributed to the discovery of the integrin intermediate state. Furthermore, the subtle difference of diabetic platelets was amplified for detection in this device using only one-drop of whole blood sample, which is highly unlikely to achieve by current techniques with such limited sample. In addition, neutrophil integrin LFA-1 activation was assessed by separating the stimulation and behavior reporting. The activation requirement and the effect of two parameters were studied.

The same integrin expressed on neutrophil also exist on T cells. Studying the stimulation of LFA-1 by T cell receptor in cell moving condition could contribute to our understanding of T cell activation. CHAPTER 4 investigated the interaction of T cell receptor with its ligand pMHC and the resulting activation of integrin LFA-1 measured by the rolling behavior on ICAM-1 and activation of the cell measured by calcium flux. By controlling the density and length of the surface-immobilized ligands, I was able to characterize the stimulation dose-dependency of T cell activation.

The knowledge of pMHC-activated T cell rolling gained from CHAPTER 4 contributed to the development of an antigen-specific T cell sorting platform in CHAPTER 5. The platform consists of two parts: an activation zone for target T cell stimulation and a sorting zone coated with a pattern of integrin ligand ICAM-1 allowing activated T cells to move with an angle to the flow direction. I validated the platform with mouse primary OT1 T cell sorting from non-target B6 T cells. Based on the activation response rather than direct receptor affinity, this platform successfully identified the functionally active target

cells. Considering its advantages including short time scale, continuous sorting manner, and module compatibility, this platform can certainly be implemented for enumeration and isolation of functional T cells in the future, provided that repeated sorting can be realized systematically.

6.2 Further works

Hardware and fabrication processes can certainly be improved to make the platforms more user-friendly for broader applications. Advances of the systems I developed in this dissertation can be explored in the further to make them more powerful. Additional biological questions can then be investigated.

6.2.1 Broader applications of the multi-zone device

Our device has demonstrated its ability of studying cooperative receptors; it is reasonable to speculate that it can also be used to study the antagonistic effect between receptors [155-157], such as the inhibitory effect of programmed cell death protein 1 (PD1) [158] and CTLA-4 to T cell receptor (TCR) [159], which has been known to play a critical role in tumour immunology [158], or even more complex systems involving multiple receptor species where both cooperative and antagonistic concurrently play a role [160]. This would largely extend our understanding of cell mechano-signaling, for instance understanding the acute inhibitory effect of antagonistic receptors to T cell should contribute to the discovery of T cell noise rejection and self-immunity.

6.2.2 Coupling other techniques for multi-parameter analysis

Adherent cell density and translocation velocity are the two major readout of our current system; calcium flux can be applied to certain cells as well. However, more parameters of response can certainly be measured by incorporating other techniques [161, 162]. For instance, DNA force probe [162] that reports the binding force between a receptor and a ligand can be patterned on the stimulation region to assess the requirement of stimulation force or on the reporting region for the measurement of cell receptor activation.

In quite a few biological processes such as inflammation, multiple types of cells are involved [163-165], which communicate with one another. Cells, instead of purified proteins, can be patterned on the multi-zone device surface, such as a layer of adhered endothelial cells, which will allow the study of direct cell-cell crosstalk. Future study can explore the platelet-leukocyte recruitment such that one step forward can be accomplished to the cellular mechanistic processes such as development of atherosclerotic lesions [166] and acute inflammation [165].

6.2.3 Improvement on sorting with mechanism study on cell rolling signature

Although Figure 4-8 (Page 81) showed the considerable difference of rolling velocities between Q4R7- and Q4H7- activated T cells, an enrichment limitation was demonstrated in Figure 5-11 (Page 112) between OT1 cells activated by these pMHCs. Even with a statistically significant difference of the lateral movement of the two

populations, the enrichment level within one round of sorting was imperfect. It remained a question of what are the parameters of the cell adhesion signatures that affects the lateral movement on inclined ligand stripes if rolling velocity was not enough for prediction. One can further investigate on the rolling properties that contributes to the effective lateral movement such that a clear sorting of polyclonal T cell spectrum can be realized for multiple outlet collections of single population.

6.2.4 T cell sorting with unknown antigen

All the current approaches can only be applied to sort T cells to known and synthetic ligands. However, in numerous disease cases, we could not acquire the ligands before we determine the target molecule. Sorting of T cells targeting tumor cells without knowing or acquiring the ligands would have tremendous value in clinics. In this practice, tumors including the tumor cells and leukocytes can be broken down to make membrane micro-vesicles by ultracentrifuge. The micro-vesicles can then be delivered to the activation zone and seeded on the surface. Since the membrane contains the specific pMHC from the leukocytes trapped in the tumor, corresponding T cells have the chance to interact with the surface through the TCR-pMHC interactions. Resolving the lipid seeding, noise discrimination and specificity enhancement, one can sort T cells targeting an unknown antigen and collect the sorted cells for sequencing and expansion, which is of great value in immunotherapy.

APPENDIX

Appendix A. Multi-zone device assembling for identifying zone location

The location of the cell relative to the starting point of the interaction is an estimation of the cell experiencing time. Transient or changing state exist in a lot of cell activation process. In these applications, the zone locations on the substrate need to be identified for accurate estimation of activation changing over time.

To provide the accurate zone location, especially the boundary of the stimulation zone and reporting zone, markers on the channel device PDMS was designed for identification purpose. Process to assemble the device was illustrated as below (A 1)

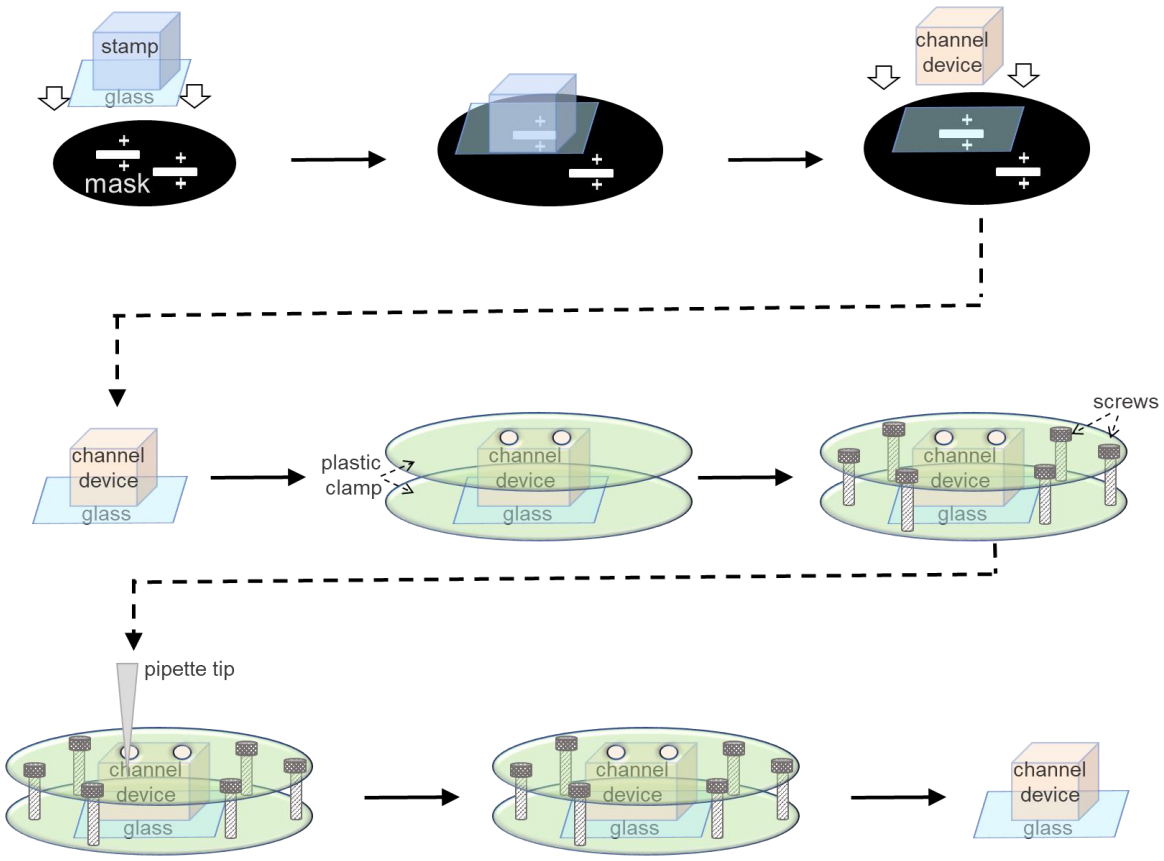

A 1. Process to align markers on channel device to the zone location. Stamp and contacted substrate glass were placed and taped onto a mask with markers. Took off the stamp before put channel device onto the glass according to the markers on the mask. Held the device and delivered coating solution with the clamp.

A preliminary study of platelet activation changing over time was investigated on multi-zone device. After activation by VWF-A1, platelets entered the zone of Fg or FN. Instead of measuring the velocity or adherent density of the cells, we tracked the cells along the reporting zone to observe their velocity changes on the Fg (A 2 a) or FN (A 2 b) surface. Comparison of the velocities on reporting surface across the time indicating a more

activated state through time when intermediate-state platelet interacting with FN and Fg (A 2 c).

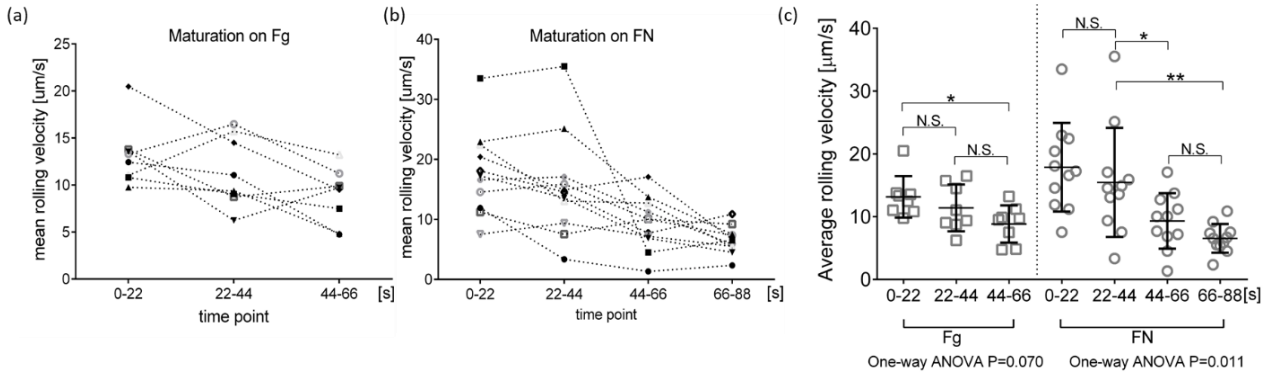

A 2. Activation maturation of platelets on reporting zone. Individual platelet velocities on Fg (a) or FN (b) were plotted after activation by VWF-A1. c) A summary of the velocities was plotted, and velocities were compared across the time of platelets on reporting zone. Dots indicated individual experiment. *, **, * and **** denotes p < 0.05, 0.01, 0.001 and 0.0001, respectively, by One-way ANOVA.**

Appendix B. Antibody Kim127 production and purification

The key conformation antibody to report intermediate state of integrin LFA-1 was produced and purified from hybridoma B cells.

B.1. Hybridoma culture

Hybridoma B lymphocyte (mouse) was purchased and cultured for antibody KIM127 production. Initial recovery and cell expansion culture were conducted as standard cell culture procedures. After expansion, cells were gradually transferred to a protein-free media (Thermo Fisher Scientific) so that extraction of antibody would not be affected by the albumin in culture media. The adaptation of the protein-free environment took 4 steps:

0% protein-free media (100% normal RPMI 1640 media), 50% protein-free media, 80% protein-free media, and 100% protein-free media. After the adaption, supernatant media was then collected after 2-3 days of culture and ready for purification.

B.2. Antibody purification

We first ran gel electrophoresis to validate the existence of the antibody KIM127 in cell media (A 3). The structure of heavy chains and light chains in the antibody was verified by the reduced sample. Heavy chains of ~50 kd and light chains of ~20kd creates the dimer antibody ~150kd.

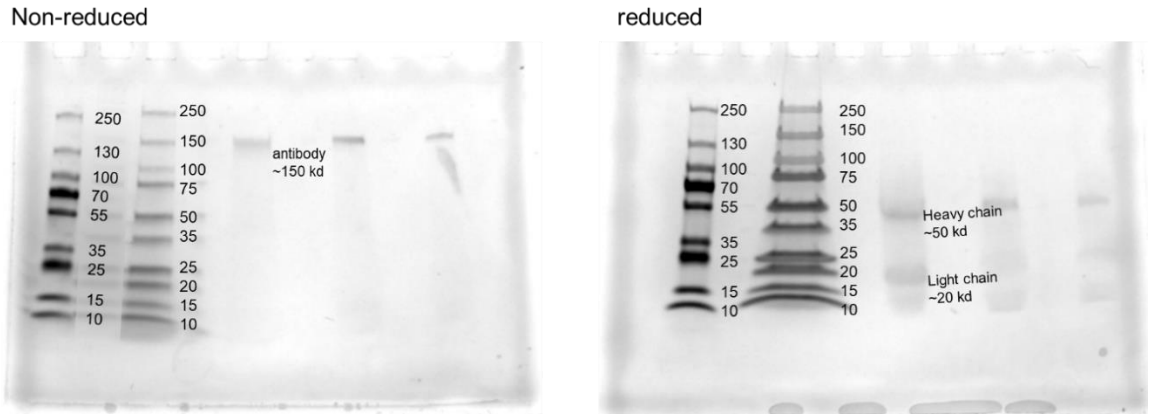

A 3. Existence of the antibody KIM127 by gel electrophoresis. Three difference concentrated media supernatant was compared to the calibration. Left was the original supernatant, protein detected at ~150KD (supposed to be the antibody KIM127). right was reduced (break the disulfide), heavy chain and light chain can be observed.

Column G was used for antibody purification. Gel electrophoresis showed depletion of the antibody after going through the column G (A 4).

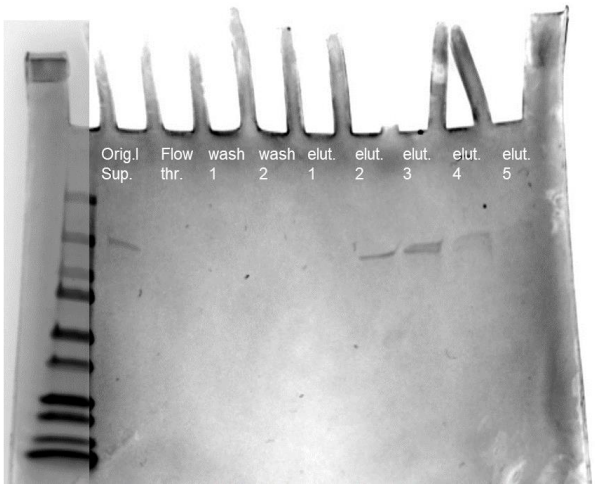

A 4. Extraction and purification of antibody KIM127. Protein was shown to exist in original supernatant and elution solution, but not in flow through or wash solution.

Appendix C. Cell sorting system

C.1. Components

A microscope to monitor and image.

A two-way syringe pump to deliver cell solution and buffer.

A computer to record video and control syringe pump. Computer and syringe pump were connected with a cable: network cable to PC and to "to computer" network port on pump.

A heater to control temperature on chip.

C.2. Code for stop-flow pattern

To create a stop-flow pattern, MATLAB code was modified for syringe pump controlling. The GUI file was created before and I modified the following part to control the time of running and pause.

```
% --- Executes on button press in togglebutton13.
function togglebutton13_Callback(hObject, eventdata, handles)
% hObject    handle to togglebutton13 (see GCBO)
% eventdata  reserved - to be defined in a future version of MATLAB
% handles    structure with handles and user data (see GUIDATA)

% Hint: get(hObject,'Value') returns toggle state of togglebutton13
if handles.pumpvalidity(1) == 1
num1 = 5;
ptime = 3;%pause time can be changed



for i = 1:10 %cycle number to end
dstart = tic;
fwrite(handles.pSer,['1 RUN' 13 10]);
set(handles.light1,'BackgroundColor','green');


toc(dstart);
%run ptime and stop
while toc(dstart) < ptime*2
toc(dstart);
pause(.005);
end

fwrite(handles.pSer,['1 STP' 13 10]);
set(handles.light1,'BackgroundColor','red');
toc(dstart);

%pause another ptime
while(toc(dstart) < ptime*3)
toc(dstart);
pause(.005);
end
end
```

```
else

   fwrite(handles.pSer,['1 STP' 13 10]);
    set(handles.light1,'BackgroundColor','red');
end
```

REFERENCES

1. Ruoslahti, E. and M. Pierschbacher, *New perspectives in cell adhesion: RGD and integrins.* Science, 1987. **238**(4826): p. 491-497.

2. Smith-Garvin, J.E., G.A. Koretzky, and M.S. Jordan, *T cell activation.* Annual review of immunology, 2009. **27**: p. 591-619.

3. McEver, R.P. and C. Zhu, *Rolling cell adhesion.* Annu Rev Cell Dev Biol, 2010. **26**: p. 363-96.

4. Zhou, D.W. and A.J. García, *Measurement systems for cell adhesive forces.* Journal of biomechanical engineering, 2015. **137**(2): p. 020908-020908.

5. Albrecht, C., et al., *DNA: A Programmable Force Sensor.* Science, 2003. **301**(5631): p. 367-370.

6. Su, Q.P. and L.A. Ju, *Biophysical nanotools for single-molecule dynamics.* Biophysical Reviews, 2018. **10**(5): p. 1349-1357.

7. Humphrey, J.D., E.R. Dufresne, and M.A. Schwartz, *Mechanotransduction and extracellular matrix homeostasis.* Nat Rev Mol Cell Biol, 2014. **15**(12): p. 802-12.

8. BrianSavage, EnriqueSaldívar, and Z. MRuggeri, *Initiation of Platelet Adhesion by Arrest onto Fibrinogen or Translocation on von Willebrand Factor.* Cell, 1996.

9. Nesbitt, W.S., et al., *Distinct glycoprotein Ib/V/IX and integrin alpha IIbbeta 3-dependent calcium signals cooperatively regulate platelet adhesion under flow.* J Biol Chem, 2002. **277**(4): p. 2965-72.

10. Ruggeri, Z.M. and G.L. Mendolicchio, *Adhesion mechanisms in platelet function.* Circ Res, 2007. **100**(12): p. 1673-85.

11. Merten, M. and P. Thiagarajan, *P-selectin expression on platelets determines size and stability of platelet aggregates.* Circulation, 2000. **102**(16): p. 1931-6.

12. Leytin, V., et al., *Quantification of Platelet Activation Status by Analyzing P-Selectin Expression.* Biochemical and Biophysical Research Communications, 2000. **273**(2): p. 565-570.

13. Liu, Z., et al., *Differential regulation of human and murine P-selectin expression and function in vivo.* J Exp Med, 2010. **207**(13): p. 2975-87.

14. Zarbock, A. and K. Ley, *Mechanisms and consequences of neutrophil interaction with the endothelium.* The American journal of pathology, 2008. **172**(1): p. 1-7.

15. Chen, W., et al., *Measuring Receptor-Ligand Binding Kinetics on Cell Surfaces: From Adhesion Frequency to Thermal Fluctuation Methods.* Cell Mol Bioeng, 2008. **1**(4): p. 276-288.

16. Huang, J., et al., *The kinetics of two-dimensional TCR and pMHC interactions determine T-cell responsiveness.* Nature, 2010. **464**(7290): p. 932-6.

17. Chesla, S.E., P. Selvaraj, and C. Zhu, *Measuring two-dimensional receptor-ligand binding kinetics by micropipette.* Biophysical journal, 1998. **75**(3): p. 1553-1572.

18. Benoit, M. and H.E. Gaub, *Measuring Cell Adhesion Forces with the Atomic Force Microscope at the Molecular Level.* Cells Tissues Organs, 2002. **172**(3): p. 174-189.

19. Zhang, H. and K.-K. Liu, *Optical tweezers for single cells.* Journal of the Royal Society, Interface, 2008. **5**(24): p. 671-690.

20. Kaplanski, G., et al., *Granulocyte-endothelium initial adhesion. Analysis of transient binding events mediated by E-selectin in a laminar shear flow.* Biophysical Journal, 1993. **64**(6): p. 1922-1933.

21. Alon, R., D.A. Hammer, and T.A. Springer, *Lifetime of the P-selectin-carbohydrate bond and its response to tensile force in hydrodynamic flow.* Nature, 1995. **374**(6522): p. 539-542.

22. Dong, C. and X.X. Lei, *Biomechanics of cell rolling: shear flow, cell-surface adhesion, and cell deformability.* Journal of Biomechanics, 2000. **33**(1): p. 35-43.

23. J. Azeredo, A.P.P., I. Lopes, R. Oliveira and M.J. Vieira, *Monitoring cell detachment by surfactants in a parallel plate flow chamber.* 2003.

24. Takalkar, A.M., et al., *Binding and detachment dynamics of microbubbles targeted to P-selectin under controlled shear flow.* J Control Release, 2004. **96**(3): p. 473-82.

25. King, M.R., et al., *Nano-to-micro scale dynamics of P-selectin detachment from leukocyte interfaces. III. Numerical simulation of tethering under flow.* Biophys J, 2005. **88**(3): p. 1676-83.

26. E. Evans, D. Berk, and A. Leung, *detachment of agglutinin-bonded red blood cells.* 1991.

27. Evans, E. and K. Kinoshita, *Using Force to Probe Single‐Molecule Receptor–Cytoskeletal Anchoring Beneath the Surface of a Living Cell*, in *Methods in Cell Biology*. 2007, Academic Press. p. 373-396.

28. Christ, K.V., et al., *Measurement of single-cell adhesion strength using a microfluidic assay.* Biomedical Microdevices, 2010. **12**(3): p. 443-455.

29. Murthy, S.K., *Effect of Flow and Surface Conditions on Human.* 2004.

30. Plouffe and S.K. Murthy, *Peptide-Mediated Selective Adhesion of Smooth Muscle and Endothelial Cells in Microfluidic Shear Flow.* 2007.

31. Hang Lu, et al., *Microfluidic Shear Devices for Quantitative Analysis of Cell Adhesion.* 2004.

32. Wankhede, S.P., et al., *Cell Detachment Model for an Antibody-Based Microfluidic Cancer Screening System.* Biotechnology Progress, 2006. **22**(5): p. 1426-1433.

33. Simone, G., et al., *Cell rolling and adhesion on surfaces in shear flow. A model for an antibody-based microfluidic screening system.* Microelectronic Engineering, 2012. **98**: p. 668-671.

34. Nesbitt, W.S., et al., *A shear gradient-dependent platelet aggregation mechanism drives thrombus formation.* Nat Med, 2009. **15**(6): p. 665-73.

35. Juliano, R.L., *Signal Transduction by Cell Adhesion Receptors and the Cytoskeleton: Functions of Integrins, Cadherins, Selectins, and Immunoglobulin-Superfamily Members.* Annual Review of Pharmacology and Toxicology, 2002. **42**(1): p. 283-323.

36. Kong, F., et al., *Demonstration of catch bonds between an integrin and its ligand.* The Journal of Cell Biology, 2009. **185**(7): p. 1275-1284.

37. Rosetti, F., et al., *A Lupus-Associated Mac-1 Variant Has Defects in Integrin Allostery and Interaction with Ligands under Force.* Cell reports, 2015. **10**(10): p. 1655-1664.

38. Schurpf, T. and T.A. Springer, *Regulation of integrin affinity on cell surfaces.* EMBO J, 2011. **30**(23): p. 4712-27.

39. M. ARYA, et al., *Glycoprotein Ib–IX-mediated activation of integrin aIIbb3: effects of receptor clustering and von Willebrand factor adhesion.* J of Thrombosis and Haemostasis, 2003.

40. El Haouari, M. and J.A. Rosado, *Platelet function in hypertension.* Blood Cells Mol Dis, 2009. **42**(1): p. 38-43.

41. Ju, L., et al., *Compression force sensing regulates integrin αIIbβ3 biomechanical adhesive function on diabetic platelets.* Nature Communications (Resubmitted), 2017.

42. Goyal, A., et al., *Attained Educational Level and Incident Atherothrombotic Events in Low- and Middle-Income Compared With High-Income Countries.* Circulation, 2010. **122**(12): p. 1167-1175.

43. Fisher, M. and J. Loscalzo, *The Perils of Combination Antithrombotic Therapy and Potential Resolutions.* Circulation, 2011. **123**(3): p. 232-235.

44. Chakraborty, A.K. and A. Weiss, *Insights into the initiation of TCR signaling.* Nat Immunol, 2014. **15**(9): p. 798-807.

45. Courtney, A.H., W.L. Lo, and A. Weiss, *TCR Signaling: Mechanisms of Initiation and Propagation.* Trends Biochem Sci, 2018. **43**(2): p. 108-123.

46. Phillips, R.E., et al., *Human immunodeficiency virus genetic variation that can escape cytotoxic T cell recognition.* Nature, 1991. **354**(6353): p. 453-459.

47. Lehmann, P.V., et al., *Spreading of T-cell autoimmunity to cryptic determinants of an autoantigen.* Nature, 1992. **358**(6382): p. 155-157.

48. Gaud, G., R. Lesourne, and P.E. Love, *Regulatory mechanisms in T cell receptor signalling.* Nat Rev Immunol, 2018. **18**(8): p. 485-497.

49. Tian, S., et al., *CD8⁺ T Cell Activation Is Governed by TCR-Peptide/MHC Affinity, Not Dissociation Rate.* The Journal of Immunology, 2007. **179**(5): p. 2952-2960.

50. McKeithan, T.W., *Kinetic proofreading in T-cell receptor signal transduction.* Proceedings of the National Academy of Sciences, 1995. **92**(11): p. 5042-5046.

51. Dushek, O., R. Das, and D. Coombs, *A Role for Rebinding in Rapid and Reliable T Cell Responses to Antigen.* PLOS Computational Biology, 2009. **5**(11): p. e1000578.

52. Altan-Bonnet, G. and R.N. Germain, *Modeling T Cell Antigen Discrimination Based on Feedback Control of Digital ERK Responses.* PLOS Biology, 2005. **3**(11): p. e356.

53. Mukhopadhyay, H., et al., *Systems Model of T Cell Receptor Proximal Signaling Reveals Emergent Ultrasensitivity.* PLOS Computational Biology, 2013. **9**(3): p. e1003004.

54. Voisinne, G., et al., *T Cells Integrate Local and Global Cues to Discriminate between Structurally Similar Antigens.* Cell reports, 2015. **11**(8): p. 1208-1219.

55. Govern, C.C., et al., *Fast on-rates allow short dwell time ligands to activate T cells.* Proceedings of the National Academy of Sciences, 2010. **107**(19): p. 8724-8729.

56. Valitutti, S., et al., *Serial triggering of many T-cell receptors by a few peptide–MHC complexes.* Nature, 1995. **375**(6527): p. 148-151.

57. Kim, S.T., et al., *The alphabeta T cell receptor is an anisotropic mechanosensor.* The Journal of biological chemistry, 2009. **284**(45): p. 31028-31037.

58. Liu, B., et al., *Accumulation of dynamic catch bonds between TCR and agonist peptide-MHC triggers T cell signaling.* Cell, 2014. **157**(2): p. 357-368.

59. Davis, S.J. and P.A. van der Merwe, *The kinetic-segregation model: TCR triggering and beyond.* Nature Immunology, 2006. **7**(8): p. 803-809.

60. Bunting, M., et al., *Leukocyte adhesion deficiency syndromes: adhesion and tethering defects involving β 2 integrins and selectin ligands.* Current Opinion in Hematology, 2002. **9**(1): p. 30-35.

61. Savinko, T., et al., *Filamin A Is Required for Optimal T Cell Integrin-Mediated Force Transmission, Flow Adhesion, and T Cell Trafficking.* J Immunol, 2018. **200**(9): p. 3109-3116.

62. Dustin, M.L. and K. Choudhuri, *Signaling and Polarized Communication Across the T Cell Immunological Synapse.* Annu Rev Cell Dev Biol, 2016. **32**: p. 303-325.

63. Fooksman, D.R., et al., *Functional anatomy of T cell activation and synapse formation.* Annual review of immunology, 2010. **28**: p. 79-105.

64. Huppa, J.B. and M.M. Davis, *T-cell-antigen recognition and the immunological synapse.* Nature Reviews Immunology, 2003. **3**(12): p. 973-983.

65. Hogg, N., I. Patzak, and F. Willenbrock, *The insider's guide to leukocyte integrin signalling and function.* Nat Rev Immunol, 2011. **11**(6): p. 416-26.

66. Lefort, C.T. and K. Ley, *Neutrophil arrest by LFA-1 activation.* Front Immunol, 2012. **3**: p. 157.

67. Salas, A., et al., *Transition from rolling to firm adhesion can be mimicked by extension of integrin alphaLbeta2 in an intermediate affinity state.* J Biol Chem, 2006. **281**(16): p. 10876-82.

68. Corum, L.E., et al., *Using microcontact printing of fibrinogen to control surface-induced platelet adhesion and activation.* Langmuir : the ACS journal of surfaces and colloids, 2011. **27**(13): p. 8316-8322.

69. Chiu, D.T., et al., *Patterned deposition of cells and proteins onto surfaces by using three-dimensional microfluidic systems.* Proceedings of the National Academy of Sciences, 2000. **97**(6): p. 2408-2413.

70. Cabezas, M.D., et al., *Combinatorial screening of mesenchymal stem cell adhesion and differentiation using polymer pen lithography.* Methods in cell biology, 2014. **119**: p. 261-276.

71. You, C. and J. Piehler, *Functional protein micropatterning for drug design and discovery.* Expert Opinion on Drug Discovery, 2016. **11**(1): p. 105-119.

72. Kwong, G.A., et al., *Modular nucleic acid assembled p/MHC microarrays for multiplexed sorting of antigen-specific T cells.* J Am Chem Soc, 2009. **131**(28): p. 9695-703.

73. Didar, T.F. and M. Tabrizian, *Adhesion based detection, sorting and enrichment of cells in microfluidic Lab-on-Chip devices.* Lab Chip, 2010. **10**(22): p. 3043-53.

74. Kumar, A. and G.M. Whiteside, *Features of gold having micrometer to centimeter dimensions can be formed through a combination of stamping with an elastomeric stamp and an alkanethiol ''ink'' followed by chemical etching.* Appl. Phys. Lett, 1993.

75. James, L.W., et al., *Microcontact printing of self-assembled monolayers: applications in microfabrication.* Nanotechnology, 1996. **7**(4): p. 452.

76. Kim, E., Y. Xia, and G.M. Whitesides, *Polymer microstructures formed by moulding in capillaries.* Nature, 1995. **376**(6541): p. 581-584.

77. Takayama, S., et al., *Patterning cells and their environments using multiple laminar fluid flows in capillary networks.* Proceedings of the National Academy of Sciences, 1999. **96**(10): p. 5545-5548.

78. Williams, T.E., et al., *Concurrent and Independent Binding of Fcγ Receptors IIa and IIIb to Surface-Bound IgG.* Biophysical Journal, 2000. **79**(4): p. 1867-1875.

79. Chemnitz, J.M., et al., *SHP-1 and SHP-2 associate with immunoreceptor tyrosine-based switch motif of programmed death 1 upon primary human T cell stimulation, but only receptor ligation prevents T cell activation.* J Immunol, 2004. **173**(2): p. 945-54.

80. Ju, L., et al., *Dual Biomembrane Force Probe enables single-cell mechanical analysis of signal crosstalk between multiple molecular species.* Sci Rep, 2017. **7**(1): p. 14185.

81. Perl, A., D.N. Reinhoudt, and J. Huskens, *Microcontact Printing: Limitations and Achievements.* Advanced Materials, 2009. **21**(22): p. 2257-2268.

82. Berthier, E., et al., *Pipette-friendly laminar flow patterning for cell-based assays.* Lab on a Chip, 2011. **11**(12): p. 2060-2065.

83. Kane;, R. and G.M. Whitesides, *Patterning proteins and cells using soft lithography.* Biomaterials, 1999.

84. Lee, C.H., et al., *Studying cell rolling trajectories on asymmetric receptor patterns.* J Vis Exp, 2011(48).

85. Frelinger, A.L., et al., *Monoclonal Antibodies to Ligand-occupied Conformers of Integrin aIIbP3 (Glycoprotein IIb-IIIa) Alter Receptor Affinity, Specificity, and Function.* J Biol Chem, 1991.

86. Bunch, T.A., *Integrin alphaIIbbeta3 activation in Chinese hamster ovary cells and platelets increases clustering rather than affinity.* J Biol Chem, 2010. **285**(3): p. 1841-9.

87. Hanley, W., et al., *Single molecule characterization of P-selectin/ligand binding.* J Biol Chem, 2003. **278**(12): p. 10556-61.

88. Plow, E.F. and M.H. Ginsberg, *Specific and Saturable Binding of Plasma Fibronectin to Thrombin stimulated Human Platelets".* J Biol Chem, 1981.

89. Yago, T., et al., *Platelet glycoprotein Ibalpha forms catch bonds with human WT vWF but not with type 2B von Willebrand disease vWF.* J Clin Invest, 2008. **118**(9): p. 3195-207.

90. Remijn, J.A., *Role of ADP Receptor P2Y12 in Platelet Adhesion and Thrombus Formation in Flowing Blood.* Arteriosclerosis, Thrombosis, and Vascular Biology, 2002. **22**(4): p. 686-691.

91. Chen, Y., et al., *Receptor-mediated cell mechanosensing.* Mol. Biol. Cell, 2017.

92. Huang, J., et al., *Integrin alpha(v)beta(3) on human endothelial cells binds von Willebrand factor strings under fluid shear stress.* Blood, 2009. **113**(7): p. 1589-1597.

93. Nuyttens, B.P., et al., *Platelet adhesion to collagen.* Thrombosis Research, 2011. **127**: p. S26-S29.

94. Zhang, D., et al., *Two disparate ligand-binding sites in the human P2Y1 receptor.* Nature, 2015. **520**(7547): p. 317-321.

95. Hollopeter, G., et al., *Identification of the platelet ADP receptor targeted by antithrombotic drugs.* Nature, 2001. **409**(6817): p. 202-207.

96. Coughlin, S.R., *How the protease thrombin talks to cells.* Proceedings of the National Academy of Sciences of the United States of America, 1999. **96**(20): p. 11023-11027.

97. Yago, T., et al., *Selectins and chemokines use shared and distinct signals to activate beta2 integrins in neutrophils.* Blood Adv, 2018. **2**(7): p. 731-744.

98. Knobler, H., et al., *Shear-Induced Platelet Adhesion and Aggregation on Subendothelium Are Increased in Diabetic Patients.* Thrombosis Research, 1998. **90**(4): p. 181-190.

99. Ju, L., et al., *Von Willebrand factor-A1 domain binds platelet glycoprotein Ibalpha in multiple states with distinctive force-dependent dissociation kinetics.* Thromb Res, 2015. **136**(3): p. 606-12.

100. Dittmar, S., R. Polanowska-Grabowska, and A.R.L. Gear, *Platelet adhesion to collagen under flow conditions in diabetes mellitus.* Thrombosis Research, 1994. **74**(3): p. 273-283.

101. Jackson, S.P., W.S. Nesbitt, and E. Westein, *Dynamics of platelet thrombus formation.* J Thromb Haemost, 2009. **7 Suppl 1**: p. 17-20.

102. Jackson, S.P., *Arterial thrombosis--insidious, unpredictable and deadly.* Nat Med, 2011. **17**(11): p. 1423-36.

103. Beste, M.T. and D.A. Hammer, *Selectin catch–slip kinetics encode shear threshold adhesive behavior of rolling leukocytes.* Proceedings of the National Academy of Sciences, 2008. **105**(52): p. 20716-20721.

104. Yago, T., et al., *Catch bonds govern adhesion through L-selectin at threshold shear.* The Journal of cell biology, 2004. **166**(6): p. 913-923.

105. Sigal, A., et al., *The LFA-1 Integrin Supports Rolling Adhesions on ICAM-1 Under Physiological Shear Flow in a Permissive Cellular Environment.* The Journal of Immunology, 2000. **165**(1): p. 442-452.

106. Santilli, F., et al., *Platelet activation in obesity and metabolic syndrome.* Obesity Reviews, 2012. **13**(1): p. 27-42.

107. Dustin, M.L. and L.C. Kam, *Tapping out a mechanical code for T cell triggering.* J Cell Biol, 2016. **213**(5): p. 501-3.

108. Mallaun, M., et al., *The T cell receptor's alpha-chain connecting peptide motif promotes close approximation of the CD8 coreceptor allowing efficient signal initiation.* Journal of immunology (Baltimore, Md. : 1950), 2008. **180**(12): p. 8211-8221.

109. Bromley, S.K. and M.L. Dustin, *Stimulation of naïve T-cell adhesion and immunological synapse formation by chemokine-dependent and -independent mechanisms.* Immunology, 2002. **106**(3): p. 289-298.

110. Tybulewicz, V.L.J., *Chemokines and the immunological synapse.* Immunology, 2002. **106**(3): p. 287-288.

111. Hong, J., et al., *A TCR mechanotransduction signaling loop induces negative selection in the thymus.* Nature Immunology, 2018. **19**(12): p. 1379-1390.

112. Marki, A., et al., *Rolling neutrophils form tethers and slings under physiologic conditions in vivo.* J Leukoc Biol, 2018. **103**(1): p. 67-70.

113. Le Borgne, M., et al., *Real-Time Analysis of Calcium Signals during the Early Phase of T Cell Activation Using a Genetically Encoded Calcium Biosensor.* Journal of immunology (Baltimore, Md. : 1950), 2016. **196**(4): p. 1471-1479.

114. Wülfing, C., M.D. Sjaastad, and M.M. Davis, *Visualizing the dynamics of T cell activation: Intracellular adhesion molecule 1 migrates rapidly to the T cell/B cell interface and acts to sustain calcium levels.* Proceedings of the National Academy of Sciences, 1998. **95**(11): p. 6302-6307.

115. Pennock, N.D., et al., *T cell responses: naive to memory and everything in between.* Advances in physiology education, 2013. **37**(4): p. 273-283.

116. Roetynck, S., et al., *Phenotypic and Functional Profiling of CD4 T Cell Compartment in Distinct Populations of Healthy Adults with Different Antigenic Exposure.* PLOS ONE, 2013. **8**(1): p. e55195.

117. Kosub, D.A., et al., *Gamma/Delta T-Cell Functional Responses Differ after Pathogenic Human Immunodeficiency Virus and Nonpathogenic Simian Immunodeficiency Virus Infections.* Journal of Virology, 2008. **82**(3): p. 1155-1165.

118. Apetoh, L., et al., *Consensus nomenclature for CD8(+) T cell phenotypes in cancer.* Oncoimmunology, 2015. **4**(4): p. e998538-e998538.

119. Jäger, A. and V.K. Kuchroo, *Effector and regulatory T-cell subsets in autoimmunity and tissue inflammation.* Scandinavian journal of immunology, 2010. **72**(3): p. 173-184.

120. Golubovskaya, V. and L. Wu, *Different Subsets of T Cells, Memory, Effector Functions, and CAR-T Immunotherapy.* Cancers, 2016. **8**(3): p. 36.

121. Klebanoff, C.A., L. Gattinoni, and N.P. Restifo, *Sorting through subsets: which T-cell populations mediate highly effective adoptive immunotherapy?* Journal of immunotherapy (Hagerstown, Md. : 1997), 2012. **35**(9): p. 651-660.

122. Clay, T.M., et al., *Assays for Monitoring Cellular Immune Responses to Active Immunotherapy of Cancer.* Clinical Cancer Research, 2001. **7**(5): p. 1127-1135.

123. Butler, N.S., J.C. Nolz, and J.T. Harty, *Immunologic considerations for generating memory CD8 T cells through vaccination.* Cellular microbiology, 2011. **13**(7): p. 925-933.

124. Sibener, L.V., et al., *Isolation of a Structural Mechanism for Uncoupling T Cell Receptor Signaling from Peptide-MHC Binding.* Cell, 2018. **174**(3): p. 672-687 e27.

125. Newell, E.W., et al., *Simultaneous detection of many T-cell specificities using combinatorial tetramer staining.* Nature methods, 2009. **6**(7): p. 497-499.

126. Batard, P., et al., *Dextramers: New generation of fluorescent MHC class I/peptide multimers for visualization of antigen-specific CD8+ T cells.* Journal of Immunological Methods, 2006. **310**(1): p. 136-148.

127. Huang, J., et al., *Detection, phenotyping, and quantification of antigen-specific T cells using a peptide-MHC dodecamer.* Proceedings of the National Academy of Sciences, 2016. **113**(13): p. E1890-E1897.

128. Chattopadhyay, P.K., et al., *Quantum dot semiconductor nanocrystals for immunophenotyping by polychromatic flow cytometry.* Nature Medicine, 2006. **12**(8): p. 972-977.

129. Dimitrov, S., et al., *Activated integrins identify functional antigen-specific CD8(+) T cells within minutes after antigen stimulation.* Proc Natl Acad Sci U S A, 2018. **115**(24): p. E5536-E5545.

130. Gossett, D.R., et al., *Label-free cell separation and sorting in microfluidic systems.* Analytical and bioanalytical chemistry, 2010. **397**(8): p. 3249-3267.

131. Shields, C.W.t., C.D. Reyes, and G.P. López, *Microfluidic cell sorting: a review of the advances in the separation of cells from debulking to rare cell isolation.* Lab on a chip, 2015. **15**(5): p. 1230-1249.

132. Shen, Y., Y. Yalikun, and Y. Tanaka, *Recent advances in microfluidic cell sorting systems.* Sensors and Actuators B: Chemical, 2019. **282**: p. 268-281.

133. Murthy, S.K., *Micro- and nanotechnology in cell separation.* 2006.

134. Choi, S., et al., *Microfluidic Self-Sorting of Mammalian Cells to Achieve Cell Cycle Synchrony by Hydrophoresis.* Analytical Chemistry, 2009. **81**(5): p. 1964-1968.

135. Zheng, S., et al., *Membrane microfilter device for selective capture, electrolysis and genomic analysis of human circulating tumor cells.* Journal of Chromatography A, 2007. **1162**(2): p. 154-161.

136. Di Carlo, D., et al., *Continuous inertial focusing, ordering, and separation of particles in microchannels.* Proc Natl Acad Sci U S A, 2007. **104**(48): p. 18892-7.

137. Choi, S., et al., *Continuous blood cell separation by hydrophoretic filtration.* Lab on a Chip, 2007. **7**(11): p. 1532-1538.

138. Petersson, F., et al., *Free Flow Acoustophoresis: Microfluidic-Based Mode of Particle and Cell Separation.* Analytical Chemistry, 2007. **79**(14): p. 5117-5123.

139. Vahey, M.D. and J. Voldman, *An Equilibrium Method for Continuous-Flow Cell Sorting Using Dielectrophoresis.* Analytical Chemistry, 2008. **80**(9): p. 3135-3143.

140. Bartels, K.E., et al., *Separation of breast cancer cells from peripherally circulating blood using antibodies fixed in microchannels.* 2004. **5312**: p. 278-293.

141. Chang, W.C., L.P. Lee, and D. Liepmann, *Biomimetic technique for adhesion-based collection and separation of cells in a microfluidic channel.* Lab Chip, 2005. **5**(1): p. 64-73.

142. Kumar, A. and A. Srivastava, *Cell separation using cryogel-based affinity chromatography.* Nat Protoc, 2010. **5**(11): p. 1737-47.

143. Mahara, A. and T. Yamaoka, *Antibody-immobilized column for quick cell separation based on cell rolling.* Biotechnol Prog, 2010. **26**(2): p. 441-7.

144. Shimaoka, M., et al., *Structures of the alpha L I domain and its complex with ICAM-1 reveal a shape-shifting pathway for integrin regulation.* Cell, 2003. **112**(1): p. 99-111.

145. Stone, J.D., A.S. Chervin, and D.M. Kranz, *T-cell receptor binding affinities and kinetics: impact on T-cell activity and specificity.* Immunology, 2009. **126**(2): p. 165-76.

146. Choi, S., J.M. Karp, and R. Karnik, *Cell sorting by deterministic cell rolling.* Lab Chip, 2012. **12**(8): p. 1427-30.

147. Gleghorn, J.P., J.P. Smith, and B.J. Kirby, *Transport and collision dynamics in periodic asymmetric obstacle arrays: Rational design of microfluidic rare-cell immunocapture devices.* Physical Review E, 2013. **88**(3).

148. Chung, K., et al., *Imaging single-cell signaling dynamics with a deterministic high-density single-cell trap array.* Anal Chem, 2011. **83**(18): p. 7044-52.

149. Gotoh, K., *Migration of a Neutrally Buoyant Particle in Poiseuille Flow: a Possible Explanation.* Nature, 1970. **225**(5235): p. 848-850.

150. SegrÉ, G. and A. Silberberg, *Radial Particle Displacements in Poiseuille Flow of Suspensions.* Nature, 1961. **189**(4760): p. 209-210.

151. Clarke, S.R., et al., *Characterization of the ovalbumin-specific TCR transgenic line OT-I: MHC elements for positive and negative selection.* Immunology & Cell Biology, 2000. **78**(2): p. 110-117.

152. Vickers, D.A., E.J. Chory, and S.K. Murthy, *Separation of two phenotypically similar cell types via a single common marker in microfluidic channels.* Lab Chip, 2012. **12**(18): p. 3399-407.

153. Moon, H.-S., et al., *Continual collection and re-separation of circulating tumor cells from blood using multi-stage multi-orifice flow fractionation.* Biomicrofluidics, 2013. **7**(1): p. 14105-14105.

154. Daniels, M.A., et al., *Thymic selection threshold defined by compartmentalization of Ras/MAPK signalling.* Nature, 2006. **444**(7120): p. 724-729.

155. Itoh, F., et al., *Synergy and antagonism between Notch and BMP receptor signaling pathways in endothelial cells.* The EMBO Journal, 2004. **23**(3): p. 541-551.

156. Kohn, J., et al., *Functionally Antagonistic Interactions between the TrkA and p75 Neurotrophin Receptors Regulate Sympathetic Neuron Growth and Target Innervation.* The Journal of Neuroscience, 1999. **19**(13): p. 5393-5408.

157. Dambly-Chaudière, C., N. Cubedo, and A. Ghysen, *Control of cell migration in the development of the posterior lateral line: antagonistic interactions between the chemokine receptors CXCR4 and CXCR7/RDC1.* BMC Developmental Biology, 2007. **7**(1): p. 23.

158. Mizuno, R., et al., *PD-1 Primarily Targets TCR Signal in the Inhibition of Functional T Cell Activation.* Frontiers in Immunology, 2019. **10**(630).

159. Odorizzi, P.M. and E.J. Wherry, *Inhibitory Receptors on Lymphocytes: Insights from Infections.* The Journal of Immunology, 2012. **188**(7): p. 2957-2965.

160. Acuto, O., V.D. Bartolo, and F. Michel, *Tailoring T-cell receptor signals by proximal negative feedback mechanisms.* Nature Reviews Immunology, 2008. **8**: p. 699.

161. Sekar, R.B. and A. Periasamy, *Fluorescence resonance energy transfer (FRET) microscopy imaging of live cell protein localizations.* The Journal of cell biology, 2003. **160**(5): p. 629-633.

162. Zhang, Y., et al., *DNA-based digital tension probes reveal integrin forces during early cell adhesion.* Nature communications, 2014. **5**: p. 5167-5167.

163. Zhang, D., et al., *Neutrophils, platelets, and inflammatory pathways at the nexus of sickle cell disease pathophysiology.* Blood, 2016. **127**(7): p. 801-809.

164. Morrell, C.N., et al., *Emerging roles for platelets as immune and inflammatory cells.* Blood, 2014. **123**(18): p. 2759-2767.

165. Zarbock, A., R.K. Polanowska-Grabowska, and K. Ley, *Platelet-neutrophil-interactions: Linking hemostasis and inflammation.* Blood Reviews, 2007. **21**(2): p. 99-111.

166. Huo, Y., et al., *Circulating activated platelets exacerbate atherosclerosis in mice deficient in apolipoprotein E.* Nature Medicine, 2003. **9**(1): p. 61-67.